EXPERIMENTAL STUDY OF CO-AXIAL FREE JETS

By
RAFIA BEGUM

Thesis submitted to the
Department of Mechanical Engineering
in partial fulfillment of the requirements of the degree of
Master of Science
in
Mechanical Engineering

BANGLADESH UNIVERSITY OF ENGINEERING AND TECHNOLOGY
DHAKA-1000, BANGLADESH

MAY, 2004

CERTIFICATE OF APPROVAL

The thesis titled "EXPERIMENTAL STUDY OF CO-AXIAL FREE JETS" submitted by RAFIA BEGUM, Roll No.100010002F, Session: Oct, 2000 to Mechanical Engineering Department of Bangladesh University of Engineering & Technology has been accepted as satisfactory for partial fulfillment of the requirements for the degree of Master of Science in Mechanical Engineering on May, 2004.

BOARD OF EXAMINERS:

1. Dr. M.A. Taher Ali
   Professor
   Department of Mechanical Engineering
   BUET,Dhaka-1000
   — Chairman (Supervisor)

2. Dr. Md.Quamrul Islam
   Professor and Head
   Department of Mechanical Engineering
   BUET,Dhaka-1000
   — Member (Ex-Officio)

3. Dr. Amalesh Chandra Mandal
   Professor
   Department of Mechanical Engineering
   BUET,Dhaka-1000
   — Member

4. Dr. Md.Tazul Islam
   Professor
   Department of Mechanical Engineering
   CUET,Chittagong
   — Member (External)

CERTIFICATE OF RESEARCH

This is to certify that the work presented in this thesis is the outcome of the investigation carried out by the candidate under the supervision of Dr.M.A.Taher Ali, Professor, Department of Mechanical Engineering of Bangladesh University of Engineering & Technology.

M A Taher Ali
Supervisor

Rafia Begum
Candidate

DECLARATION

I do hereby declare that this work has not been submitted elsewhere for the award of any degree or diploma or for publication.

Rafia Begum

Candidate

ABSTRACT

Experimental study on the mixing of two circular coaxial free jets has been performed. Coaxial flow arrangement has been made by issuing two jets at different velocities from a compound nozzle. One jet is emitted through an inner nozzle of 42 mm inner diameter and is known as inner jet. Another jet which is passed through the annular space between the outer and the inner nozzle is known as the annular jet. Three outer nozzles of inner dia of 80, 63 and 52.5 mm are used and thus the area ratios of the two nozzles are varied. The flow characteristics in the mixing zone of these two jets and the way how these characteristics differ from those of a single jet are the point of interest of the present study.

For this purpose four values of velocity ratios of outer to inner jet have been taken for each coaxial jet configuration. These values lie within 0.10 to 0.90 while the values of area ratios are 2.61,1.25 and 0.56. Measurements of velocity are taken with 1.6mm OD pitot static tube for Reynolds number ranging from 1.04×10^4 to 4×10^4.

In the exit velocity profiles the curvature effect of nozzle is prominent in reshaping the thickness of inner and outer boundary of the coaxial jet. Centerline velocity profiles show that for coaxial jets potential core length elongates from that of single jet but remains more or less constant for all velocity ratios and increases with the increase in area ratio. Mixing of coaxial jets takes place earlier for lower values of both velocity and area ratios. Spread rate of the coaxial jet is decreased in comparison to the single jet. It is also decreased with the increase in area ratio.

ACKNOWLEDGEMENT

The author wishes to express her sincerest gratitude and indebtedness to Prof. M.A. Taher Ali, Department of Mechanical Engineering, BUET for his guidance, supervision and moral support throughout the entire period of the research work. His initiative, encouragement, patience and invaluable suggestions are gratefully acknowledged.

The author wishes to express thanks to Prof. Md.Quamrul Islam, Head, Mechanical Engineering Department, BUET, Prof. Amalesh Chandra Mandal, Mechanical Engineering Department, BUET and Prof. Md. Tazul Islam, Mechanical Engineering Department, CUET for serving on her committee. Their comments and suggestions have certainly improved the quality of the work.

The author would like to thank Dr. Ashraful Islam and Dr.Rashid Sarker for their guidance and inspiration for making the work into a successful end.

Special thanks are offered to Dr. Md. Mosharrof Hossain, for offering assistance and moral support during the whole period of the research work. Special thanks are also offered to Mr.Kafiluddin Mahmud, Assistant Foreman, Carpentry Shop for his continuous co-operation in AutoCAD drawing.

The author also extends her gratitude equally to all staffs of Machine Shop, Carpentry Shop, Fluid Mechanics Lab. and photographic sections of DAERS Office for their co-operations at different stages of work.

The final expression of gratitude is offered to her parents who supported her, in all means, during the whole period.

CONTENTS

LIST OF FIGURES

LIST OF PLATES

NOMENCLATURE

- Latin Letters

Symbol	Meaning
b	Length Scale
C_g	Geometric Virtual Origin
C_k	Kinematic Virtual Origin
D_i, d	Diameter of the Inner Nozzle
D_o, D_2	Diameter of the Outer Nozzle
C	Proportionality Factor
h	Manometric Height
K_c	Decay Rate
K_s	Spread Rate
M	Mach Number
n	Power Index
P_s	Mean Static Pressure
P_a	Atmospheric Pressure
Re	Reynolds Number
U	Axial Mean Velocity
V	Transverse Mean Velocity
U1	Central Jet Velocity
U2	Annular Jet Velocity
U_c	Centerline Velocity
U_{1m}	Inner Jet Centerline Velocity at the exit plane
$A_i = (\pi d^2/4)$	Area of Inner Nozzle

$A_2=(\pi(D_0^2-d^2))/4$	Area of Annular Space
L_P	Length of Potential Core
x	x-Co-ordinate
y	y-Co-ordinate
z	z-Co-ordinate
$y_{0.10}$	Outer Edge of the Shear Layer
$y_{0.50}$	Half-width of the Shear Layer
$y_{0.90}$	Inner Edge of the Shear Layer

- Greek Letters

Symbol	Meaning
γ	Specific Weight
η	Self-preservation Variable
μ	Viscosity
ν	Kinematic Viscosity
ρ	Density
τ	Shear Stress

- Subscript

Symbol	Meaning
a	Air
c	Centerline
d	Diameter
co	Centerline at Origin
g	Geometric
k	Kinematic
p	Potential Core

CHAPTER 1: INTRODUCTION

1.1 An Overview

Fluid flow cases are most common both in nature and in engineering fields and there are innumerable types of flow situations viz boundary layer flows, free shear layer flows, wake flows, flow through pipes and ducts, flow through turbo machines, flow through reducers and diffusers, flow through orifices and nozzles, jet flows and many others. Again each of the flow types may occur in varieties of boundary conditions. Because of the diversity and vastness of the fluid flow situations there is enough scope to know the flow behavior of a particular flow situation. Jet flow is one of such flow which is generally found in nature in different forms and boundary conditions and also is used extensively in engineering installations, such as burners of combustion chambers, rocket engines, fluid injectors and many others.

1.2 Jet Flow

A jet is created by the flow of fluid from a high-pressure region to a low-pressure region through a nozzle or an orifice. Depending on the surrounding in which jet is discharged it can be broadly classified into three categories: i) Confined or bounded Jet, ii) Wall jet and iii) Free Jet.

Combination of any number of basic jets can form another type of jet and may be termed as compound jet and coaxial jet is one of its kind.

i. **Confined or Bounded Jet**: In the bounded jet, fluid discharges into a confined region bounded by solid surface(Fig.1.2a). Jets of this kind are encountered in the design of water jet pumps, furnaces, stream-jet ejector of air conditioning plants etc.

ii. **Wall Jet**: In the case of a wall jet, jet impinges on a rigid wall(Fig.1.2b) and flows over the wall along its length. The wall may be straight and parallel to or at some angle with the flow or it may be curved. Fluid flow in the pelton wheel is a classic example of a wall jet.

iii. **Free Jet** : Free jet is formed when the jet flows in an infinite fluid reservoir having no influence of solid surface(Fig.1.2c). The exhaust from an engine is expelled into the atmosphere in the form of a free jet.

Coaxial turbulent jet is produced when two streams of fluid are emitted from a compound nozzle with different velocities one from an inner and the other from an outer annular one, into a region of fluid with which each of the streams is freely miscible(Fig.1.2d). It is a simple way by which two fluid streams can easily be mixed together.This configuration is used, for instance, in combustion chambers of rocket engines, gas turbines,boilers etc. In the combustor, usually the flow comes out as a coaxial jet with fuel flowing as the inner jet and air flowing as the outer annular jet. Often, one of the jets (the inner one) is in a liquid state and has to be atomized by a high-speed annular gas jet, which is known as airblast atomization. The near- field flow structure of coaxial jets is, therefore, expected to be relevant to the understanding of liquid jet atomization. Other applications are in different types of chemical and food processing industries where mixing of chemicals and other fluid materials are performed.

1.3 Shear Layer and Flow Regions in the Free Jet

When an incompressible jet discharges into still air, the shear layer grows continuously, with the entrainment of ambient air surrounding the jet. The turbulence originates as instabilities in laminar flow when Reynolds number exceeds some critical value. It has been shown that these instabilities due to interaction of viscous terms and non-linear inertia terms in the equation of motion, generate waves. These waves starting from the nozzle outlet grow with unstable amplitude within two or three wave lengths from the exit. These waves interact with each other and form ring of vortex core which roles down-stream. After one or two revolution the vortices interact strongly with the waves behind and break down into turbulent eddies. The eddy structures in the shear layer is complicated in nature. The characteristics behavior of these eddies enables the researchers to

divide the turbulent jets into three principal region, viz, Initial region, transition region and developed region as shown in Fig.1.3. The initial region extends until the centerline mean axial velocity remains constant and the transition region starts after this initial region. Further downstream, there exits a developed region where the eddy structures become uniform.

In the initial region, turbulence generated at the shear layer progresses towards the centerline of the jet, creating a wedge like region of constant mean velocity known as the potential core which is surrounded by a mixing layer and this initial region extends until the potential core disappears. For axisymmetric jet the length of the potential core is about four times the diameter of the nozzle. The transition region starts after the initial region and depends upon the Reynolds number. The higher the Reynolds number, the smaller the transition length. The combined initial and transition region is called the developing region, where the entrainment of ambient fluid creates a continuous transfer of momentum and energy from the jet to its surroundings and generates instability due to intensive shearing of the ambient fluid forming the shear layer. The thickness of the shear layer increases as the jet travels downstream from the jet exit. Further downstream there exists a developed region where the flow variables(i.e. mean velocity, turbulent intensity, Reynolds shear stress, etc.) become approximately self-preserving and at any section, the axial mean velocity decreases continuously from its maximum value at the centre to zero value far away in the radial direction.

1.4 Flow Field Generated by Co-axial Free Jets

The initial region of a co-axial jet consists of two potential cores separated by an annular mixing region. In the stream wise direction the central jet interacts with the annular one only but the later interacts both with the inner one near the centre and the ambient room air at the boundary. Thus, near the exit of a co-axial jet two distinct potential cores exist, one at the centre and other along the central circumference of the annular jet forming a wedge shape ring. Of the two mixing

regions one is between the central and inner boundary of the annular jet and the other is between the ambient room air and the outer boundary of the annular jet. As the flow proceeds the width of each core decreases approximately linearly with the downstream distance and the cores terminate when the two(inner and outer) annular mixing regions meet together as shown in Fig.1.4. As the flow is developing it is in a state of intense mixing and it becomes fully turbulent in its developed state. In the developing stage the inner mixing layer spreads in the outward direction more rapidly to meet the outer one and in further downstream direction the co-axial jet produces the velocity profile identical to the simple axisymmetric one, indicating the complete mixing and fully developed flow condition. The characteristics of flow properties in this zone become self-preserving.

1.5 Motivation Behind the Present Study

Jet flow is a common flow field occurring both in nature and in many engineering applications and most of the jets are turbulent in nature. Considering the various use of jet flow extensive research has been done on turbulent flow into a still air or a secondary stream and the essential features of the jet have been explored. The simple flows are well understood and can be handled theoretically but when flow pattern becomes complicated by the interaction of two or more turbulent jets it becomes impossible to handle theoretically. Therefore, to know about the flow characteristics of interacting jet flows experimental investigation is required to be carried on to know about the nature of the flow field.

Though the use of co-axial jet is numerous in engineering applications,available research work on this flow field is relatively much less than that of simple jet flow. Thus experimental research work on co-axial jet flow is considered to be of prime importance and is selected for the present investigation.

1.6 Research Highlight

Two concentric circular air jets are used in the present investigation. A 42 mm diameter nozzle is introduced in the centre of the 80mm diameter nozzle set up which has already been installed by the previous researcher(24).

Despite of the extensive use of coaxial jets particularly in the combustion chambers of gas turbines, boilers, propulsion of rockets, chemical process plants, even in domestic burners and many others, research on its mixing process is much less than that on single jet. In the present research work emphasis is put on the mean flow characteristics of coaxial jets with varying area ratios and velocity ratios at different Reynolds number in an aim to find its flow characteristics which will indicate the mixing and spread rate of this compound air jet system.

1.7 Objectives:

The Objectives of the present research are to investigate the near field flow characteristics of co-axial free jets at different initial and boundary conditions and also to compare those with single jet in certain cases. The investigations include:

1. Measurement of the axial mean velocity, in the free shear layer at different centreline location from the nozzle exit to find:
   -The initial mixing Zone
   - Partial self preserving Zone
   - Fully developed zone
2. Jet Spread from the different constant velocity lines.
3. Centerline mean velocity variation along axial distance for determining:
   - The length of potential core.
4. Effect of velocity ratio and area ratio on mean velocity profile.
5. Comparison of the properties of the co-axial jet with those of the single jet.

CHAPTER-2: LITERATURE REVIEW

Over decades jet flow has become the subject of many investigators and both experimental and numerical works have been performed on free jets by previous researchers. The reviews of some of these works related to the present investigation are given under the heading of Single Jet, Co-axial Jet and Annular Jet.

2.1 **Single Jet**:

Islam[11] carried out experimental investigation on the flow characteristics of circular jets at different exit conditions which he obtained by varying the lengths of the nozzles (1.5d,5d and 8.5d), by attaching vertical flanges of different diameter(1.5d, 2.5d 4.2d and 2d), by making wedges of different angles(60^0, 45^0 and 30^0) at the exit section and by changing the Reynolds number in the range $2x10^4$ to $1x10^5$. He worked out that the mean static pressure within the potential core was positive and that in the mixing region was negative. The centerline mean velocity near the exit decreased slightly and corresponding mean static pressure increased and these were suppressed due to the increase of the exit length, Reynolds number and wedge angle. But for vertical flange, the centerline velocity near the exit increased sharply and corresponding centerline mean static pressure decreased. The stream wise velocity profile showed saddle shaped behavior which moved towards the downstream distance and disappeared at the end of the potential core. The peak value of the saddle shaped profile increased due to exit vertical flange and decreased due to the increase of the exit Reynolds number, length and wedge angle. The increase of nozzle exit length, Reynolds number and the presence of vertical flange were found to increase the potential cone.

Islam[10] performed his experiment in jets issued out from nozzles having triangular shaped splines parallel to the flow. He investigated the effect of splined tips on the near-field flow characteristics of a circular jet. He measured mean

velocity and longitudinal turbulence quantities with the help of pitot-static tube and hot-wire anemometer respectively. From his result, exit boundary layer mean velocity profiles were found to be very close to the Blasius profile and centerline mean velocity was observed to be decelerated upto 1.5% of the exit value within potential core region. Kinematic and Geometric virtual origins were located at the downstream and upstream of the nozzle exit respectively. Due to the presence of spline the saddle shaped mean velocity profiles were found to be diminishing. The spread rate and entrainment of the splined jet were also decreased in comparison to other nozzles studied.

Gama[8] studied various mean and turbulent quantities of a circular air jet in both acoustically excited and unexcited condition. He showed that rate of decay of centerline mean velocity was higher when the initial flow was turbulent compared to initially laminar cases. The kinematic virtual origin moved downstream with increasing Reynolds number. He found that the centerline turbulence intensities started to be enhanced at lower excitation frequency and after reaching the maximum started to decrease with further increase in excitation frequencies.

Selim[22] worked on both axisymmetric and asymmetric jets and studied the effect of displacement thickness and Reynolds number on the free shear layers. According to his result, the thickness of the initial boundary layer suppressed the peak value of turbulent intensities and increased the spread rate of the jet. Self-preservation characteristics of the axisymmetric jets were found to be independent of Reynolds number and initial boundary layer thickness. Asymmetry in the jet flow in one axis had little effect on mean velocity in other axis but suppressed turbulent intensities in those axis.

Lighthill[17] studied how the shearing motions in a turbulent jet manage to shed some of their energy as sound radiation. He concluded that the rms turbulent velocity was one parameter which affected the total acoustic power generation and

which was also dependent on jet velocity. For noise reduction he suggested to decrease the jet speed. Without reducing jet speed there were two more ways of noise reductions, they were, by reducing the turbulence intensity by diminishing the relative velocity of the jet to the adjacent air and by using the multiple jets when the peak noise generated from the cluster of nozzles would cancel each other resulting in a less noise than the sum of the peak noise from each separately. Using both of these two alternatives, reduction upto 10 db in peak sound was reported.

Husain and Zedan[9] measured the mean velocity and determined the jet boundaries at different boundary layer thickness. From their experimental results they found that the mean velocity was self-preserving at a distance from the exit which varied with the initial turbulence level and boundary layer thickness. For a turbulent boundary layer, the geometric virtual origin was found close to the physical origin at the nozzle exit.

Ko and Davis[13] studied the pressure field inside the potential core of a subsonic jet having Mach number less than 0.45. They showed that a near field exists within the core, except that in the first half diameter downstream. Differences in the characteristics of the pressure field within the potential core exist between the vortex generated noise at very low jet velocity and the eddy generated noise at higher velocity. They observed that the higher frequency noise was generated near the orifice while the lower frequency noise originated from further downstream.

Bradshaw[3] investigated the effect of initial conditions on the development of a free shear layer produced by a circular nozzle(exit diameter 5.08 cm and Reynolds number $Re_d = 3x10^5$). The parallel circular sections of various lengths could be screwed at the end of the nozzle to alter the initial boundary layer thickness. The initial boundary layer state was changed by tripped concentric rings(to make the exit boundary layer turbulent). He concluded that the shear layer became fully developed at $x=7(\gamma/U_e)x10^5$ from the exit for any boundary layer thickness used in

the experiment. He also noticed a significant change of geometric virtual origin with the change of boundary layer thickness.

Wygnanski and Fiedler [25] studied the axisymmetric isothermal turbulent incompressible jet issued from a round nozzle (dia 2.6 cm) having Reynolds number $Re_d = 1x10^5$ and exit turbulent intensity at 0.1%. They showed that mean velocity profiles became self-preserving after 20 diameter downstream from the exit. The location of kinematic virtual origin was found to be at 3 diameter downstream when measurements considered up to 50 diameter and that at 7 diameter when measurements considered up to 100 diameter.

2.2 **Co-axial Jet**:

Rehab, et.al. [21] experimentally investigated the near-field(x/d=5.0) flow structure of coaxial axisymmetric water jets, of large outer to inner velocity ratio, $r_u(1<r_u<\infty)$ discharging into a tank where the fluid(water)was at rest. They had their convergent nozzle configurations of area ratio=1.82 for co-axial flow arrangements. They applied flow visualization technique to identify the interaction of different mixing layers present in the near field(Fig.2.2a). They observed that the growth of the inner shear layer between the central and annular jets depended on r_u while the external layer between the annular jet and the ambient fluid at rest grows independently of the velocity ratio r_u.(Fig.2.2b).

Lenzo, and Dalal[16] performed an experimental investigation on the effect of the initial non-uniformities in the exit velocity profiles of incompressible coaxial air jets, exhausting into still air, on the fully developed region of the jets. They showed that central line velocity decay in the fully developed region of co-axial jets depends on primary jet exit velocity profile and the ratio of the central to annular jet average velocities. But it does not depend on annulus to primary jet exit area ratio which is evident from the equations they developed:

$$U_c/U_{1m} = C/X$$

$$\overline{X} = 1+(X/D_2)(U_1/U_2)^{1/2}$$

Champagne and Wygnanski [5] provided mean velocity distribution, turbulence intensities and shear stresses for various area ratios of the external and internal nozzles and the ratios of the velocity issuing out from each of the nozzles. They had their measurements at area ratios 2.94 and 1.28 with the corresponding Reynolds number ranging from 0 to about 10^5 for both nozzles, and at velocity ratio, ranging from 0 to 10.They worked out that the flow became fully developed and self-preserving sufficiently far downstream(X/D_0~ 40 or X/D_i~ 60). The decay of centerline velocity and the growth of half-width $Y_{0.5}$ were insensitive to changes of velocity and area ratios. They found that close to the nozzle exit the flow consisted of two potential cores. The length of the external core appeared to be independent of the initial velocity ratio and was equal to approximately 8 times the width of the annular nozzle. But the length of the inner core was strongly dependent on velocity ratio as well as on the area ratio. They concluded from the results of axial and radial measurements of mean velocity and turbulent intensities,that,for a fixed area ratio, velocity ratio of the outer to inner jet should be greater than one to enhance mixing between the two streams.

Morton[18] proposed a theoretical model of co-axial turbulent jets. The model was based on double jet consisted of a core(inner) and an annular(outer)jet, each having uniform but different velocities. The mixing between the jets and between the annular jet and the surrounding ambient fluid were represented by constant entrainment rate. Equations describing the velocities of the jets and the growth of the jet boundaries were derived and numerically integrated. Also, equations governing the mixing of two fluids emitting from the inner and outer jets, respectively were treated.

Murakami, et al[19] experimentally investigated mean flow development and potential core lengths of single and dual stream compressible air jets using co-

axial and eccentric nozzle configurations. They observed that, in the co-axial arrangements, the secondary flow reduced the growth rate of the primary shear layer and increased the length of the primary potential core. As a result, the mass entrainment rate of the co-axial jet was less than that of the single jet. On the other hand, the eccentric configuration showed substantial improvement in mixing over the co-axial case and achieved an entrainment rate roughly equal to that of the single jet when the exit areas of the primary and secondary streams were approximately equal.

Williams, et al[24] examined the noise emitted from external and internal mixing of co-axial jets and also from an annular nozzle and compared the results to the flow patterns of the jets. For external mixing, they observed that as the velocity of the annular jet was increased in relation to a given central jet velocity, an initial attenuation of the jet noise was observed. On further increasing the annular jet velocity until the velocities of the two streams were equal , the noise was in excess of that of the central jet alone.

Alpinieri [1] presented experimental results on the turbulent mixing process between coaxial jets of different density. In his experiment, carbon dioxide and Hydrogen were used as central jets, alternatively, exhausting into a moving concentric stream of air. The temperature of both streams were maintained equal. His objectives were to investigate the nature of turbulent diffusion process between jets when the velocity ratio as well as the mass flow rate per unit area between them approached unity. From the radial and axial distribution of concentration and velocity he concluded that the product of local density and eddy kinematic viscosity coefficient($\rho\varepsilon$) depends on axial co-ordinate(x). He showed that no tendency towards segregation of the streams was found when either the velocities or the mass flows of the streams were equal. He also showed that diffusion of mass occurred more readily than that of momentum.

Au and Ko[2,15] investigated the flow structures of coaxial jets for different values of velocity ratios, of inner to outer jet, U_1/U_2, ranging from 0.15 to 1.0. They studied the characteristics of mean velocity, turbulence intensity and pressure intensity and obtained the corresponding similarity profiles. According to their measurement of mean velocity, the initial region of coaxial jets, for the mentioned values of velocity ratios, U_1/U_2, can be divided into the initial merging, intermediate merging and fully merged zones. With the help of spectral measurement and flow visualization system, they detected the presence of two trains of vortical structures in the mixing regions of coaxial jets. The vortices, in the outer mixing region, were found to possess characteristics similar to those of a single jet and were independent on U_1/U_2. But the inner train of vortices, found in the inner mixing region, was dependent on $U_1/U_2$and resembled the characteristics of annular jet at lower values of velocity ratios ($0.15< U_1/U_2<0.5$). Therefore, at low U_1/U_2, the coaxial jet had an intermediary role between single and coaxial jet.

Elbanna and Sabbagh[6] investigated the flow field generated by the interaction of two non equal plane parallel jets. They presented the measurements of mean static pressure and mean and fluctuating velocities of the flow field for different values of velocity ratios(0.25,0.50,0.75 and 1.0) of the two jets. From axial and centerline distribution of mean velocity profiles, they figured out the location of the complete confluence of the two jets. They showed that the confluence phenomenon of the ventilated jet occurred at a much larger distance from the exit plane than that for unventilated jets, i.e., air ventilation causes weaker interaction between the two jets. They also pointed out that the axis of the combined jet came closer to the power jet as the velocity of the weaker jet was decreased. Negative static pressure was encountered upstream of the merging region while the highest pressure was developed in the confluence region. Total momentum was constant at each cross

section of the two interacting jets which is consistent with the principle of law of conservation of momentum.

2.3 **Annular Jet**

Ko and Chan [14] provided a detailed study of the initial region of three annular jets. The configurations were the basic annular jet(without any bullet in the centre) and the annular jet with a conical and an elliptical bullet. From the result of the mean velocity and turbulent intensity measurement,it was found that the initial region can be divided into the initial merging, the intermediate merging and fully merged zones. Within these three zones similarity of both mean velocity and turbulence intensity profiles were found. The similarity curves were compared with those for a single jet and a good agreement between them was found.

CHAPTER 3: THEORY

3.1 General

The co-axial turbulent jet is produced when two miscible streams of fluid are emitted from a compound nozzle with different velocities in the same direction one from an inner and other from an outer annular one into a region of fluid with which each of the streams is freely miscible.

When the central jet velocity U_1 is assumed to be uniform at the discharge of the nozzle, as well as the ambient velocity U_2 (no boundary-layer effects), then just behind the nozzle exit the turbulent mixing zone has zero width which increases with the increasing distance from the exit, up to a distance X_c such that the mixing zone covers the entire jet (Fig: 3.1). The velocity at the axis maintains its constant value U_{co} up to this distance X_c upto which the jet contains a central potential core region. Further downstream from the exit the velocity at the axis of the jet decreases with increasing distance. It will be some distance farther before the jet flow becomes fully developed and the flow characteristics in consecutive sections become self-preserving. Usually the transition region between core region and fully developed turbulent region is quite short.

3.2 Governing Equations

The turbulent motion of free jet is governed by the mass conservation and the Navier-Stokes equations. Exact analytical solutions of these equations are yet to obtain because of their non-linear forms. Hypothesis and empirical assumptions are to be introduced for obtaining a set of equations with time averaged dependent variables. Conventional order of magnitude analysis is applied to the general momentum equations to obtain the equations in a simpler form. These simpler equations used for evaluating the free jet flow parameters are:

$$\frac{dU}{dx} + \frac{dV}{dy} = 0 \qquad 3.1$$

$$U\frac{dU}{dx}+V\frac{dV}{dy}=\frac{d}{dx}\left(\frac{\tau}{\rho}\right) \qquad 3.2$$

Where τ is the shear stress and ρ is the density of the fluid; U & V are axial and transverse mean velocities; x & y are the co-ordinates in axial and transverse directions respectively.

3.3 Empirical Relations

Forstall and Shapiro [7] obtained empirical relations for the spread of the jet as a function of the distance from the orifice and for the decrease in the jet velocity, both for different ratios between the surrounding velocity U_2 of the secondary flow and the axial velocity U_1 of the jet.

The length of the core region X_c was determined mainly by the value of the ratio of U_2/U_1 and it increased with increasing U_2/U_1. According to Forstall [7] the following empirical relation held:

$$\frac{X_c}{d}=4+12\frac{U_2}{U_1} \qquad 3.3$$

The relationship was valid for the range $U_2/U_1 \sim 0.2$ to 0.5. From the above equation it is seen that $X_c = 4d$ for $U_2/U_1 = 0.0$

According to Forstall measurements the relative velocity of the jet at the axis decreased hyperbolically with increasing X

$$\frac{U_{x,\max}}{U_1-U_2}=\frac{X_c}{X}\ for \quad X>X_c \qquad 3.4$$

For the change in the jet half-width ($y_{0.5}$) he obtained

$$\frac{2y_{0.5}}{d}=\left(\frac{X}{X_c}\right)^{1-\frac{U_2}{U_1}}\ for \quad X>X_c \qquad 3.5$$

The empirical hyperbolic relation Eq^{n}3.4 between mean velocity and distance seems to apply even at large distances from the exit (for U_2/U_1=.5 Forstall's measurements

covered the range from X=0 to X=120d). But if this result were correct, one would expect a linear increase of the jet width with increasing X, not the relation Eq^{n}3.5. For, on the basis of the momentum-integral equation, equation Eq^{n}3.5 does not agree with equation Eq^{n}3.4; at any rate this is so if the velocity profiles in consecutive sections are similar. And, according to Forstall's measurement, the profiles were practically similar if at each section the velocities were expressed in terms of $U_{x,max}$ and the radial distances in terms of the jet half-width.

According to the empirical relation Eq^{n}3.5, the increase in the jet width becomes zero if U_2/U_1 approaches the value 1. This seems logical, provided that both the primary and secondary flows are free from turbulence.

Self-Preservation Variable:

It is a common practice to plot velocity against self-preserving or similarity variables. The self-preserving independent variable was defined in different ways by different authors to express the flow to be self-preserving.

Islam [10] used $\eta = (y-y_{0.5})/x$ as the self-preserving variable for expressing the flow to be self-preserving in the developing region.

Rajaratnam [19] used $\eta = (y-y_{0.95})/(y_{.50}-y_{0.95})$.

Champagne and Wygnanski [5] used $\eta = (y/x-x_h)$; where x_h is the distance of virtual origin from the nozzle exit plane.

Ko and Chan [13] used $\eta = (y-y_{0.5})/(y_{.9}-y_{.1})$ for initial merging zone

$\eta = (y-1/2De)/x$ for intermediate and fully merged zone

$\eta = y/y_c$ for fully merged zone of the annular jet.

where, y_c is the radial distance at which the local mean velocity is equal to 0.5 of U_m. U_m is the maximum mean velocity in the x-y plane and D_e is the equivalent diameter of the fully- merged jet.

Shear Layer Width, b: The shear layer width is defined by :

$$b = y_{.10} - y_{.95}$$

where, $y_{.10}$ is the y co-ordinate at $U/U_{ec}=.10$ and

$y_{0.95}$ is the y co-ordinate at $U/U_{ec}=0.95$

Virtual Origin: The origin of the co-ordinate system of a jet has been taken as the geometric origin. But practically it is observed by many researchers that the jet seems to be discharged from either downstream or upstream of the lip of jet producing component. Thus the virtual origin comes in defining jet characteristics instead of geometric origin and is classified as :

i) Kinematic Virtual Origin and ii) Geometric Virtual Origin.

i) **The Kinematic Virtual Origin**, C_k is determined from the decay of the centerline mean velocity, U_c.The non-dimensional inverse centerline velocity can be expressed by the following equation:

$$\left(\frac{U_{ec}}{U_c}\right)^2 = K_c\left(\frac{x}{d} - C_K\right)$$

where C_K is the location of the kinematic virtual origin and K_c is the rate of decay of the centerline mean velocity.

ii) **The Geometric Virtual Origin**, C_g is determined from the growth of the jet half-width $Y_{0.50}$.

$$\frac{Y_{0.5}}{d} = K_s\left(\frac{x}{d} - C_g\right)$$

Dimensionless Number: The dimensionless number associated with the jet flow is Reynolds number which is the ratio of inertia force to the viscous force. Reynolds number based on exit diameter is given by:

$$\mathrm{Re}_d = \frac{U_{ec}d}{\nu}$$

CHAPTER 4: EXPERIMENTAL SET-UP, MEASUREMENT AND CALCULATION PROCEDURE

4.1 Co-axial Jet Flow System

The co-axial jet flow system is developed by adding a central circular air flow system in the existing jet flow facility of the laboratory (P.1). The jet flow facility has overall length of 8.0m having 80 mm diameter exit nozzle. In the delivery side of the flow facility the diameter of the pipe is reduced in two stages from 475mm to 80mm where the experimental nozzle is fitted as shown in Figs. 4.1.1 and 4.1.2. To convert this circular jet flow system into a coaxial jet flow system a 62 mm PVC line is taken out from the 100 mm diameter delivery line of the centrifugal blower which has already been installed for the air supply to the calibration rig placed below the jet flow system. The 62 mm PVC pipe is inserted radially into the 475 mm main pipe and placed centrally by means of four pin centralizers in three places viz. the 475mm pipe flange,the 250 mm pipe flange and the 80 mm discharge flange as shown in P.2a,P.2b,P.2c and P.2d. These centralizers are at 75mm and 19mm apart. The purpose of these centralizers is to place the central nozzle along the central axis of the 80 mm nozzle. In between the centralizers 100 mm PVC pipe of 520 mm length is placed and it is connected to the inlet through 62mmx100mm diffuser and its outlet is connected to 42 mm central nozzle through 100mmx42mm reducer. The 100 mm PVC pipe is introduced to act as a plenum chamber. Inside this pipe two pairs of wire screens of 24x24 mesh one at the entry and other at the exit are placed. The wire screens are breaking big eddies created in the upstream producing smooth uniform flow with low levels of turbulent intensity. The flow through the central nozzle can be regulated both by controlling the inlet valve or the exit valve of the blower or by changing the pulley of the v-belt drive.

In the main flow system(Fig..4.1.1) air enters into the fan unit through the butterfly valve which controls the air flow. Air flow can also be controlled by

regulating the fan motor speed. A silencer is fitted at the discharge of the fan unit through vibration isolator to reduce both noise and vibration generated at the fan. Flow from the silencer enters to the first settling chamber through a diffuser. At the discharge side of this chamber there is a flow straightner and wire screen of 12 mesh to straighten the flow as well as to breakdown large eddies generated at the fan discharge. Settled air from this chamber flows to the second settling chamber through a nozzle and the second diffuser. The flow straightner and wire screens are also used here for ensuring axial flow, free of large eddies which may be present in the upstream side of the flow. Flow from the second settling chamber enters into the 80 mm circular nozzle of 100 mm length.

The whole set up is mounted on rigid frames made of M.S. pipes and plates and these frames are securely fixed with the ground so that any possible unwanted vibration of the system may be reduced to a minimum.

In the experiment, three nozzles of the same length(100 mm) but of different inner diameter such as 80, 63 and 52.5 mm (Fig.4.1.3 and P.3) are used. The inner diameter of the central nozzle is kept constant(42 mm). The resulting area ratios are 2.61,1.25 and 0.56.

4.2 Co-Ordinate System

In the present investigation nozzle exit center is chosen as the origin. The centerline of the nozzle in the direction of flow is taken as positive x-axis and radial distance pointing upwards as positive y-axis and the axis 90^0 anticlockwise looking from positive y-axis as the positive z-axis(Fig.4.2.1).

4.3 Traversing Mechanism and Probe Settings

The pitot static tube is traversed in the air stream with the help of a Mitutoyo(Japan)coordinate measuring machine(Type CS 652)with ranges X co-ordinate 800 mm, Y co-ordinate 500 mm and Z co-ordinate 400 mm. The probe

traverse is made by rotating the respective wheels through rack and pinion arrangement in each axis. A position can be fixed with resolutions of 0.01 mm with the help of the wheel driving the rack and pinion mechanism and this can be read in the dial gauge.

To minimize the effect of any boundary on the jet flow, the nozzle centerline is set at 1400 mm above the ground and the traversing mechanism is placed on a hydraulically operated table designed for the purpose. The table is also placed 900 mm away from the nozzle axis to avoid any possible disturbance. The table top can be moved up and down hydraulically and is mounted on two 4500 mm long V-shaped rails and wheels. The rails are placed parallel to the nozzle axis. Thus the table with the traversing mechanism can move along the jet in axial direction through a distance of 4500 mm. The parallelism of both the axes is secured with the help of plumb bob and cathetometer. The measuring probe is mounted on the z-arm of the traversing mechanism and can be placed in the centerline of the nozzle from the side by moving the z-arm. The probe could be moved in the x and y-axis direction by moving the z-arm in the x and y directions respectively. In the case of further movement of the probe in the axial direction the whole table could be moved on the rail by rotating the lead screw made for the purpose.

Great care is taken to set the probe as correctly as possible with respect to the flow direction and centerline of the nozzle. The base of the coordinate measuring machine is kept parallel to the centerline of the circular jet facility and kept horizontal with the help of high precision spirit level, plum bob and cathetometer.The alignment of coordinate measuring machine is necessary to ensure correct axial and cross movement of the probe.

4.4 **Velocity Measurement**

The mean velocities are measured by United Sensor (USA)pitot static tube of 1.6mm outside diameter with a Furnace Control Ltd.(UK) pressure

transducer(Model MDC FC001)with data logger(Cathley,USA) and computer(Fig.4.4).The pressure signals of the pitot static tube are transmitted to pressure transducer through a 1.4 mm bore flexible plastic tube. The signal of the pressure transducer corresponds to the velocity head of the pitot static tube. The velocity from the pitot static tube signal is expressed by $U^2=2(P_0-P_s)/\rho$, where P_0 and P_s are the stagnation and static pressures respectively. Before starting the experiment, the output voltage of the pressure transducer for its different range of scale is calibrated with an inclined tube manometer(Appendix B.2.1).

4.5 Data Analysis and Calculation Technique

In presenting measurement points all distances are non-dimensionalized by central nozzle exit diameter d and axial distance x while the velocities are made non dimensional by exit centerline velocity at the origin U_{co}. All raw data found from data logger in volt are converted to velocity(m/s) by calibration equation and all measurements are carried out for inner velocity U_{co} ranging from 3.89 m/s to 14.86 m/s with corresponding Reynolds number, Re_d ranging from $1.04x10^4$ to $4.0x10^4$.

The computer programming (Excel) is used for working with parameters extracted from the data logger.

CHAPTER 5: RESULTS AND DISCUSSIONS

5.1 General

Analysis of velocity profiles of co-axial jets along with those of single jets are the main theme of the present research. Flow characteristics of coaxial jet flow are investigated by varying the velocity ratio of the annular jet and the jet issuing from the inner nozzle, as well as the area ratio of the annular to inner nozzle respectively. Four values of velocity ratios(U_2/U_1) are used in each coaxial nozzle configuration.Values are in the range $0.10<U_2/U_1<0.90$.The values of area ratios(A_2/A_1) are 2.61,1.25 and 0.56. The Reynolds number is calculated on the basis of velocity of the inner nozzle at the exit plane and the dia of the inner nozzle.

For comparing the results of co-axial jet with that of single jet, two circular jets issuing from nozzles of dia 80 mm and 42 mm with velocities of 10 m/s and 13.76 m/s respectively are studied individually. The corresponding Reynolds numbers are $5.3x10^4$ and $3.7x10^4$.

5.2 Exit Velocity

A comparison between the exit velocity profile of co-axial jet and that of single jet is made in Fig.5.2.1. For single jet, at the exit, the potential core should extend up to y/d=0.5. But the measurement shows the effect of the existence of the nozzle boundary at y/d =0.45 from where velocity starts to decrease sharply as shown in the figure. In the case of co-axial jet, due to existence of annular jet, the potential core at the exit is reduced to y/d =0.42 from 0.45. y/d =0.5 to 0.583 is the zone behind the wall thickness of the inner nozzle where wake forms both due to inner and annular jets and in this zone the velocity is minimum. Potential core of the annular jet exists from y/d =0.65 to 0.90 around the mean radius of the annular jet. The outer boundary layer(y/d =0.9 to 0.97) of the annular jet is found to be thicker

than that of the inner one(y/d =0.55 to 0.60). This difference of thickness is due to the fact that the outer one is under the influence of concave surface which gives the compressive action on the fluid thereby increasing the resistance to the flow and hence increases the thickness of the boundary layer. On the contrary, the inner one has a convex surface giving the expanding action on the fluid which gives less resistance to the flow thereby decreasing the thickness of the boundary layer. After reaching the outer wall, the velocity decreases asymptotically to zero.

Effects of Reynolds number on exit velocity profiles of co-axial jets at different velocity ratios are presented in Figs 5.2.2, 5.2.3,5.2.4 and 5.2.5. The profiles seem to be identical for inner jet but for annular jet, the profiles provide higher values for lower Reynolds number at velocity ratios 0.12,0.37 0.75&0.90.The velocity of the inner jet shows the usual potential core as found in normal jets but that of annular jet shows the point of inflection near its central zone. This may be due to the effect of asymmetrical wall boundary(concave-outer and convex-inner). Higher velocity field is noticed near the outer wall of the annular jet than the inner wall. This tendency of unequal distribution of velocity increases with the increase of velocity ratio.

Effects of velocity ratios at different Reynolds number and at different area ratios are shown in Figs. 5.2.6,5.2.7 and 5.2.8. From Fig.5.2.6, it is found that with the increase of velocity ratio, the nature of the central jet velocity profile is changed from saddle shape to parabolic form. Therefore, near the central nozzle boundary, velocity decreases with the increase of velocity ratio. For, annular jet, with the increase of velocity ratio, the profile is converted to asymmetric shape from its symmetric nature i.e. as the velocity ratio increases, the velocity towards the outer wall increases relative to its inner wall. This may be the consequence of differential curvature effect of the nozzle as discussed before. Same configuration

is observed in Fig.5.2.7 for area ratio 1.25 but the curvature effect is less due to small annular space.

Effect of area ratios on exit velocity profiles at different velocity ratios and at Re= $4x10^4$ are shown in Figs. 5.2.9, 5.2.10, 5.2.11 and 5.2.12. For velocity ratio 0.10 and 0.25 the effect of area ratio for central jet is zero. But Fig.5.2.11 for velocity ratio 0.60 shows that with the increase of area ratio the nature of velocity profile of the central jet changes near the inner nozzle boundary. There, the velocity decreases thereby decreasing the potential core region. Near the outer wall boundary, the velocity decreases asymptotically to its zero value.

5.3 Centerline Velocity

The centerline of a jet is the fundamental axis. Different important aspects of jet flow such as, potential core length, virtual origin etc. can be identified from the flow characteristics along this axis. The parameter used in this experiment is U_c/U_{co}.

The centerline velocity profiles of co-axial jets of varying area and velocity ratios are presented in Figs 5.3.1,5.3.2,5.3.3 and 5.3.4 at Reynolds number=$4x10^4$. In Fig 5.3.1 (for velocity ratio=0.10) from the regular decay of centerline velocity the potential core length can be determined as $4d<L_p<5d$, $5d<L_p<5.5d$ and 7d for area ratios 0.56,1.25 and 2.61 respectively. In the same way, the potential core length for the other velocity ratios can be worked out. For all area ratios,the deceleration of the exit centerline velocity is noticed up to x/d=1.0(about 3%, 2% and 1% of its exit value for A_2/A_1= 2.61,1.25 and 0.56 respectively) beyond which acceleration is observed up to the end of potential core. After the potential core, the centerline velocity decreases monotonically in the stream wise direction to zero value far away from the nozzle exit. In Fig.5.3.5 potential core length is plotted against velocity ratios for different area ratios. It is observed that, for a certain velocity

ratio the length of potential core increases with increase in area ratio. But potential core length remains more or less constant for different velocity ratios.

Centerline velocity profiles of co-axial jets of area ratio=2.61 and velocity ratio=0.12 at two different Reynolds number are presented in Fig.5.3.6. Almost the same length of potential core (x/d~7) can be identified for the two Reynolds number. But according to the previous researchers [12,13,24] length of potential core increases with the increase of Reynolds number. This is because the Reynolds numbers which are chosen for the present study have values very close to each other. So their effect on potential core can not be identified.

Deceleration of the exit centerline velocity is observed upto x/d=1.0(about 2.6% and 1% of its exit value for Re=$2.69\text{x}10^4$ and $3.77\text{x}10^4$ respectively) beyond which acceleration is occurred upto the end of the potential core. Beyond the end of the potential core, the centerline velocity is found to decrease in the same rate of Islam[12], and others[13,24].

A comparison between the centerline velocity profile of coaxial jets with that of single jet has been made in Fig.5.3.7. Higher potential core length (L_p=7d) is observed for coaxial jets than that of single jet(L_p=4d).

5.4 **Streamwise Mean Velocity**

The streamwise velocity profiles are the basic and most important flow parameters which show the mixing behaviour, entrainment of the surrounding fluid and hence the resulting flow pattern.

Figs 5.4.1 and 5.4.2 show the streamwise velocity profiles of two single jets of two different diameters and at two different Reynolds numbers. The profiles of both the jets are found to be saddle shaped in the mixing region near the exit but with different degree of buldging. The saddle shape nature is prominent in the profiles

of 80 mm jet while the traces of this behaviour are noticed in the velocity profiles of 42mm jet. This nature of profile is found in the work of previous researchers[12,13].According to their hypothesis, the saddle shape nature of the velocity profiles is due to the superposition of the induced velocity of vortex rings surrounding the jet upon a uniform mean streamwise velocity. In the small diameter jet the size of vortex rings formed at the shear layer may be small due to high curvature of the jet boundary. As the energy containing eddies of the small vortices are much less than those of large vortices, their effect on mean velocity profile becomes negligible in reshaping the velocity profiles of the jet.The static pressure within the jet may also play a vital role in the formation of these profiles. This saddle shaped nature of the profiles seem to disappear beyond the potential core.

Fig 5.4.3 is presented to show the effects of Reynolds number on the saddle shaped nature of the velocity profiles at x/d=1.00, 2.00 and 5.00. From the figures, it is seen that peak values of the profiles are the same at all axial locations and are equal to the centerline velocity for lower Reynolds number. But for higher Reynolds number, the maximum peak occurs at x/d=1.0 and its value is found to be 1.78% higher than the corresponding local centerline value. But the results are not consistent with those of Islam[12] who showed that the magnitude of the peak decreases and its location shifts upstream close to the exit with the increase of Reynolds numbers. He also concluded that the profiles have little Reynolds number effect on its nature. In the present investigation the profiles show that the spread rate of jet increases at higher Reynolds number indicating accelerated mixing.

Stream wise velocity profiles for co-axial jets for area ratio=2.61 at different velocity ratio are presented in Figs 5.4.4, 5.4.5 and 5.4.6. Fig 5.4.4 shows clearly the existence of central jet and annular jet near the exit(at x/d=1.0 and 2.0). After

the outer annular jet, the profiles decrease monotonically to its zero value in the boundary. Beyond x/d=2.0 the intermixing of central and annular jet takes place in such a way that no separate existence of the jets can be identified. The combined effect of the jets acts as a resultant single jet. From Figs 5.4.4, 5.4.5 and 5.4.6 it is evident that as the velocity ratio(U_2/U_1) decreases the effect of annular jet on the velocity profile of central jet decreases almost linearly.

The effect of annular jet is noticed upto x/d=3.0 for U_2/U_1=0.75 (Fig.5.4.4), upto x/d=2.0 for U_2/U_1=0.37(Fig.5.4.5)and upto x/d=1.0 for U_2/U_1=0.12(Fig.5.4.6) and after these respective positions the velocity profiles of the co-axial jet take the form of unified single jet confirming the completion of mixing of the two jet flows.

Fig 5.4.7 shows the effect of velocity ratio on the streamwise velocity profiles of co-axial jet of area ratio 2.61.In the figure three groups of curves for three axial locations(x/d=1,2&5)are shown. It is seen that the degree of influence of annular jet on the overall velocity profile decreases in the streamwise direction as well as with the decrease of velocity ratio. It is clear from the figure that the presence of annular jet shifts the combine velocity profile in the rightward direction. The profiles for all velocity ratios are similar but shift in rightward with the increase of velocity ratio.

Fig 5.4.8 shows the effects of Reynolds number on stream wise velocity profile of co-axial jets for A_2/A_1=2.61 and U_2/U_1=0.75. Reynolds number effect is found to be prominent near the exit (at x/d=1.0 and x/d=2.0),which shows that for the same velocity ratio the velocity profile deviate more from that of a single jet with the increase of Reynolds number but at x/d=5.0 the effect of Reynolds number on velocity profile becomes negligible.

Stream wise velocity profiles for the area ratios(1.25 and 0.56) are also shown in Figs. 5.4.9 and 5.4.10. With the decrease of area ratio the width of the annular jet decreases resulting in reduced mass flow rate through the annular jet comparing with that through the central jet. Due to the decreasing momentum flux the influence of annular jet on the velocity profile of the central jet decreases with the decrease of area ratio as seen in Figure 5.4.11

5.5 **Spread of the Shear Layer**:

The shear layer of the free jets is bounded by iso-velocity lines of U/U_{co} values 0.10 and 0.95. The variation of shear layer width, b with downstream distance is the manifestation of spread rate of the shear layer.

Spread rate of Iso-velocity lines of co-axial jet and single jet is compared in Fig. 5.5.1. It is found that value of outer layer($y_{0.1}/d$) of co-axial jet is greater than that of the single jet near the exit($x/d<3$) but it falls behind the single jet with the increase of downstream distance. But for inner edge($y_{0.95}/d$) the opposite result is observed. Near the half width, the co-axial and the single jet have almost the same configurations. It is also observed that within $x/d\sim6$ the iso-velocity lines are almost linear.

Reynolds number effect on iso-velocity lines for area ratio=2.61 is shown in Fig 5.5.2. Reynolds number effect is found to be negligible at the central zone but near the periphery spread rate is much more at lower Reynolds number. This is due to more viscous effect than the inertia effect of the flowing fluid particle.

Fig 5.5.3 shows the effect of area ratio at $Re=4x10^4$ on iso-velocity lines and it is found that all the iso-velocity lines spread outward in the stream wise direction. This spread rate is more with $A_2/A_1=0.56$ than that for $A_2/A_1=1.25$.

Shear layer width of co-axial jet is compared with that of the single jet in Fig. 5.5.4. Shear layer width, in the initial region($x/d \leq 6$)varies linearly having db/dx values of 0.0944 and 0.1376 for co-axial and single jets respectively.

Reynolds number effect and area ratio effects on the shear layer width, b, are presented in Fig.5.5.5 and 5.5.6.Initially (upto $x/d \leq 4$), the shear layer width varies linearly. db/dx values of 0.0739 and 0.166 are worked out for $Re=2.69 \times 10^4$ and 1.88×10^4 respectively. Again, for area ratios of 0.56 and 1.25 db/dx =0.1658 and 0.0914 respectively for $Re=4 \times 10^4$. Thus, it can be said that the shear layer width for co-axial jets decreases with increase of Reynolds number and decreases with increase in area ratio.

5.6 **Self-preservation Profiles**:

Actual self-preservation zone of a jet is occurred when all of its mean and turbulent components are in equilibrium, which is in the fully developed region of a jet. Another self-preservation is also observed which is within the potential core region called partial self-preservation region. The self-preservation variable for mean velocity taken in the present study is $(y-y_{0.5})/x$ which was also taken by Islam[10] for partial self-preservation.

Self-preservation profiles of velocity for 42 mmD jet is shown in Fig.5.6.1 while those for co-axial jets of $A_2/A_1=2.61$ at various velocity ratios(U_2/U_1) are shown in Figures 5.6.2, 5.6.3 and 5.6.4 respectively. The velocity profiles are found self-preserving in the region x/d=0.50 to 9.0 for 42 mmD jet. Reduced self-preservation regions for co-axial jets of $A_2/A_1=2.61$ are found for larger velocity ratios.

Self-preservation regions for other area ratios(1.25 and 0.56) are provided in Figs. 5.6.5 and 5.6.6 for a certain velocity ratio($U_2/U_1=0.75$).The self-preservation

regions are identified as x/d= 2 to 11 and x/d=1 to 8 for A_2/A_1=1.25 and 0.56 respectively.

CHAPTER 6: CONCLUSIONS AND RECOMMENDATIONS

6.1 Conclusions

Experimental investigations are performed to study the effect of velocity ratios, area ratios and in some cases the effect of Reynolds number on the velocity distribution of coaxial free jets. From the measurements and subsequent analysis of the data and curves the following conclusions may be drawn:

1. Due to the presence of annular jet the potential core of coaxial jets at the exit is decreased in comparison to single jet.
2. At higher velocity ratio, velocity of central jet at the exit plane decreases earlier. But for annular jet, as the velocity ratio increases the velocity towards the outer wall increases.
3. Effect of area ratio on exit velocity profile of central jet is negligible for velocity ratio =0.10 and 0.25but for velocity ratio=0.60 and 0.75 the velocity of the higher area ratio starts to decrease earlier.
4. The centerline velocity near the exit decreases just after the discharge and then it is increased to its exit value at the end of potential core before starting its normal decay in downstream direction.
5. Length of potential core increases with the increase of area ratio at a certain velocity ratio.
6. Beyond the potential core the decay rate of centerline velocity is decreased with the decrease of area ratio and with the increase of Reynolds number.
7. The stream wise velocity profiles for the single jets exhibits saddle shape behaviour which are seemed to disappear at the end of potential core.
8. The mixing of coaxial jets takes place earlier in coaxial jets with lower velocity ratios.
9. Smaller area ratios provide earlier mixing.
10. Shear layer width for coaxial jets decreases with increase in Reynolds number and area ratio prominantly.

11. Self-preservation of velocity profiles comes much earlier in single jet than in coaxial jets. For coaxial jets, lower velocity ratio and lower area ratio present self-preservation region earlier.

6.2 Recommendations

The present study is a preliminary work on coaxial free jets. The research can be modified and extended in a diversified way. The following suggestions can be made for future work on this topic:

1. Same measurements can be made for other values of area ratios. The area ratios can be varied by keeping the diameter of the outer nozzle constant while varying the diameter of the inner nozzle.
2. Higher values of velocity ratios of annular to inner jet can be used for the same measurements.
3. Static Pressure distribution can be obtained for the same configurations.
4. To perceive the flow structure of the coaxial jets more clearly some important parameters like longitudinal turbulent intensity, transverse turbulent intensity, turbulence shear stress can be measured. Constant temperature hot wire anemometer can be used for this purpose.
5. Computerized data acquisition technique can be applied for statistical calculations.
6. Flow visualization technique can be used to have a vivid picture of the mixing zone of coaxial jets.
7. All the above measurements can be taken under controllable upstream acoustic excitation.
8. Swirl velocity can be added to jets to study the effect of swirl.

APPENDIX A: MEAN PRESSURE AND VELOCITY MEASUREMENT

A.1 Pressure Probes

In the field of aeronautics, modern technology has provided different new pressure probe technique for the investigation of flow of air and other gases. There are a number of pressure probes varying in size and geometry for serving different purpose and for simultaneously measured flow quantities. However the all work on the distribution of pressure which prevails around the probe when it is immersed in a moving fluid. These pressure variation depend mainly on wind speed and direction so that with suitable chosen body shape and location of pressure holes, a probe may be calibrated in a known wind stream. The design of certain probes involving simple shapes such as cylindrical or spherical, can based on certain theory, but the final design usually becomes a compromise aimed at minimizing the effect of some factors such as Reynolds number, Mach number and turbulence.

General features which are desirable in probe selection for the measurement of flow quantities at a certain point can be summarized as follows:

i) Small size offering a minimum disturbance to the flow,

ii) Rapid response

iii) Robust and simple construction

iv) Calibration both infrequent and unaffected by flow conditions

v) All measurements close to one point

For steady incompressible flow the change of velocity head is accompanied by equal and opposite change in static head. This relationship between pressure and velocity in the flow field is widely used in flow measurement and this can be written as

$\frac{1}{2} \rho U^2 + P_s = \text{Constant} = h_0$

where, U velocity of the undisturbed stream,

ρ fluid density

P_s Static Pressure

h_o Total Pressure.

Where the kinetic pressure [½ ρU^2] can be determined directly by measuring (h_0-P_s). For determining the velocity U, to determine density, absolute pressure and temperature of the flow field at that location were needed.

A.2 Measurement of Total and Static Pressure

Total pressure is defined as the pressure attained when the fluid is brought to rest adiabatically.In practice a stagnation point can be created by introducing an obstacle into the moving fluid perpendicular to the flow direction. The pressure at such a point is referred to as the stagnation pressure. This is not necessarily equal to the total pressure of the undisturbed flow.

To disturb the flow least an obstacle is created by aligning a cylindrical tube with the flow. A pressure tapping is provided at the end facing the flow and the tube is usually bent through a right angle at some distance downstream to form a "stem". Various geometrical shapes are used for "nose" or "head" of total pressure tubes and may be square ended, hemispherical, ellipsoidal etc. Total pressure tubes of these types are usually referred to as pitot tubes, after Henri Pitot, who described such an instrument in 1732 for measuring speeds of water flow; the term impact tube is also used, mainly in America. A simplest type of total pressure or pitot tube is shown in Fig.A2.1

Some special form of stationary probe is generally employed for measuring the static pressure in a moving fluid. The pressure on the surface of a body in moving stream varies from point to point in a manner which is determined largely by the shape of the body and its orientation to the flow direction. Probe shape is generally dictated by consideration of ease of construction and reduction of interference with the flow to be measured; given by a suitable shape, the orifices are then

located where the surface pressure is equal or related in a known manner, to the static pressure of the undisturbed flow. In order to reduce errors due to the misalignment with the flow, it is usual to provide several orifices around the probe which inter communicate inside the instrument, so that a mean pressure is recorded. The simplest type of static pressure probe consists of a cylindrical shape with its axis aligned with the flow.

A.3 Measurement of Mean Velocity

For measurement of mean velocity the quantities to use most conveniently are total pressure h_0, static pressure P_s and temperature T. In incompressible flow the pressure difference (h_0-P_s) is equal to $[\frac{1}{2} \rho U^2]$; in compressible flow the pressure ratio (h_0/P_s) determines Mach number M_a. h_o and P_s is measured at the same time by using pitot-static tube. The pitot static tube consists of a static pressure tube which has been provided with an addition of orifice at the nose for measuring stagnation pressure as shown in Fig.A.3.1. It is easily constructed of two concentric tubes, which are connected to some form of manometer so that h_0, P_s, (h_0-P_s) or (h_0/P_s) can be measured as required. Various geometric shapes are used for the head, particularly hemispherical, ellipsoidal and special shapes for supersonic tapping. The design principles of pitot static combination are the same as for pitot and static tube used separately; the pitot orifice presents no special problems and does not appreciably affect the reading of the static pressure reading. For a given size of pitot orifice, however, a combination probe is necessarily of greater extent than seperate pitot and static tubes; thes considerations are importatnt in the exploration of the finer structure of a given flow field, in supersonic flow, and in regions where the flow conditions vary rapidly. Despite these limitations, the pitot static tube has one major advantage over nearly all other pressure probes; it can give a high degree of accuracy without prior calibration provided that it is used in a subsonic uniform flow and is made to specified

dimensions. In incompressible flow a combination factor K is used for a pitot static tube by the equation

$P_0-P_s = K \frac{1}{2} \rho U^2$

Where P_o denotes the reading given by the pitot orifice and P_s is that of the static pressure of the instrument. For standard designs with hemispherical, ellipsoidal or tapered conical heads, when correctly aligned with the flow, a value of K of unity gives the wind speed exactly to $\frac{1}{2} \rho U^2$ within 0.5% error. This conclusion is based on tests on tubes of 7.9 mm external diameter in air at normal atmospheric conditions and appears to be valid at least over the range of wind speeds from 6 to 60m/s[4]

APPENDIX-B: CALIBRATION PROCEDURE

B.1 Different Types of Pressure Transducer

Pressure transducers replace the conventional liquid column manometer used for pressure measurements. Pressure transducer converts the pressure into some equivalent electrical signals. Transducer's electronic circuits respond to pressure variations by the change of some resistance, capacitance or inductance which is recorded in the form of voltage or current. The magnitude of the pressure is obtained from the calibrated pattern of the output signal of the transducer.

A pressure transducer is basically constructed of two closed chambers separated by a common diaphragm. A pressure differential created between the chambers deflect the diaphragm. The deflection or strain thus produced is used to generate a suitable output signal.

In the electrical resistance type pressure transducer, a strain gage is fitted to the diaphragm to sense the pressure. The corresponding change in resistance in the gage due to the strain in the diaphragm is recorded by a galvanometer through the use of a wheatstone type of bridge, which gives the information about the applied pressure.

The deflection of the diaphragm is used to impact on a magnetic core, in the inductance type pressure transducer. Here the device consists of a primary and secondary coil. An alternating input voltage is impressed upon in the primary coil. The output voltage of the secondary coil depends on the inductive coupling between the core and the coils, which is, in turn dependent on the relative position of the coils. Thus, the output voltage gives an indication of pressure applied at the diaphragm.

In the capacitance type pressure transducer, the deflection of the diaphragm is utilized to vary a close space thus to cause the change in capacitance in a circuit. The capacitor's response is picked up by a suitable output device via a suitable bridge

circuit, giving a measure of the pressure. In the present experiment capacitance type pressure transducer is used.

B.2 Calibration of Pressure Transducer:

In the present investigation capacitor type pressure transducer (Furnace Control, UK.) is used for sensing attenuating and conditioning the pressure signals obtained from the pitot-static tube placed in the flow field of the co-axial jet. The transducer has the full range of 0 mm of H_2O to 1000 mm of H_2O in 5 steps viz 1%, 3%, 10%, 30% and 100%. The transducer has a dial gauge from where pressure can be read directly in mm of H_2O. The transducer also has the output voltage signal proportional to the pressure difference. For all the five pressure ranges the output signal gives 1 volt for full scale deflection. For calibration purpose this output signal is recorded against basic inclined tube liquid manometer deflection for different pressure ranges.

The calibration setup of the pressure transducer is shown schematically in (Fig. B.2.1). The transducer has two pressure ports one is marked 'H'(high) and other is 'L'(low). The 'H' pressure port of the transducer and the positive line of the inclined tube manometer is connected in parallel to the air chamber. The 'L' pressure port of the transducer and the negative line of the manometer are kept open to the atmosphere. The output of the transducer is connected to the data logger. The air chamber is meant to maintain desired air pressure. The air chamber is also connected to a below type rubber pump used in the blood pressure equipment.

For calibration purpose the desired air pressure is generated in air chamber. The pressure in the air chamber can be controlled accurately by the discharge controlling valve of the rubber pump. Both the data logger and the transducer are switched on at least half an hour before starting the calibration to stabilize the electronic circuits. During calibration desired pressure is generated in the air chamber and both the

output signal of the transducer and the manometer reading are recorded. In this way sufficient number of readings are taken until the full scale deflection of the transducer is obtained for each five pressure ranges. After data is taken these are plotted and calibration curves are obtained as shown in (Fig.B.2.2).During experiment these curves are used to analyze the pitot-static tube signals to find the velocity of the jet.

APPENDIX-C: UNCERTAINTY ANALYSIS

C.1 General

The term "uncertainty" is used to refer to a possible value that an error may have. Kline and McClintock [12] attributed this definition and it still seems an appropriate and valuable concept. In the single-sample measurement, proposed by Thasher and Binder,[23]the experimenter describes the uncertainty of his measurement in terms of what he believes would happen if the measurements are repeated a large number of times. In this way one can estimate the standard error and the uncertainty interval and can give odds that the error would be less than that of the uncertainty interval if the measurements are repeated a large number of times. The reliability of a result described in this manner is indicated by the size of the uncertainty interval and the magnitude of the odds.

This chapter is devoted to determine the interval around each measured parameter within which it's true value is believed to lie. The analysis is aimed to estimate the amount of uncertainties in individual measurements. An uncertainty estimate is only as good as the equations it is based on. If those equations are incomplete and do not acknowledge all the significant factors that affect the result, then the analysis will either underestimate or overestimate the uncertainty in the results. In the present experiment the uncertainty of measurement of velocity and static pressure are influenced by variation of ambient temperature, pressure, specific gravity of manometric fluid, gas constant and the angle of inclination of the sensing probe to the mean flow direction.

C.2 Basic Mathematics

In this experiment, each test point is run only once, and hence they are single sample experiment. A precise method of single sample uncertainty analysis has been described in the engineering literature by the work of Kline and McClintock

[12] If a variable X_1, has a known uncertainty G_1, then the form of representing this variable and its uncertainty is,

$$X_1 = X_1 \text{ (measured)} \pm G_1 \qquad \text{C.2.1}$$

This statement should be interpreted to mean the following:

i. The best estimate of X_1 is X_1 (measured).

ii. There is an uncertainty in X_1 that may be as large as $\pm G_1$.

It is important to note that such specification can only be made by the experimenter based on the total laboratory experience. For example, a set of measurements is made and the uncertainty in each measurement may be expressed with the same odds. These measurements are then used to calculate some desired result R using the independent variables $X_1, X_2, X_3, \ldots\ldots\ldots X_m$,

$$\text{Where, } R = R(X_1, X_2, X_3, \ldots\ldots\ldots X_m) \qquad \text{C.2.2}$$

Let, $G_1, G_2, G_3, \ldots\ldots G_m$, be the uncertainties in the independent variables given with the same odds. Then the uncertainty G_R in the result having these odds is given in Kline and McClintock [12] as,

$$G_R = \left[\left(\frac{\partial R}{\partial X_1} G_1 \right)^2 + \left(\frac{\partial R}{\partial X_2} G_2 \right)^2 + ----+ \left(\frac{\partial R}{\partial X_m} G_m \right)^2 \right]^{1/2} \qquad \text{C2.3}$$

where, the partial derivative of R with respect to X_i is the sensibility coefficient for the result R with respect to the measurement X_i [i = 1, 2, ... m]. In most situations, the overall uncertainty in a given result is dominated by only a few of its terms. Terms in the uncertainty equation that are smaller than the largest term by a factor of 3 or more can usually be ignored. This is a natural consequence of the Root-Sum-Square (RSS) combination: Small terms have very small effects. Sometimes the estimate is wanted as a fraction of reading, rather than in

engineering units. While this can always be calculated using equation Eq^n.C.2.3. It is also possible to do the calculation of relative uncertainty directly. In particular, whenever the equation describing the result is a pure product form such as equation Eq^n.C.2.3, then the relative uncertainty can be found directly. That is, if

$$R = X_1^{\,a} X_2^{\,b} X_3^{\,c} \text{ ---------- } X_m^{\,n} \qquad \text{C.2.4}$$

$$\text{then,} \quad \frac{G_R}{R} = \left[\left(a\frac{G_1}{X_1} \right)^2 + \left(b\frac{G_2}{X_2} \right)^2 + \text{-----} + \left(n\frac{G_m}{X_m} \right)^2 \right]^{1/2} \qquad \text{C.2.5}$$

C.3 Uncertainty for Velocity Measurement

Let an air stream of density ρ_a (kg/m^3) flow with a velocity U (m/sec). A pitot-static tube is placed parallel to the flow, and the dynamic head is measured by a micro volt meter in millivolt corresponding manometer reading h (mm water). Let the density of the liquid used in the manometer be ρ_1 (kg/m^3).

$$\text{So,} \quad \frac{1}{2}\rho_a U^2 = h\rho_1 g \qquad \text{C.3.1}$$

$$\text{or,} \quad U^2 = 2\left(\frac{\rho_1}{\rho_a}\right) hg$$

$$\text{or,} \quad U = \sqrt{2g\left(\frac{\rho_1}{\rho_a}\right) h}$$

$$\text{or,} \quad U = \sqrt{2g\left(\frac{\gamma_1}{\gamma_a}\right) h} \qquad \text{C.3.2}$$

where γ_1, γ_w and γ_a are the specific weights (kgf/m^3) of the liquid, water and air respectively. Suppose the sensing point of the pitot-static tube is deviated by an angle β from the direction of flow due to wrong adjustment. Then the measured velocity will be given

$$U = \sqrt{2g\left(\frac{\gamma_1}{\gamma_a}\right) h \cos\beta} \qquad \text{C.3.3}$$

$$U = \sqrt{\left(\frac{2g\gamma_w sh}{\gamma_a}\right)\cos\beta} \qquad \text{C.3.4}$$

where, s is the specific gravity of the manometer liquid.

$$U = \sqrt{2\frac{\gamma_w}{\gamma_a}}\sqrt{s\,h}\cos\beta$$

$$U = C\sqrt{s\,g\,h}\cos\beta \qquad \text{C.3.5}$$

where, $C = \sqrt{2\frac{\gamma_w}{\gamma_a}}$ C.3.6

Let us now differentiate both the sides of equation C.3.5 with respect to s, g, h and β respectively.

$$\frac{\partial U}{\partial s} = \frac{C}{2}(s\,g\,h)^{-1/2} h\,g\cos\beta = \frac{C}{2}\sqrt{\frac{hg}{s}}\cos\beta \qquad \text{C.3.7}$$

$$\frac{\partial U}{\partial g} = \frac{C}{2}(s\,g\,h)^{-1/2} s\,h\cos\beta = \frac{C}{2}\sqrt{\frac{sh}{g}}\cos\beta \qquad \text{C.3.8}$$

$$\frac{\partial U}{\partial h} = \frac{C}{2}(s\,g\,h)^{-1/2} s\,g\cos\beta = \frac{C}{2}\sqrt{\frac{sg}{h}}\cos\beta \qquad \text{C.3.9}$$

$$\frac{\partial U}{\partial \beta} = C\sqrt{sgh}(-\sin\beta) = -C\sqrt{sgh}\,\sin\beta \qquad \text{C.3.10}$$

Let G_U be the uncertainty in the result, and G_s, G_g, G_h and G_β be the uncertainties in the specific gravity of manometric fluid, acceleration due to gravity, transducer reading and angle of deviation of the sensing probe respectively.

So, $$G_U = \left[\left(\frac{\partial U}{\partial s}G_s\right)^2 + \left(\frac{\partial U}{\partial g}G_g\right)^2 + \left(\frac{\partial U}{\partial h}G_h\right)^2 + \left(\frac{\partial U}{\partial \beta}G_\beta\right)^2\right]^{1/2} \qquad \text{C.3.11}$$

Combining equation Eq^n.C.3.7 to C.3.10 and Eq^n.C3.11

$$G_U = \left[\frac{C^2}{4}\frac{hg}{s}\cos^2\beta\, G_s^{\,2} + \frac{C^2}{4}\frac{sh}{g}\cos^2\beta\, G_g^{\,2}\right.$$

$$\left. + \frac{C^2}{4}\frac{sg}{h}\cos^2\beta\, G_h^{\,2} + C^2 hgs\sin^2\beta\, G_\beta^{\,2}\right]^{1/2} \qquad \text{C.3.12}$$

$$G_U = \left[\frac{C^2}{4}\cos^2\beta\frac{hg}{s}G_s^{\,2} + \frac{sh}{g}G_g^{\,2} + \frac{sg}{h}G_h^{\,2} + 4hgs\tan^2\beta\, G\beta^2\right]^{1/2} \quad \text{C.3.13}$$

$$G_U = \frac{C\cos\beta}{2}\left[\frac{hg}{s}G_s^{\,2} + \frac{sh}{g}G_g^{\,2} + \frac{sg}{h}G_h^{\,2} + 4hgs\tan^2\beta\, G\beta^2\right]^{1/2} \quad \text{C.3.14}$$

Combining equation C.3.5 and C.3.14

$$\frac{G_U}{U} = \frac{1}{2}\left[\frac{G_s^2}{s^2} + \frac{G_g^2}{g^2} + \frac{G_h^2}{h^2} + 4G_\beta^{\,2}\tan 2\beta\right]^{1/2} \quad \text{C.3.15}$$

Putting for Room temperature 28°C and pressure 76 cm hg.

$s = 0.79 \pm 0.005$

$g = 980.6 \pm 1.0$ cm/s^2

$h = 22.735 \pm 0.099$ mm

and $\theta = 0 \pm 3^\circ$

so, $$\frac{G_U}{U} = \frac{1}{2}\left[\left(\frac{0.005}{0.79}\right)^2 + \left(\frac{1.0}{9.81}\right)^2 + \left(\frac{0.099}{22.735}\right)^2\right]$$

or, $$\frac{G_U}{U} = 0.50\%$$

C.4 Uncertainty for Reynolds number

Let Re Reynolds number

d diameter of the nozzle exit

U_e jet exit velocity

Now $$\mathrm{Re} = \frac{U_e d}{\nu} = CU_e d$$

Where $C = \frac{1}{\nu}$

Let G_{Re} G_{Ue}, and G_d be the Uncertainties in Re, U_e and d respectively.

$$U_{\mathrm{Re}} = \left[\left(\frac{\partial \mathrm{Re}}{\partial U_e}G_{Ue}\right)^2 + \left(\frac{\partial \mathrm{Re}}{\partial_d}G_d\right)^2\right]^{1/2}$$

Therefore

$$U_{\mathrm{Re}} = \left[\left(CU_e G_d\right)^2 + \left(CdG_{Ue}\right)^2\right]^{1/2}$$

or, $$G_{\mathrm{Re}} = CU_e d\left[\left(\frac{G_d}{d}\right)^2 + \left(\frac{GU_e}{Ue}\right)^2\right]^{1/2}$$

so, $$\frac{G_{\mathrm{Re}}}{\mathrm{Re}} = \left[\left(\frac{G_d}{d}\right)^2 + \left(\frac{G_{Ue}}{U_e}\right)^2\right]^{1/2}$$

Putting for room temperature 28°C and pressure 76 cm hg. d = 80.0 ± 0.5 mm.

$$\frac{G_{Ue}}{U_e} = 0.0043$$

so, $$\frac{G_{\mathrm{Re}}}{\mathrm{Re}} = \left[\left(\frac{0.5}{80.0}\right)^2 + \left(0.0043\right)^2\right]^{1/2} = 0.75\%$$

REFERENCES

1. Alpinieri, Louis J., "Turbulent Mixing of Co-axial Jets", AIAA Journal Vol.2, No.9 pp 1560-1567, 1964.
2. Au, H. and Ko, N.W.M., "Co-axial Jets of Different Mean Velocity Ratios, Part 2", Journal of Sound and Vibration,Vol. 116(3), pp 427-443, 1987.
3. Bradshaw,P., " The Effect of Initial Conditions on the Development on a Free Shear Layer", Journal of Fluid Mechanics, Vol.26, pp 225-236, 1966.
4. Bryer, D.W. and Pankhurst, R.C. " Pressure Probe Methods for Determining Wind Speed and Flow Direction", National Physical Laboratory,1971.
5. Champagne,F.H. and E.Wgnanski, I.J., "An Experimental Investigation of Coaxial Turbulent Jets", International Journal of Heat and Mass Transfer, Vol.14, pp 1445-1464, 1971.
6. Elbanna, H and Sabbagh, J.A., "Interaction of Two Non-equal Plane Parallel Jets", AIAA Journal, Vol.25,No.1, pp 12-13, 1987.
7. Forstall, W. and Shapiro,A.H., " Momentum and Mass Transfer in Coaxial Gas Jets", Journal of Applied Mechanics, Vol. 18, Trans. ASME, Vol. 73, p219, 1951,
8. Gama,B.A., "Study of the Effect of Excitation on A Circular Air Jet", MSc. Thesis, Mech. Engg. Dept., BUET, Dhaka,1993.
9. Husain, A.K.M.F. And Zedan, M.F. , " Effect of Initial Condition on the Axisymmetric Free Shear Layer: Effect of the Initial Fluctuation Level", Physics of Fluids, Vol.21, p 1475, 1978.
10. Islam, A, " Flow Characteristics in the Near Field of A Circular Splined Jet", MSc.Thesis, Mech. Engg. Dept., BUET, 1995.
11. Islam,T.,"Flow Characteristics of Unexcited and Excited Circular Wedge Shaped Jets",Ph.D. Thesis, Mech. Engg. Dept., BUET, Dhaka, 1995.

12. Kline, S.J., and Mc.-Clintock, F.A., " Describing Uncertainties in Single Sample Experiments", Mechanical Engineering, p.3, 1953.
13. Ko, N.W.M and Davis, P.O.A.L., " The Near Field within the Potential Cone of Subsonic Cold Jets", Journal of Fluid Mechanics, Vol.50, part-1, pp 49-78, 1971.
14. Ko, N.W.M and W.T. Chan, " Similarity in the Initial Region of Annular Jets: Three Configurations.", J.Fluid Mech,Vol.84,part 4,pp 641-656, 1978.
15. Ko, N.W.M. and Au.H. "Co-axial Jets of different Mean Velocity Ratios, Part 1", Journal of Sound and Vibration Vol. 100; pp 211-232, 1985.
16. Lenzo, C.S. and Dalal T.N., "Center-line Velocity Decay in Coaxial Free Jets", Journal of Applied Mechanics, Transaction of ASME, pp 514-516, June 1975.
17. Lighthill, M.J., "Jet Noise", AIAA Journal,Vol.1, No.7, pp 1507-1517, 1963.
18. Morton, B.R. , "Coaxial Turbulent Jets", International Journal of Heat and Mass Transfer,Vol.5, pp 955-965, 1962.
19. Murakami, Erina and Papamoschou, Dimitri, "Mean Flow Development in Dual Stream Compressible Jets", AIAA Journal, Vol.40,No.6 pp 1131-1138, 2002.
20. Rajaratnam,N., "Turbulent Jets", Elsevier Scientific Publishing Company, Amsterdam-Oxford-Newyork, 1976.
21. Rehab,H, Villermaux,E and Hopfinger,E.J., "Flow Regions of LargeVelocity Ratio Coaxial Jets", J.Fluid Mech,Vol 345, pp 357-381, 1997.
22. Selim, M.A., " Flow Structure of the Circular Wedge Shaped Jet", MSc. Thesis, Mech. Engg.Dept.,BUET, Dhaka,1988.
23. Thaser, L.W. and Binder, R.C. " A Practical Application of Uncertainty Calculation to Measured Data", Transactions of ASME, pp 373-376, 1957.
24. Williams, T.J., Ali, M.R.M.H and Anderson, J.S., "Noise and Flow Characteristics of Co-axial Jets" , Journal Mech. Engg. Science, Vol.11, No.2, pp 133-142, 1962.
25. Wygnanski,I. and Fiedler, H.E., "Some Measurements in the Self-Preserving Jet" Journal of Fluid Mechanics, Vo.38, pp. 577-612, 1969.

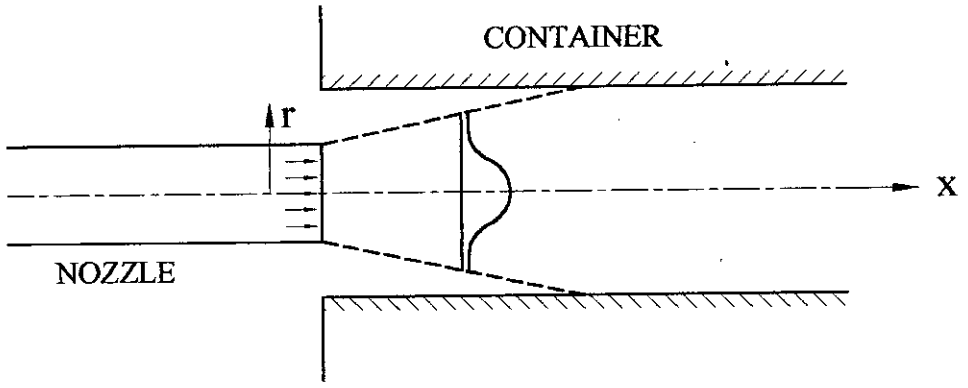

Fig. 1.2a : Confined Jet.

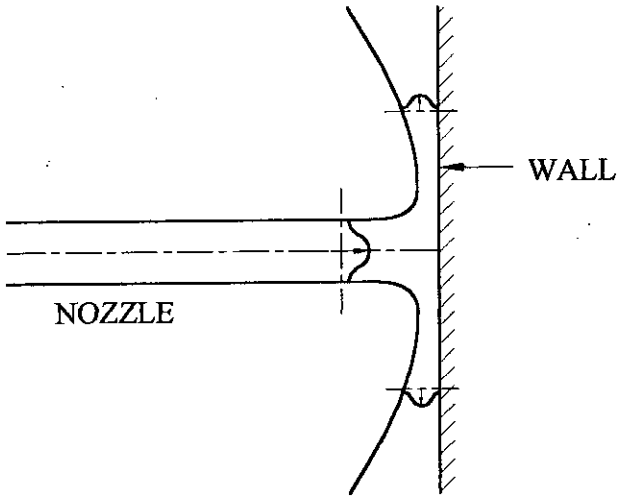

Fig. 1.2b : Wall Jet.

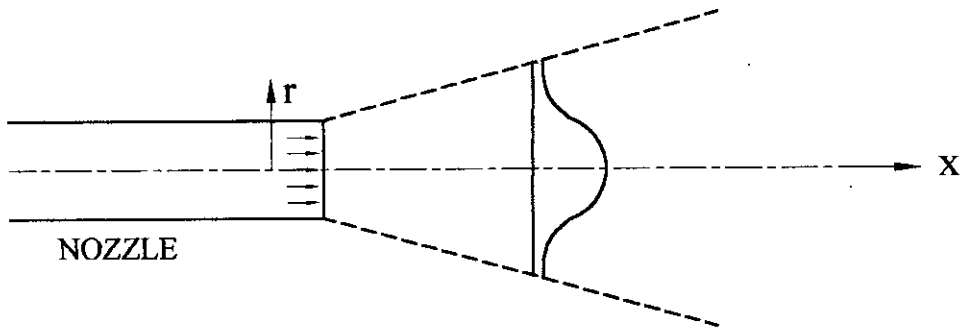

Fig. 1.2c : Free Jet.

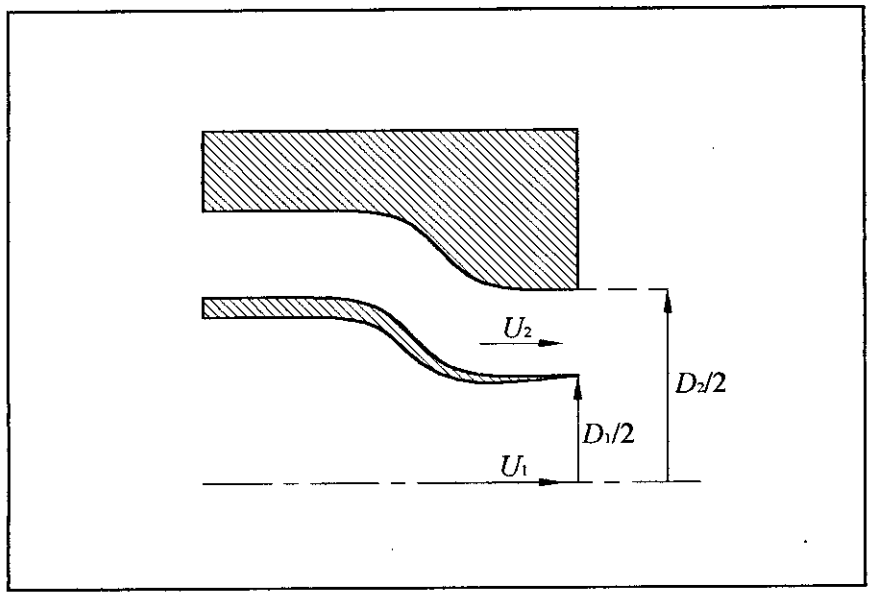

Fig. 1.2d : Co-axial Jet Nozzle Configuration.

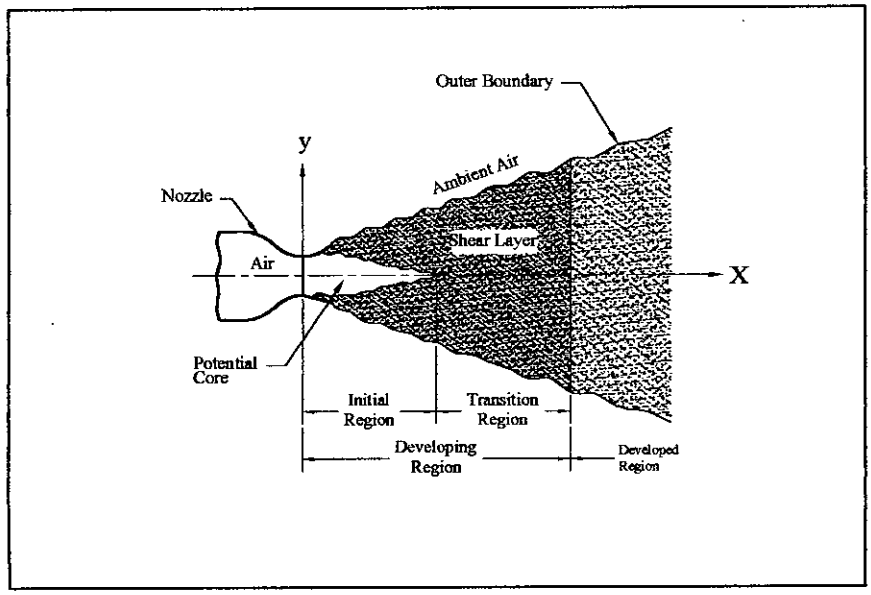

Fig. 1.3 : Schematic Diagram of the Flow Regions of a Free Jet.

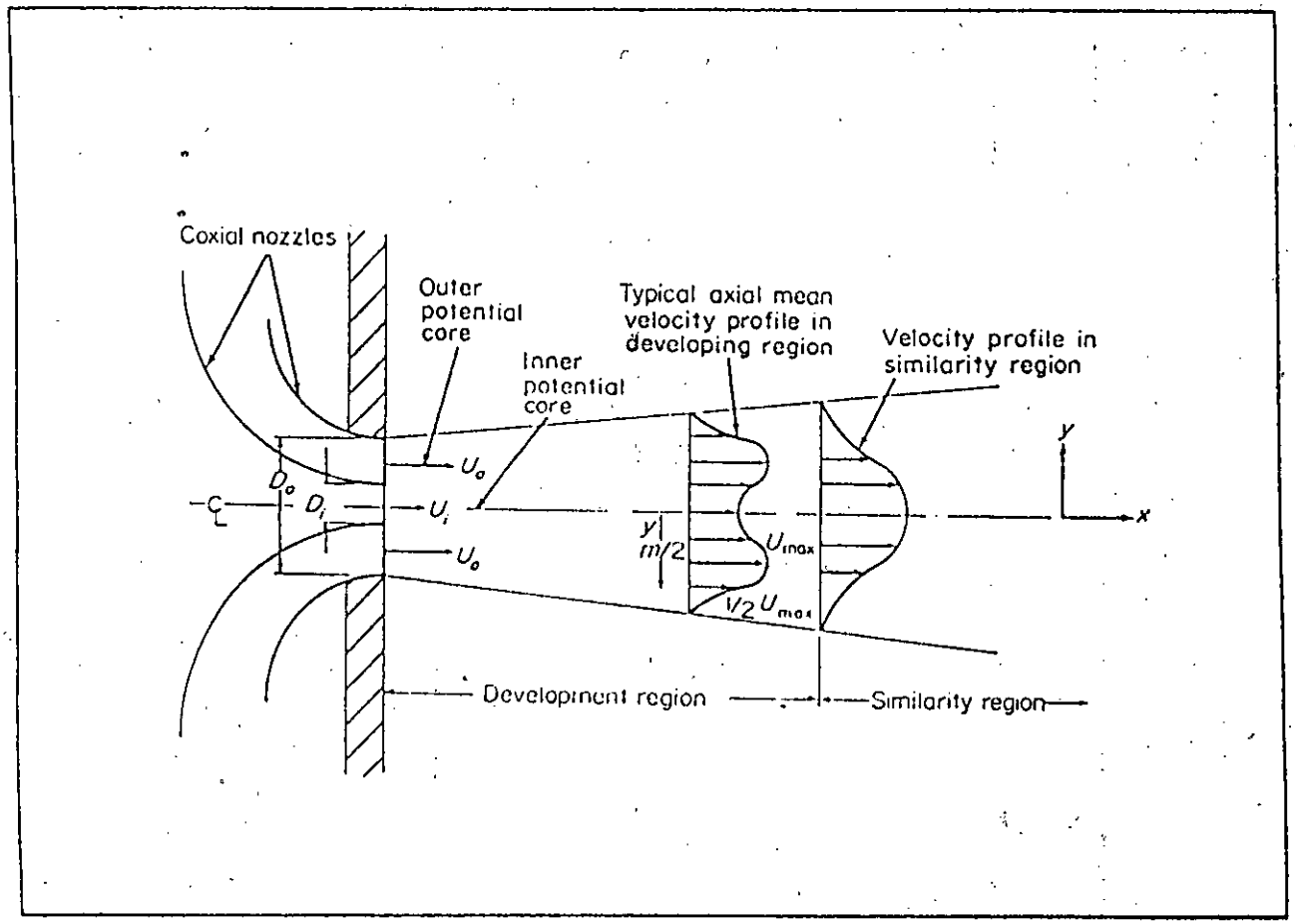

Fig. 1.4: Flow Field Generated by Co-axial Free Jet.

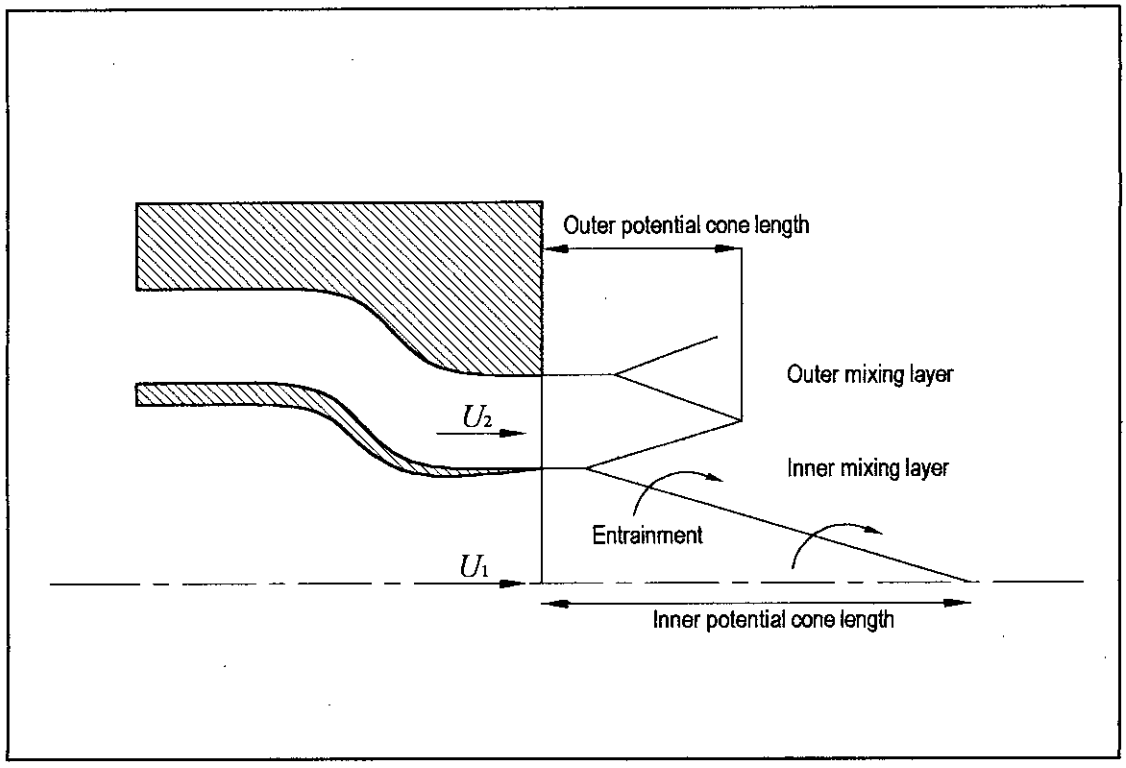

Fig. 2.2a : Schematic Diagram of the Mixing Layers in the Near Field.

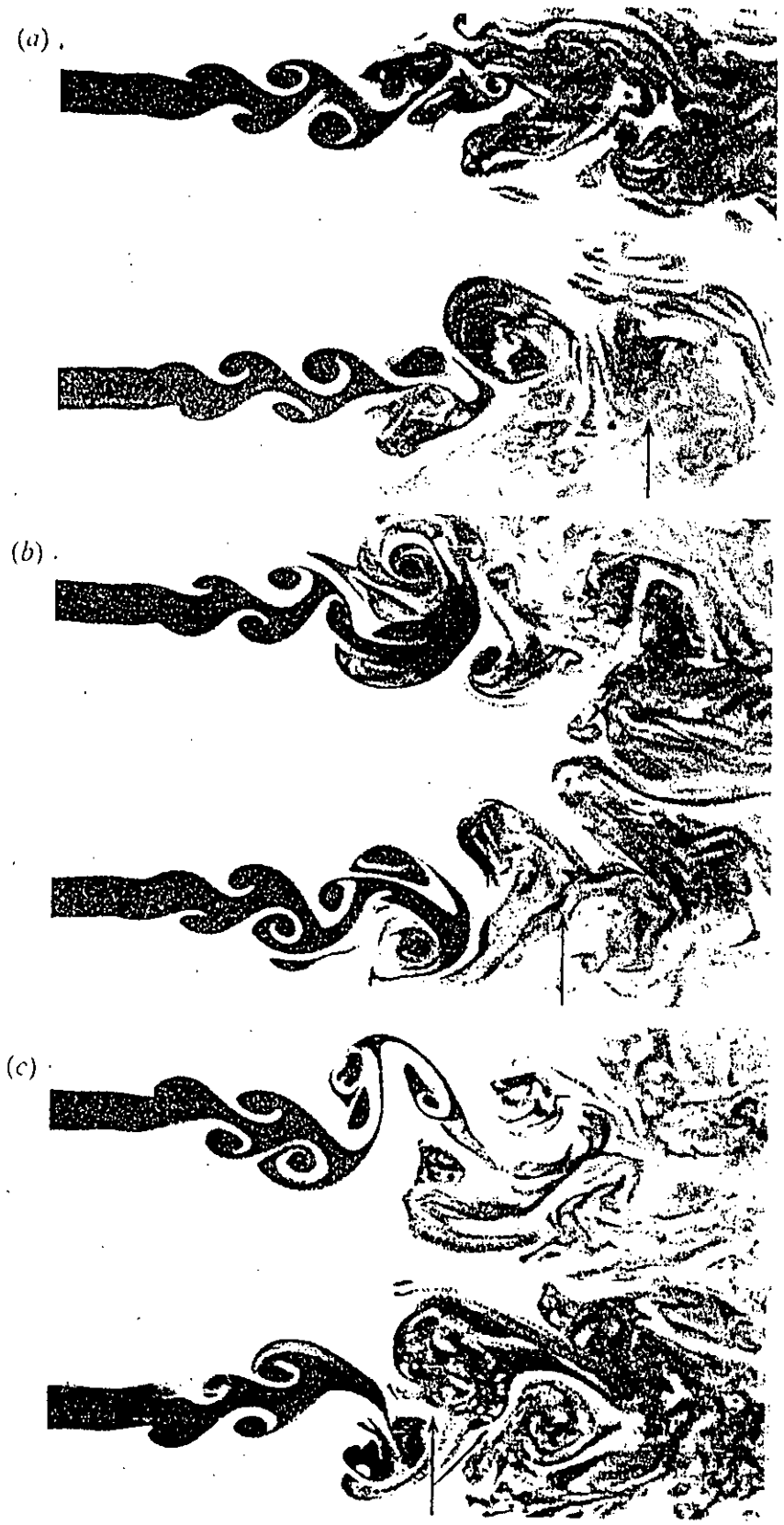

Fig. 2.2b: Instantaneous Pictures of the Flow Structure: a) r_u=2; b) r_u=3; c)r_u=4. The arrow indicates the pinching location. View from x/d=0.0 to 3.0. [20]

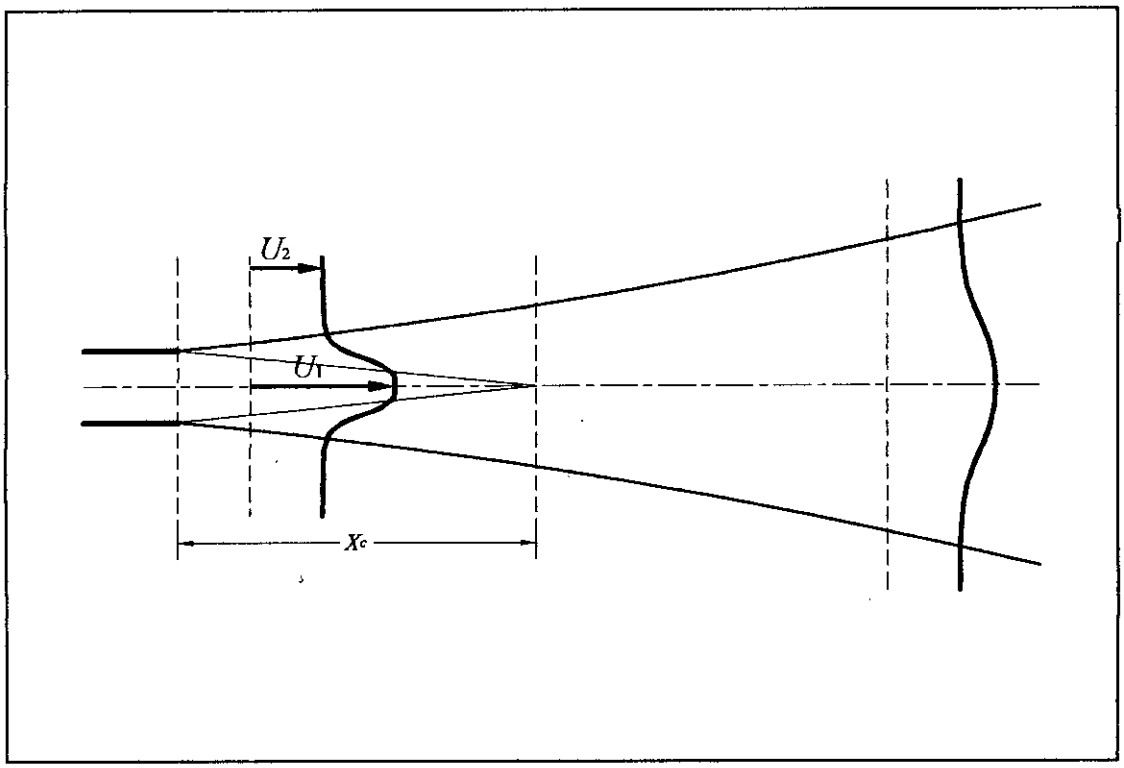

Fig. 3.1 : Mean Velocity Distribution in the First Potential Core Region & Farther Downstream of the Nozzle Exit.

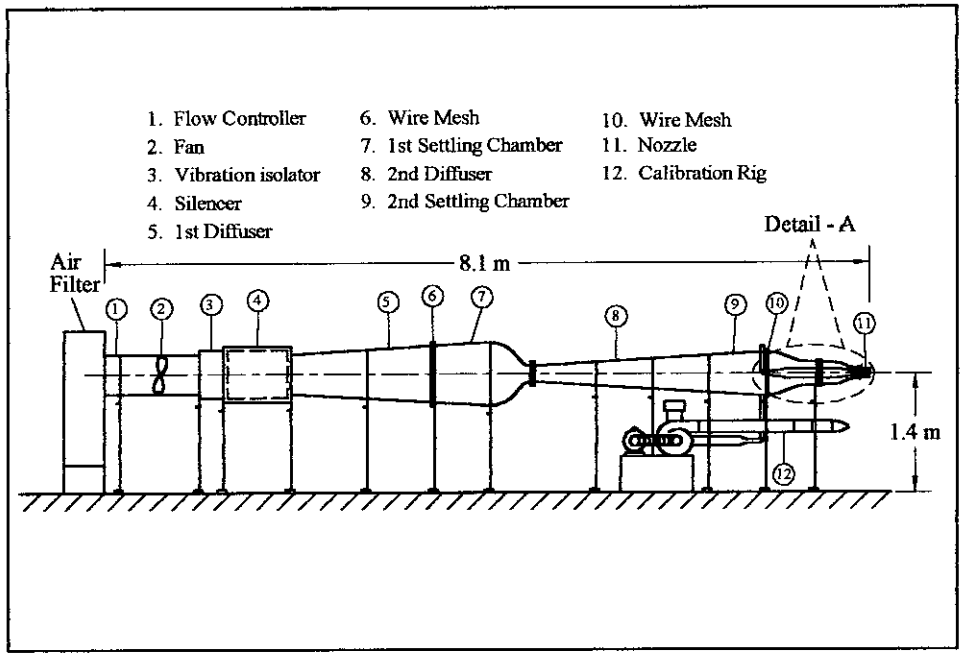

Fig. 4.1.1 : Schematic Diagram of the Jet Flow Facility and Calibration Rig.

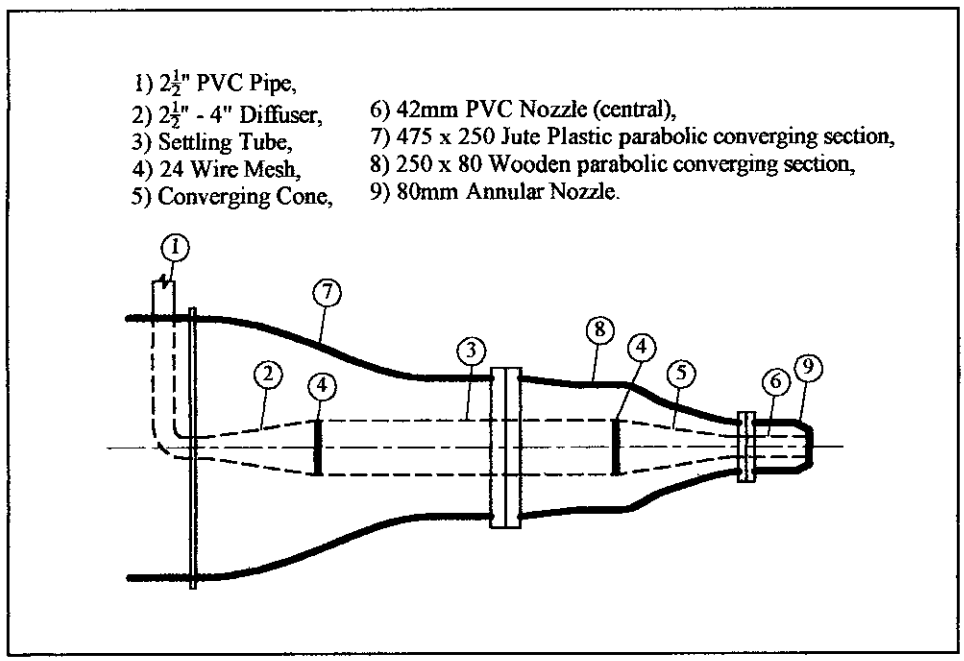

Fig. 4.1.2 : Detail - A.

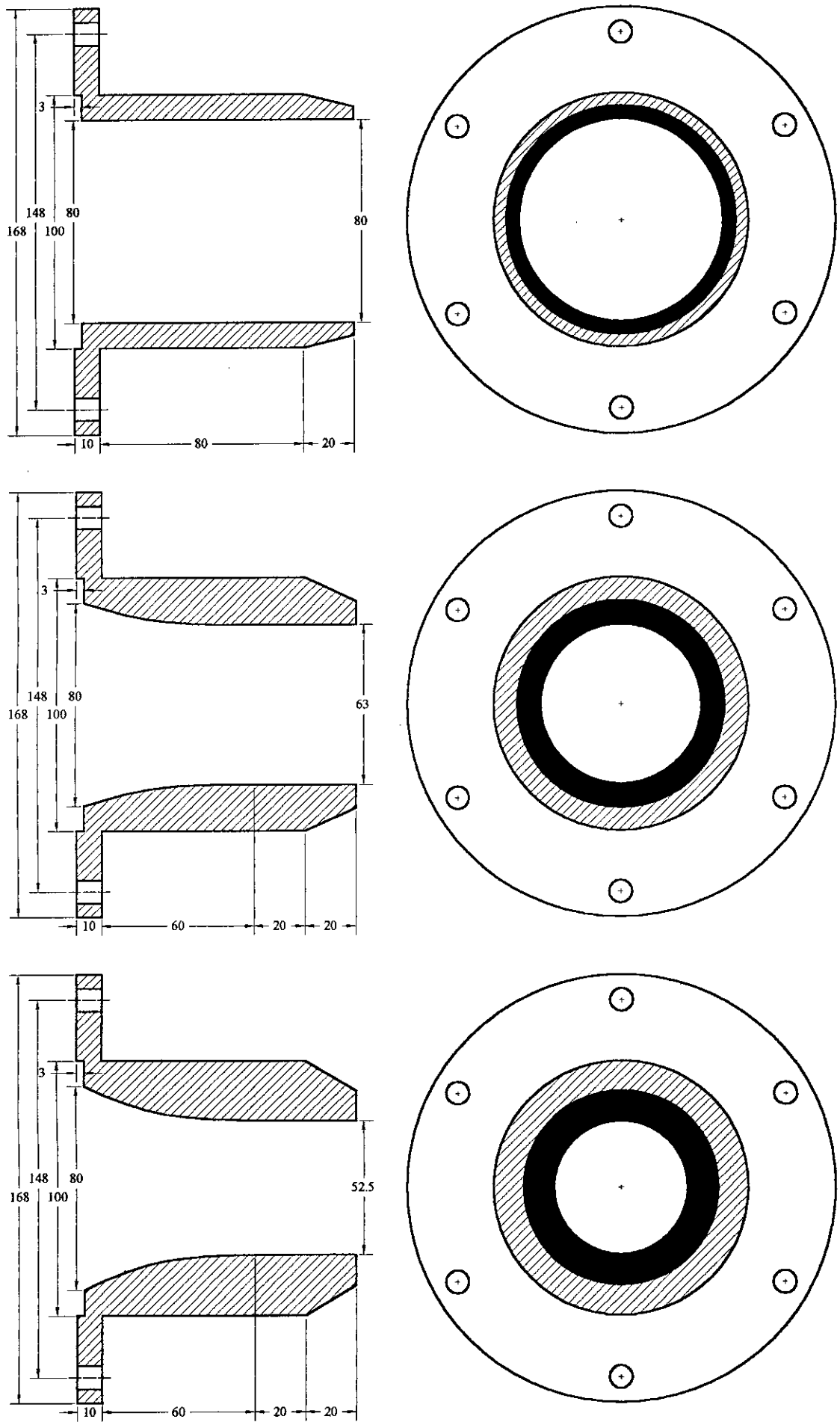

Fig. 4.1.3 : Annular Nozzles of Varying Diameter.

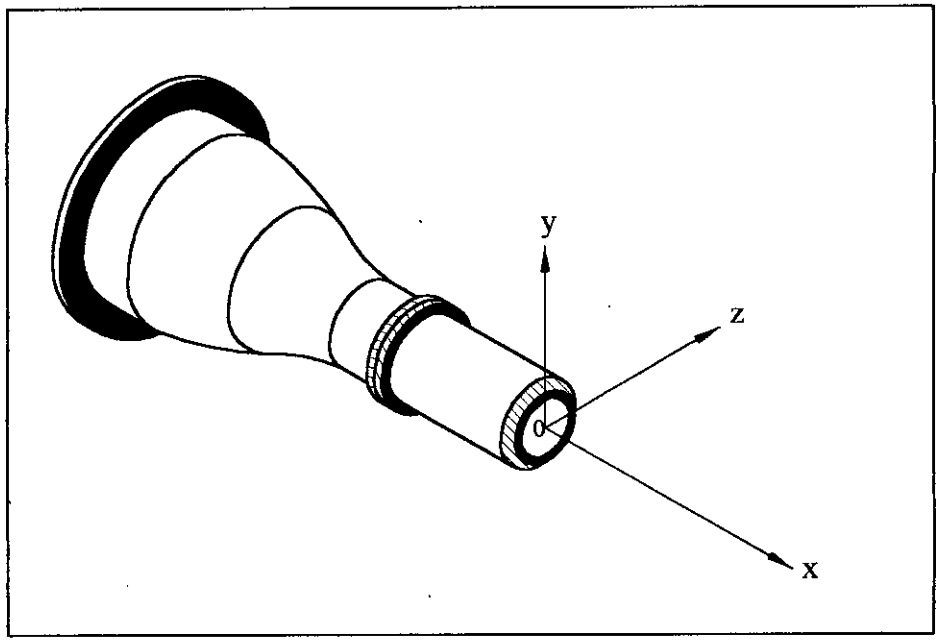

Fig. 4.2.1 : Co - ordinate System of Nozzle.

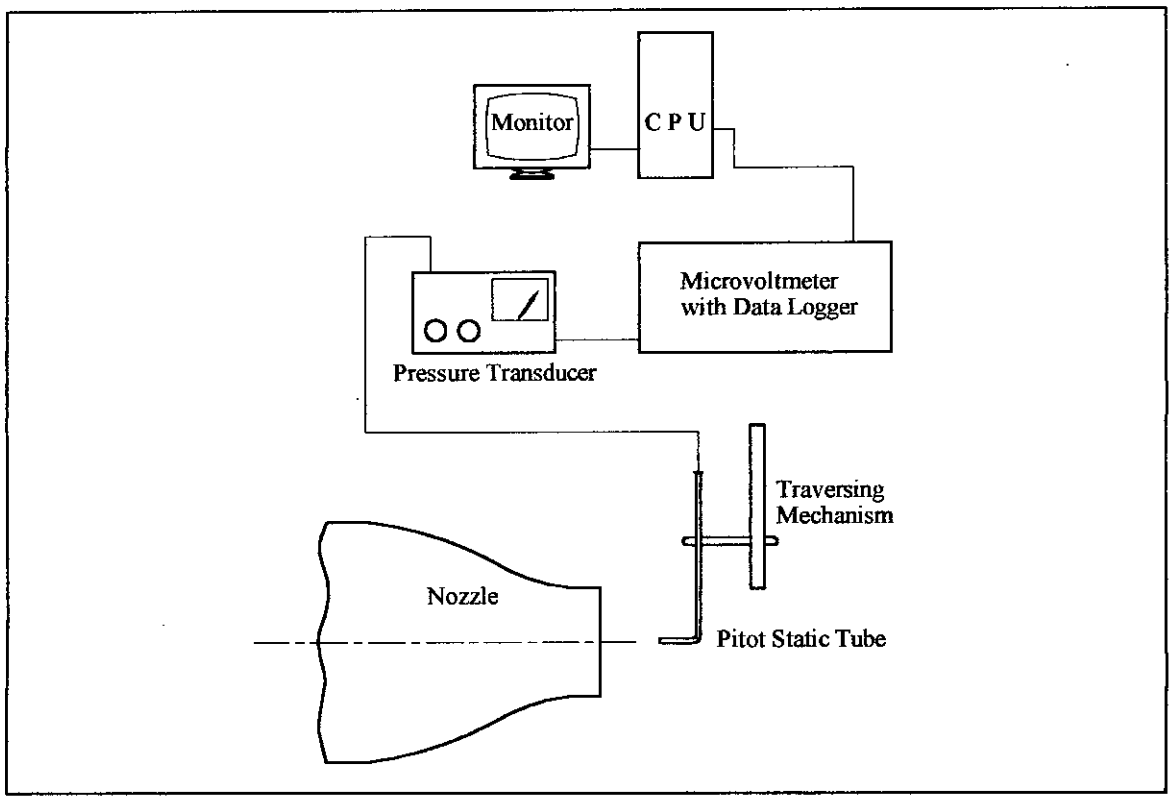

Fig. 4.4 : Schematic Diagram for Measuring Mean Velocity.

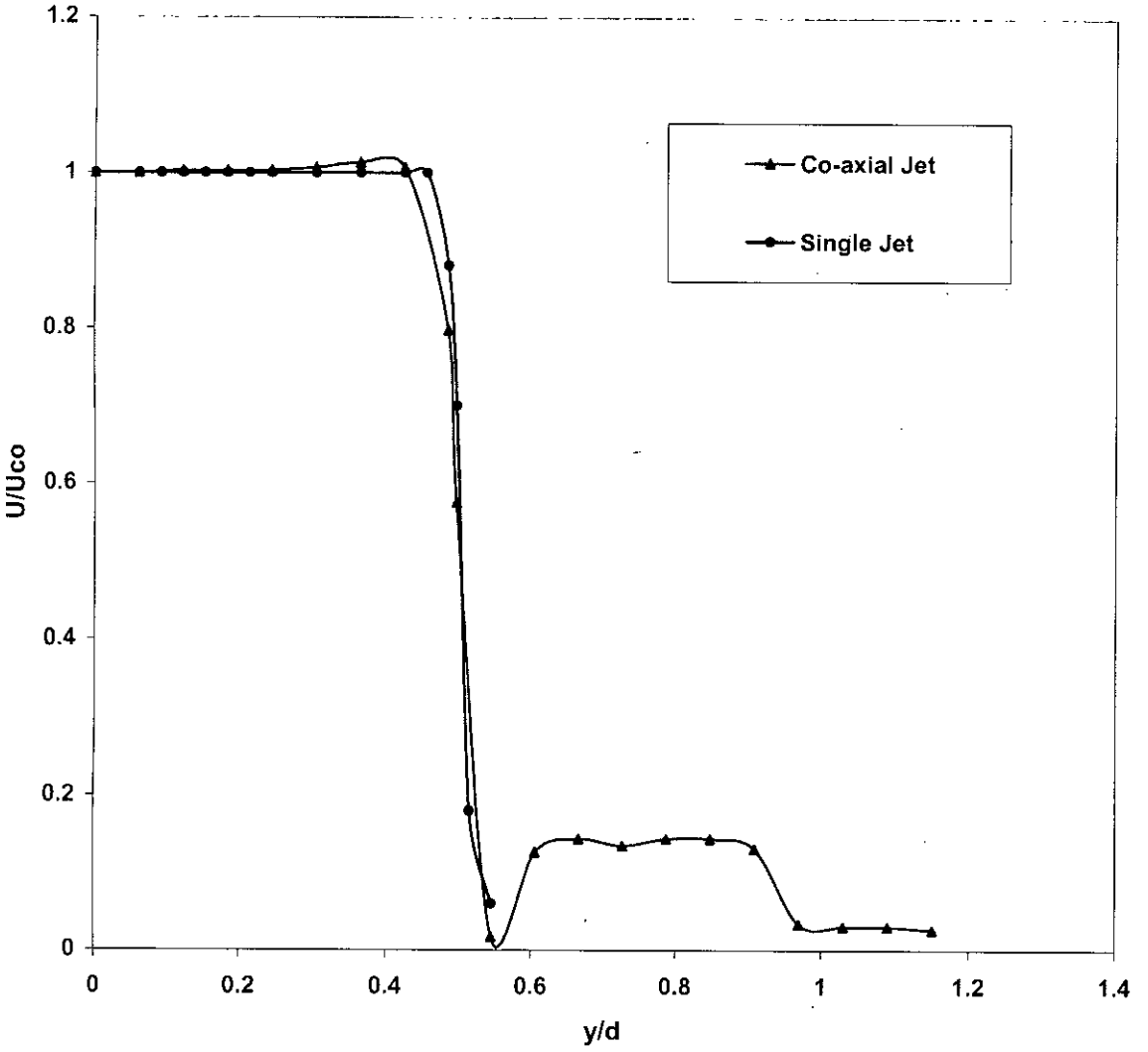

Fig 5.2.1 : Exit (x/d=0.0) Velocity Profiles of Single Jet and Co-axial Jet(U_2/U_1=0.12)At Re=3.7x10^4

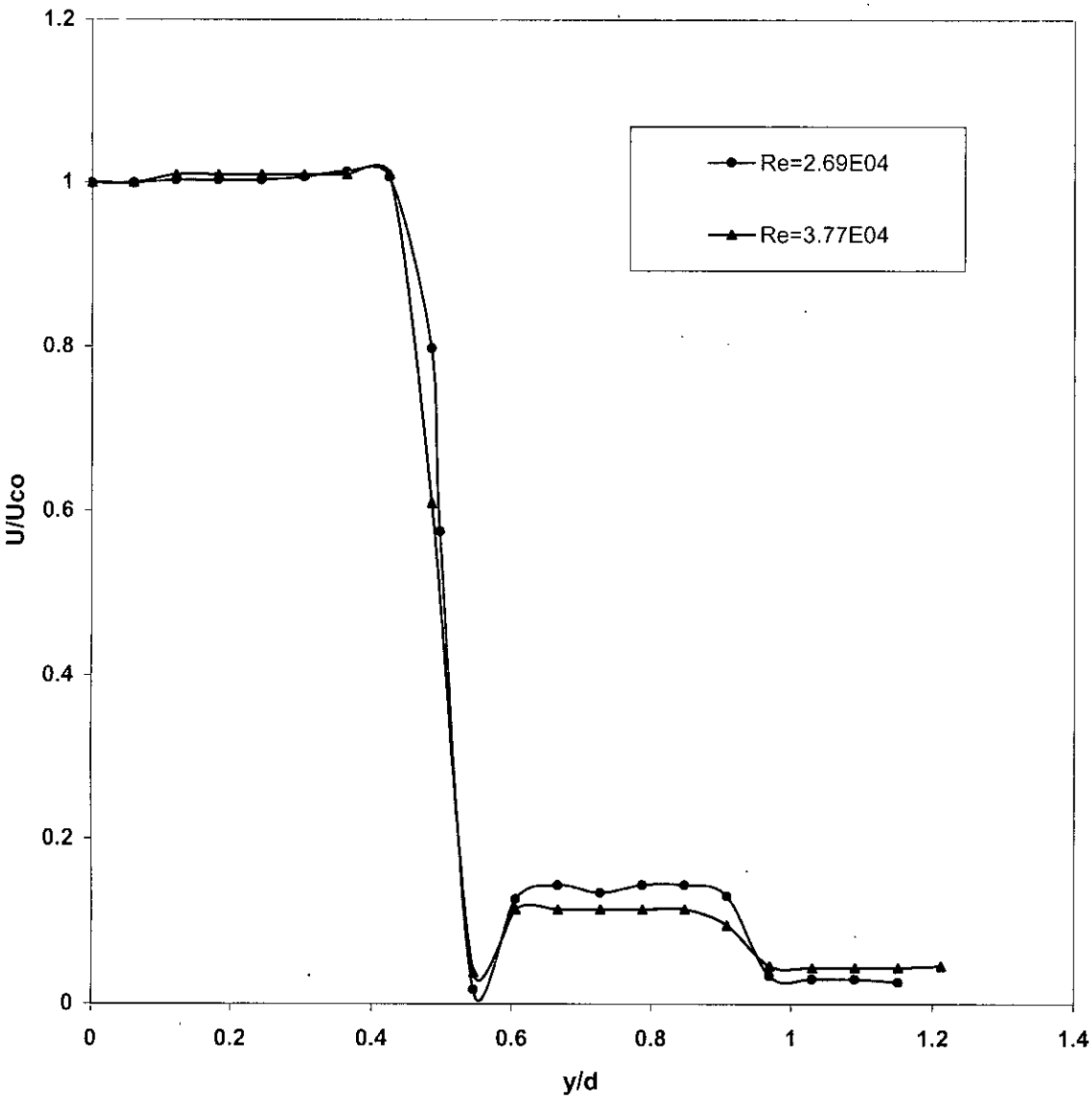

Fig 5.2.2 : Effect of Re on Exit (x/d=0.0)Velocity Profiles of Co-axial Jets at U_2/U_1=0.12 and A_2/A_1=2.61

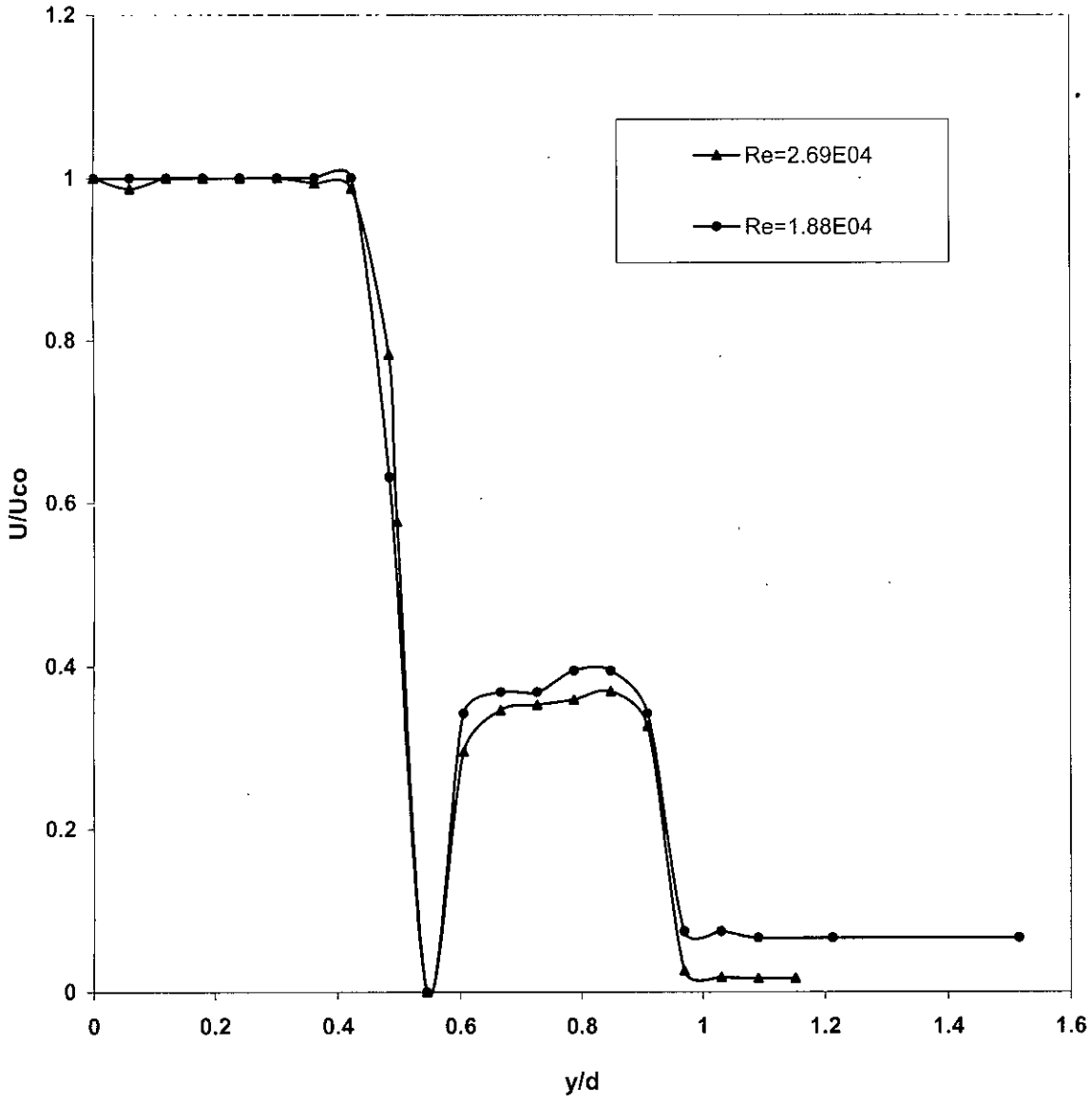

Fig 5.2.3 : Effect of Re on Exit (x/d=0.0)Velocity Profile of Co-axial Jets at U_2/U_1=0.37 and A_2/A_1=2.61

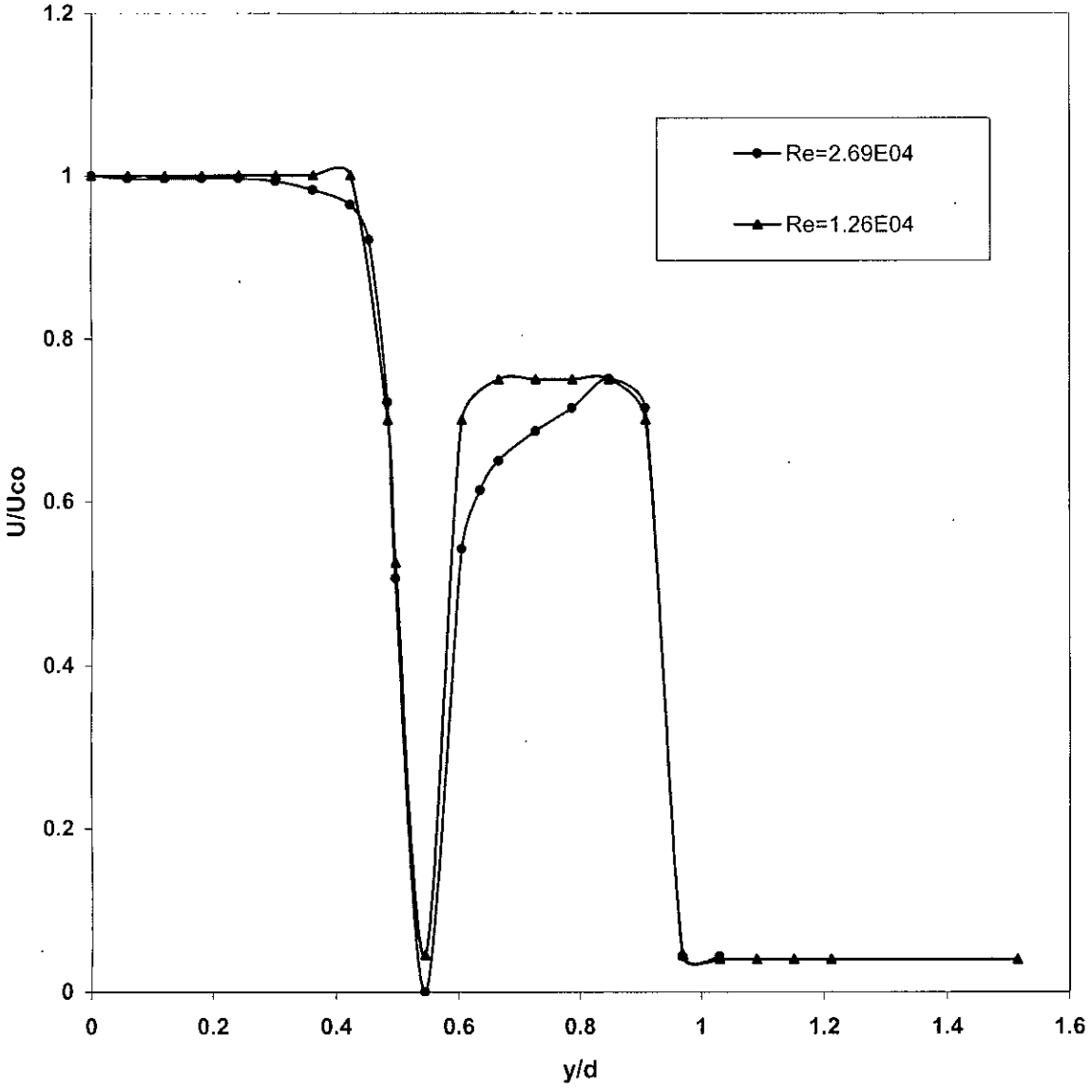

Fig 5.2.4 : Effect of Re on Exit (x/d=0.0)Velocity Profiles of Co-axial Jets at U_2/U_1=0.75 and A_2/A_1=2.61

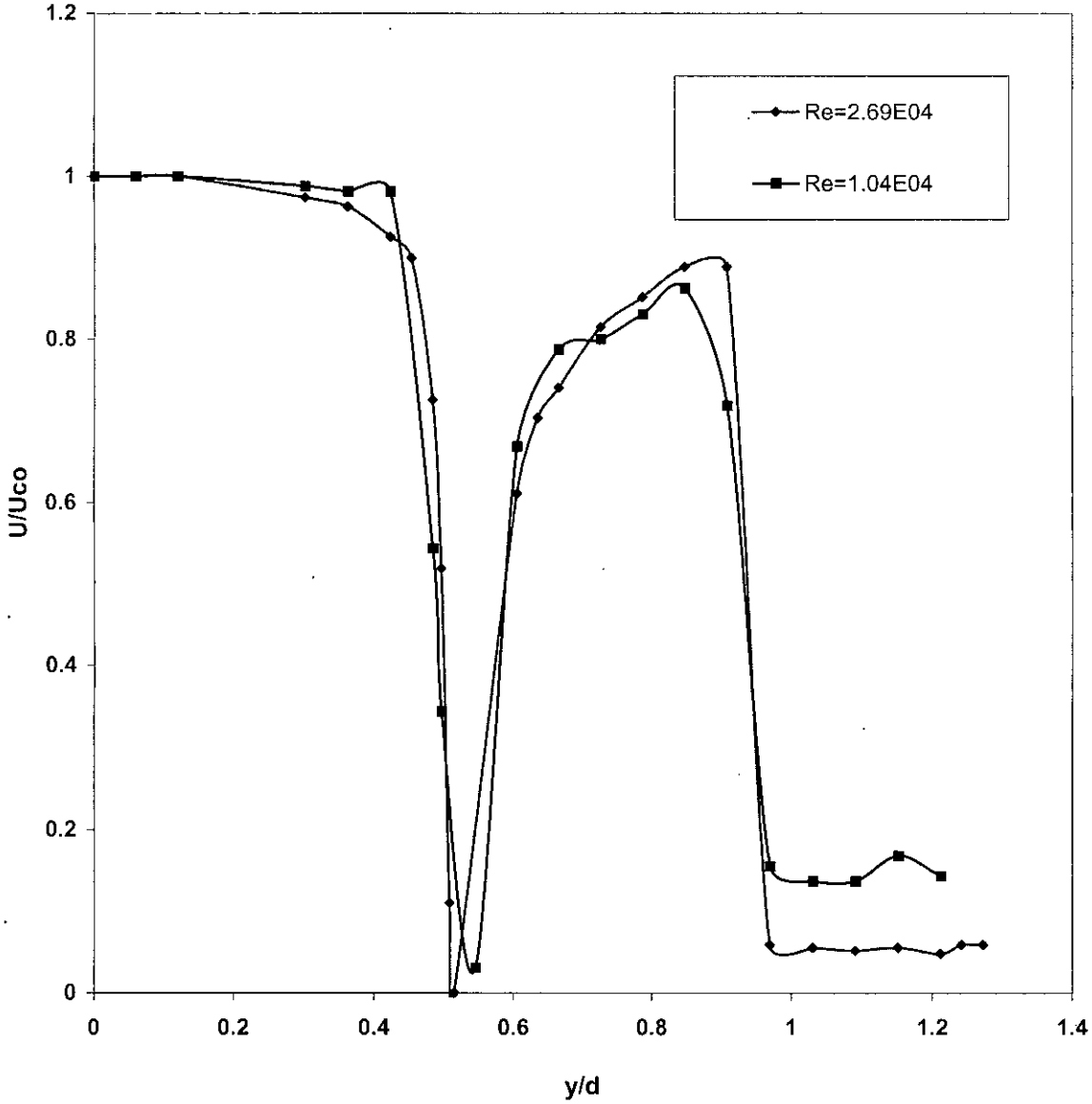

Fig 5.2.5 : Effect of Re on Exit (x/d=0.0)Velocity Profiles of Co-axial Jets at U_2/U_1=0.90 and A_2/A_1=2.61

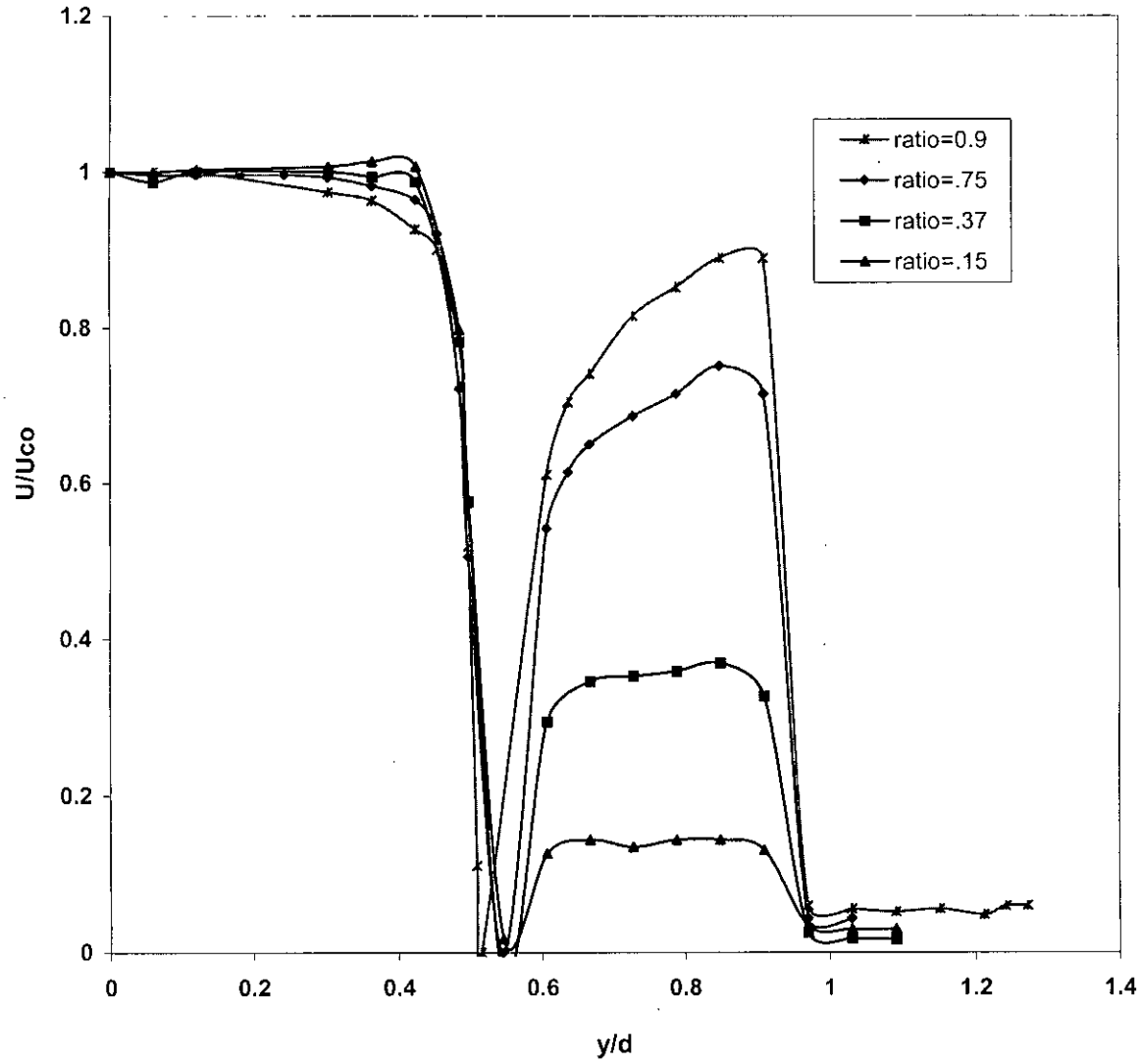

Fig 5.2.6 : Effects of Velocity Ratio on Exit (x/d=0.0)Velocity Profiles of Co-axial Jets at A_2/A_1=2.61 and Re=2.69 X 10^4

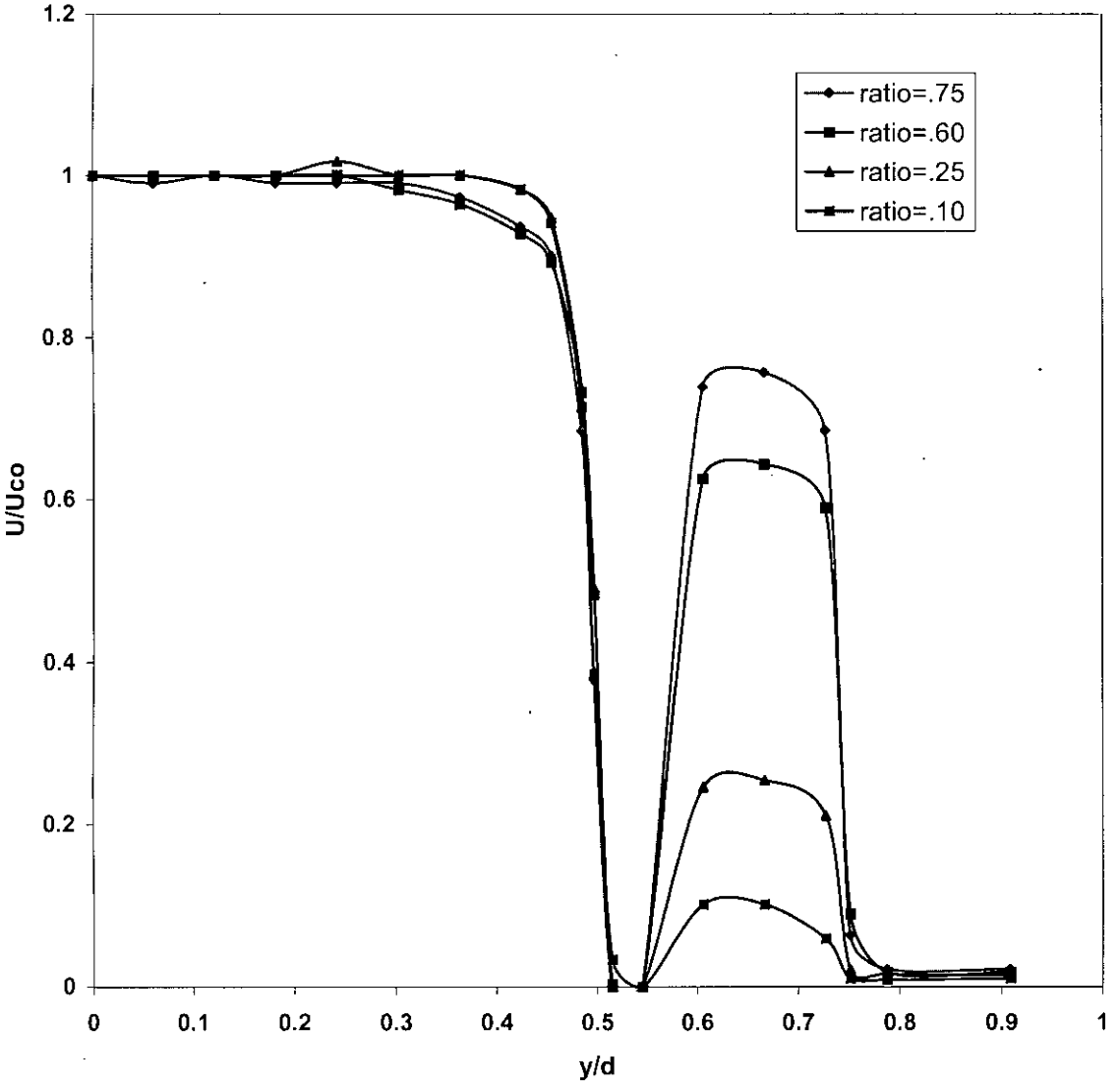

Fig 5.2.7 : Effect of Velocity Ratio on Exit(x/d=0.0) Velocity Profiles for Co-axial jets at A_2/A_1=1.25 and Re=4x10^4

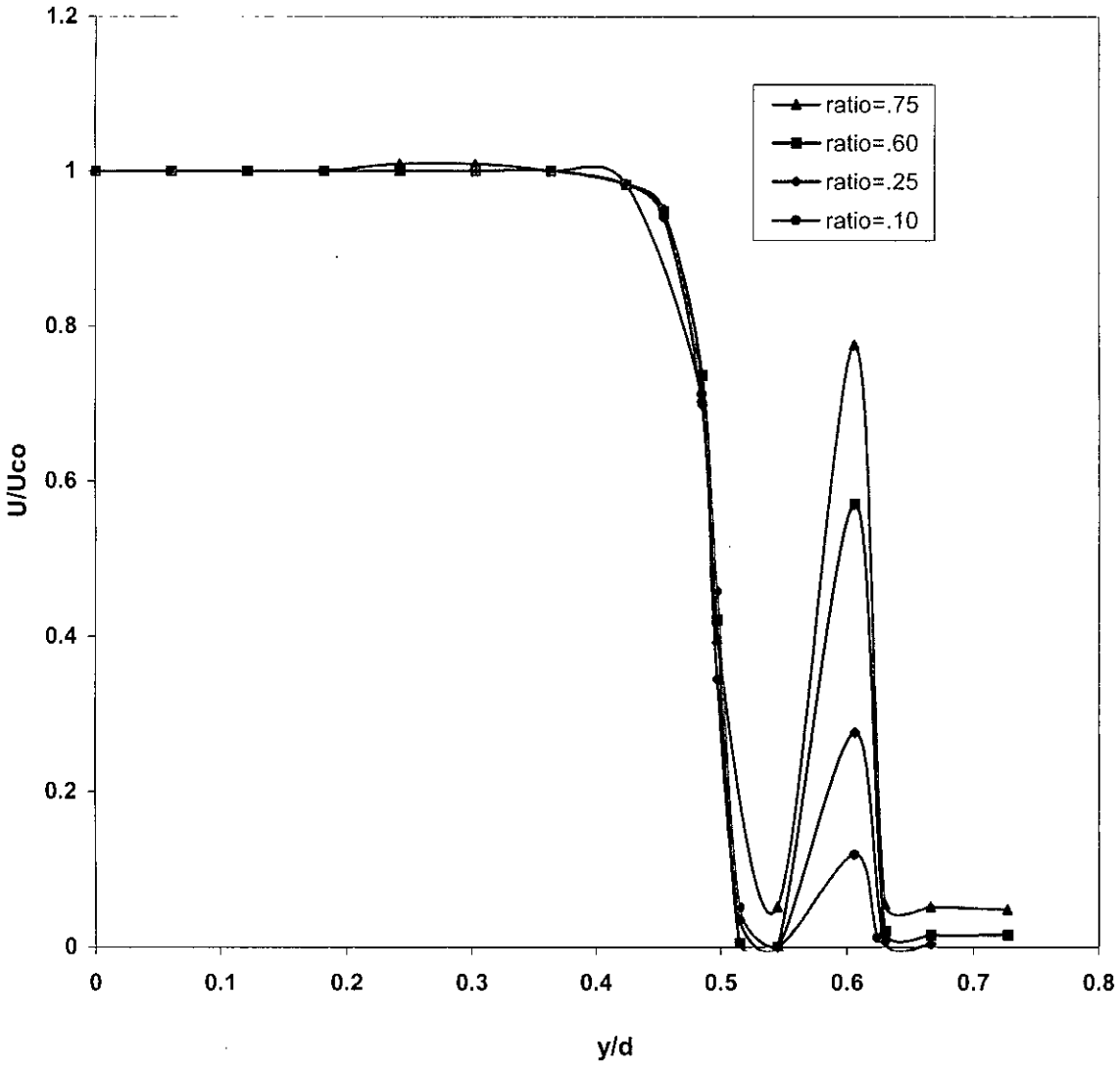

Fig 5.2.8 : Effect of Velocity Ratio on Exit (x/d=0.0) Velocity Profiles of Co-axial Jets at A_2/A_1=0.56 and Re=4X10^4

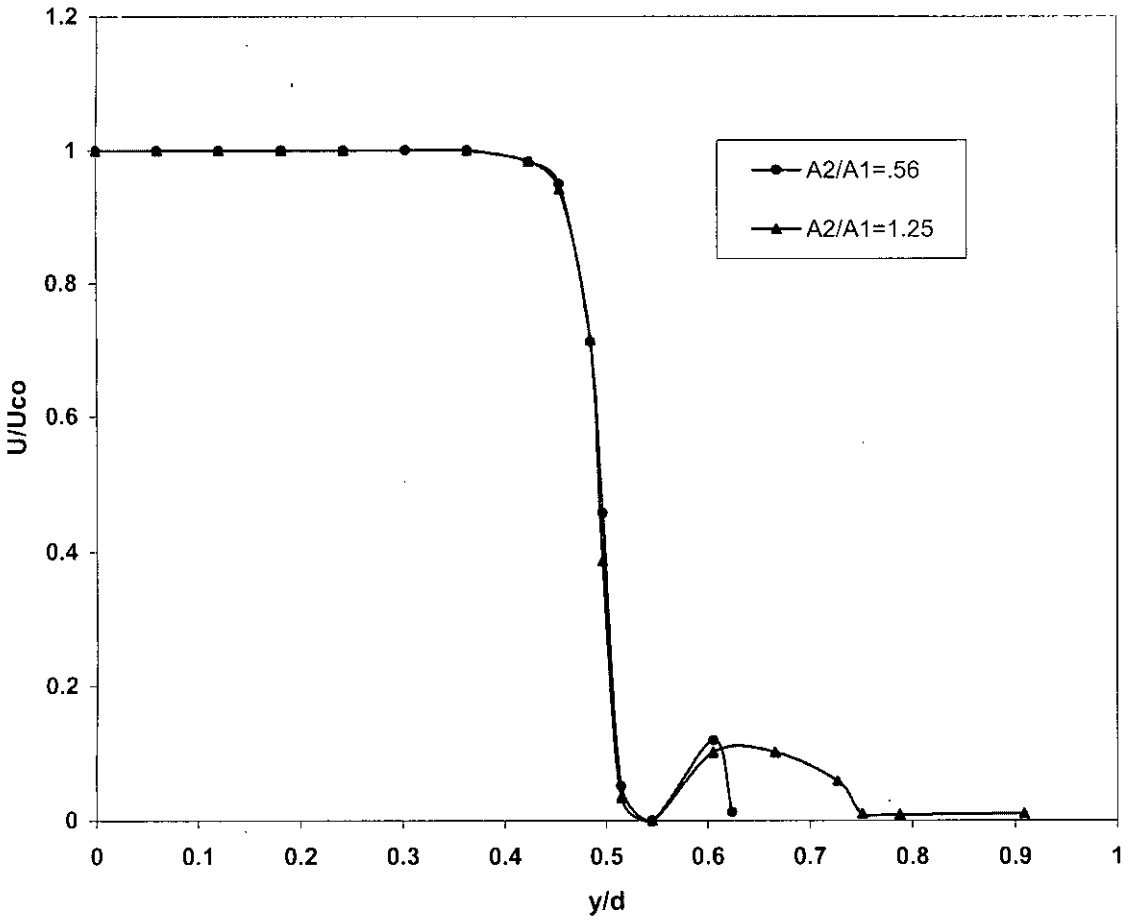

Fig 5.2.9 :Effect of Area Ratio (A_2/A_1) on Exit (x/d=0.0) Velocity Profiles at U_2/U_1=0.10 and Re=4X10^4

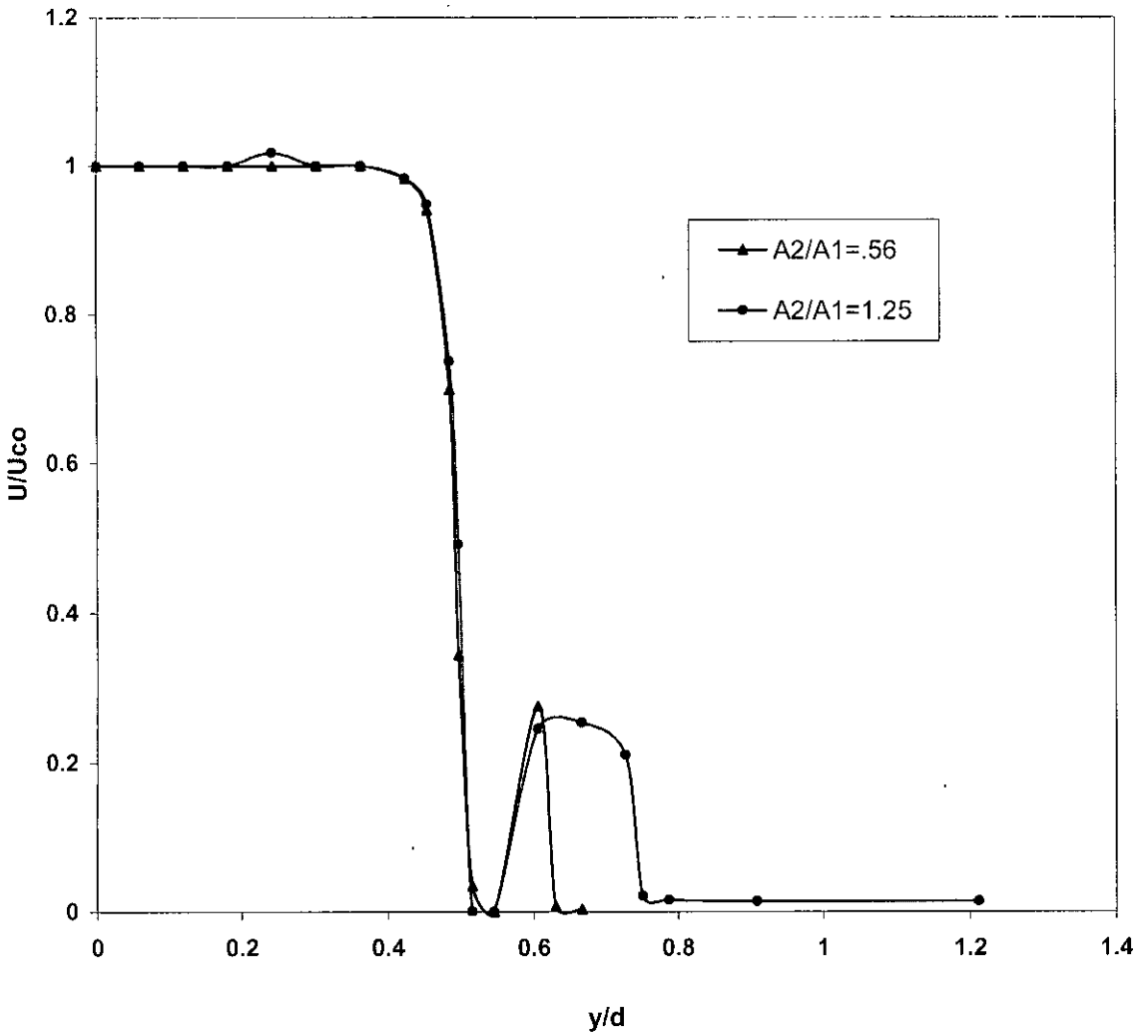

Fig 5.2.10 :Effect of Area Ratio (A_2/A_1) on Exit (x/d=0.0) Velocity Profiles at U_2/U_1=0.25 and Re=4X10^4

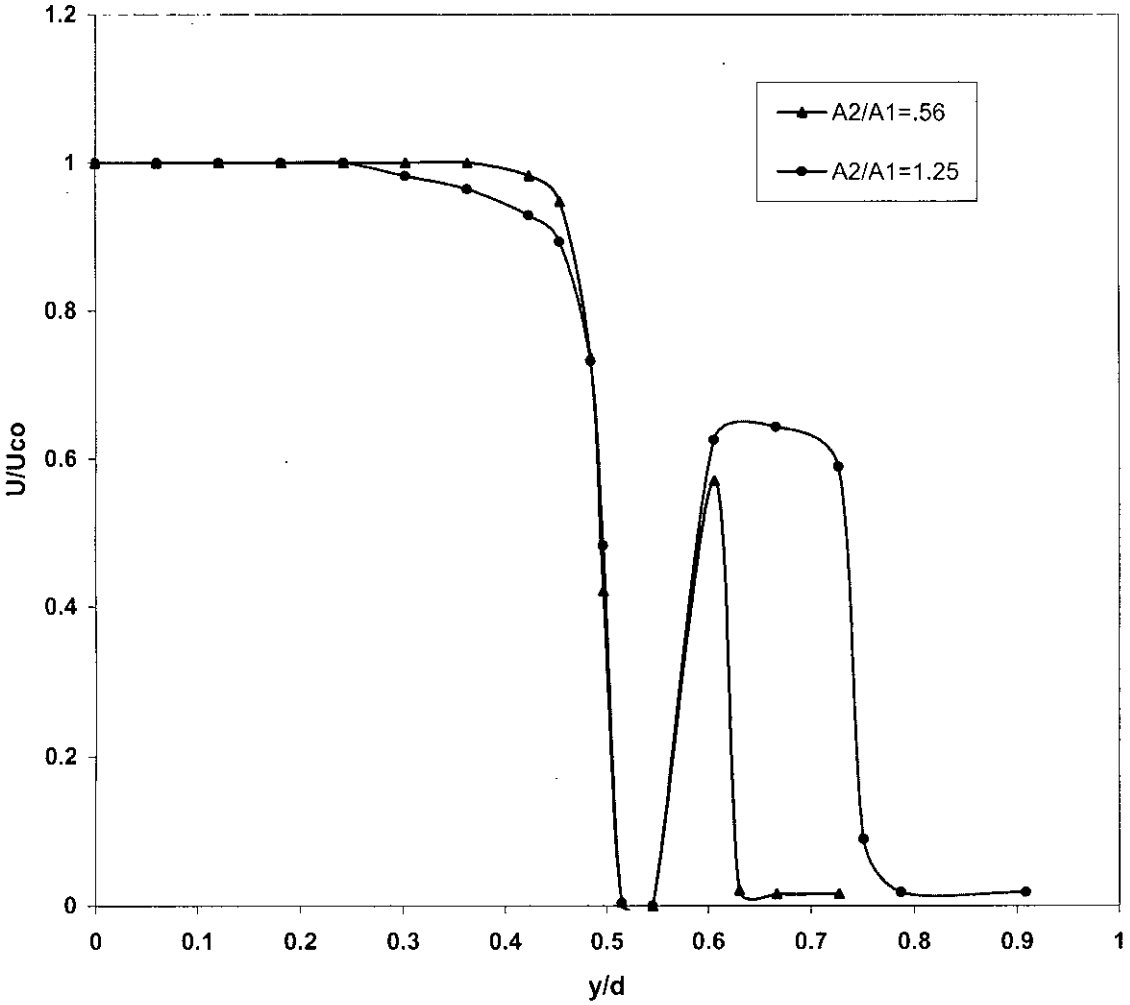

Fig 5.2.11 Effect of Area Ratio(A_2/A_1) on Exit(x/d=0.0) Velocity Profiles at U_2/U_1 =0.60 and Re=4X10^4

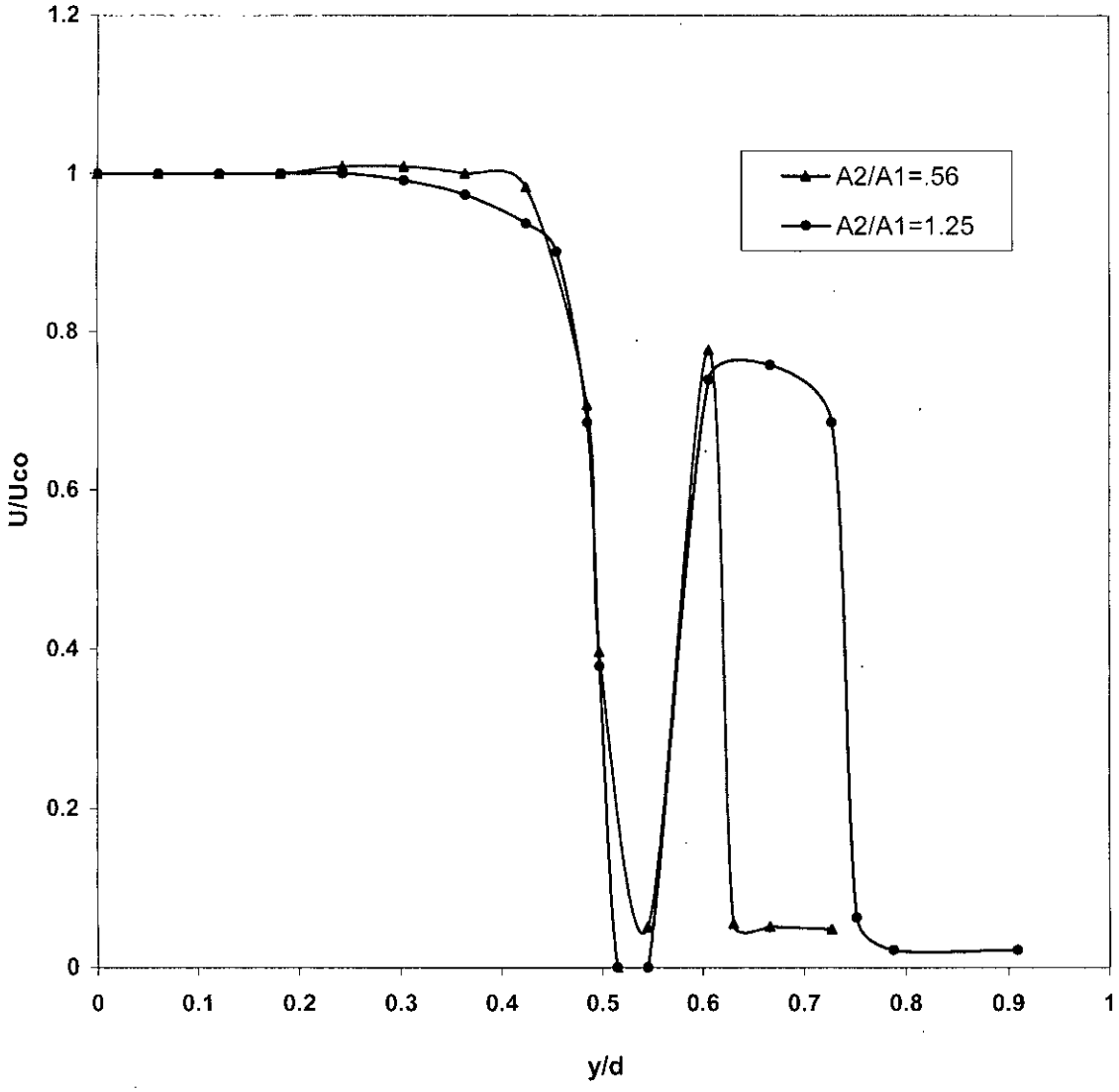

Fig 5.2.12 : Effect of Area Ratio(A_2/A_1)on Exit(x/d=0.0) Velocity Profiles at U_2/U_1=0.75 and at Re=4X10^4

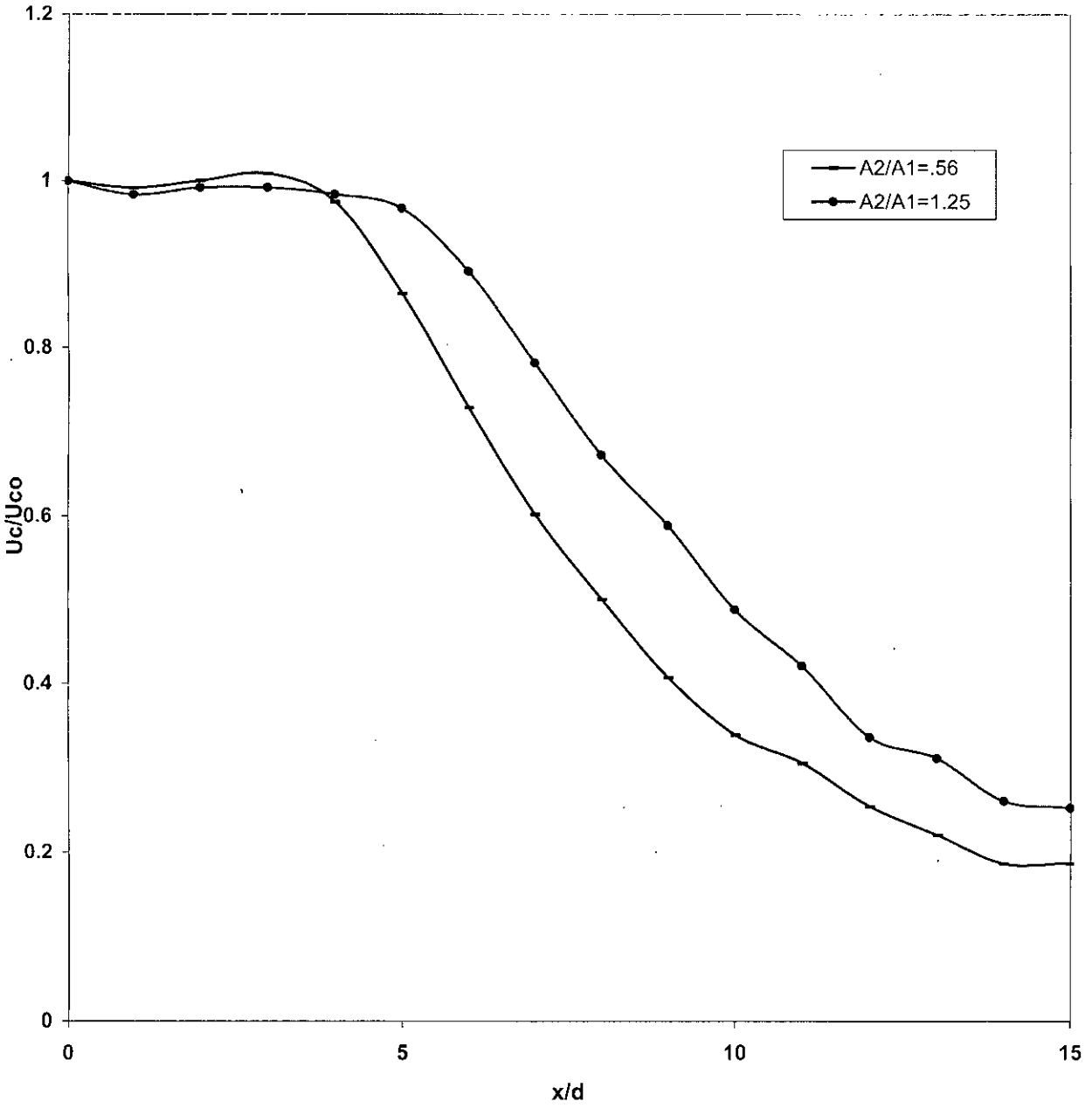

Fig.5.3.1: Effect of Area Ratio(A_2/A_1) on Centreline Velocity Profile of Coaxial Jets at U_2/U_1=0.10 and Re=4X10^4

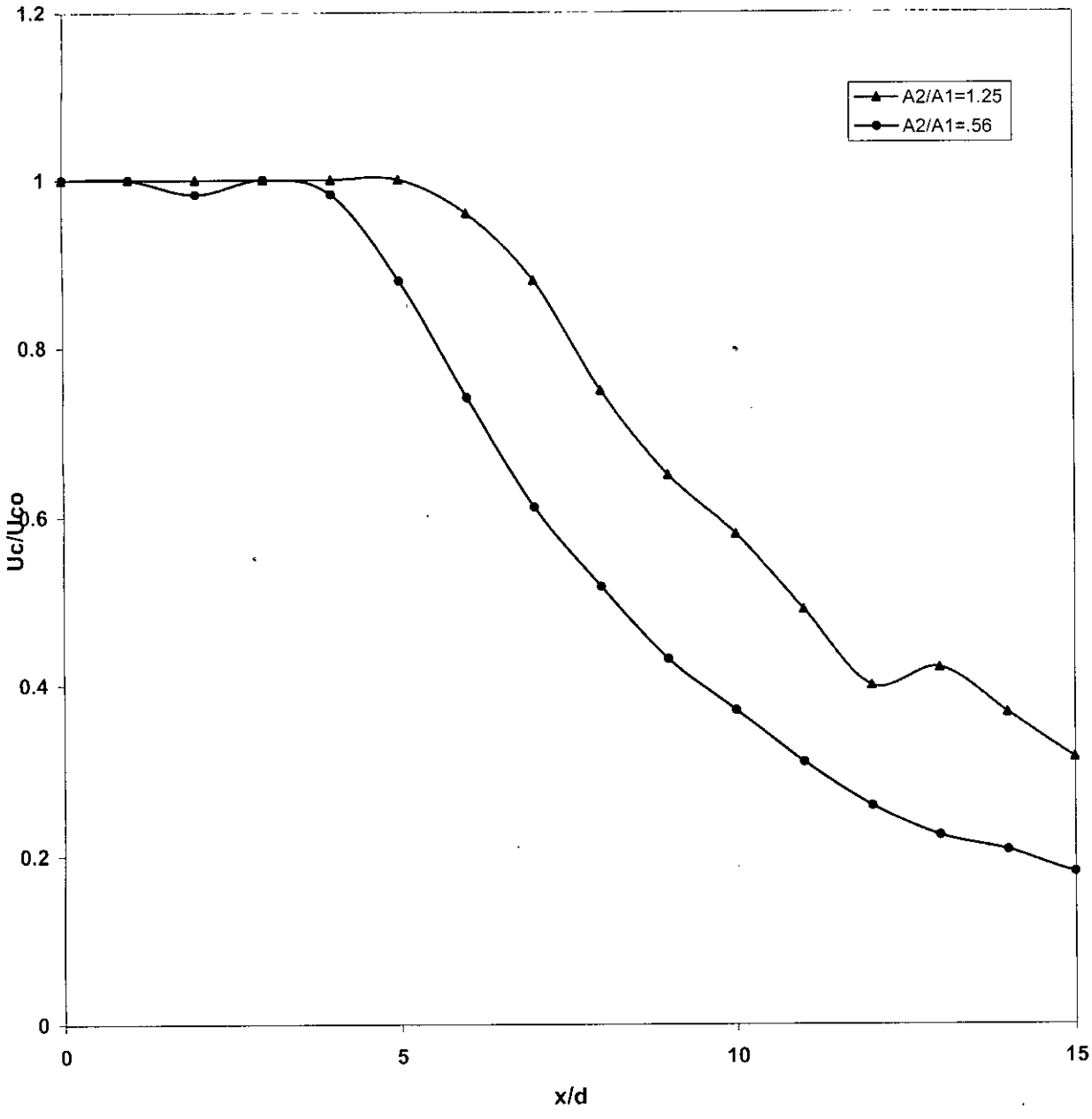

Fig5.3.2: Effects of Area Ratio(A_2/A_1) on Centreline Velocity Profiles of Coaxial Jets at U_2/U_1=0.25 and Re=4X10^4

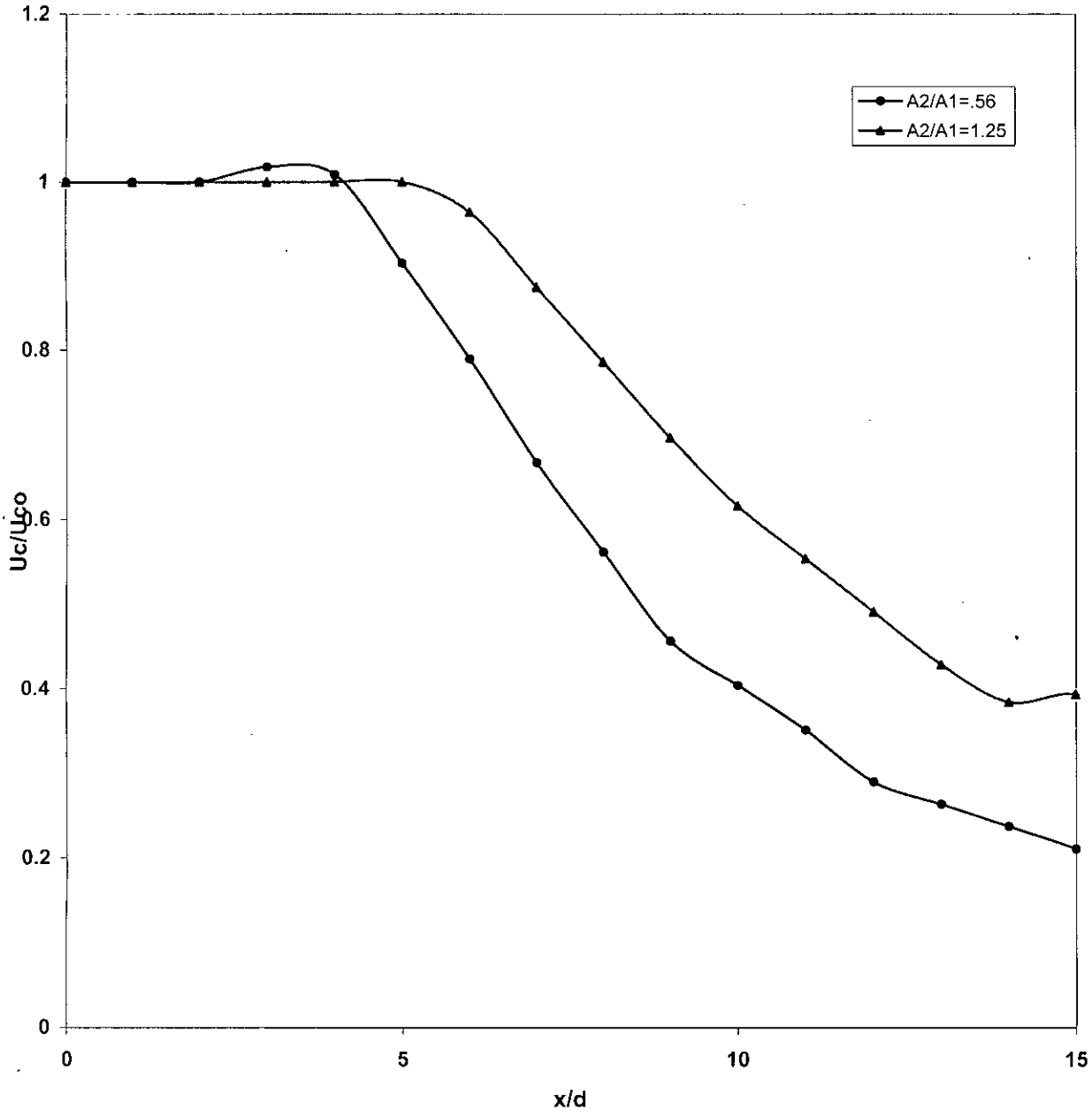

Fig5.3.3: Effects of Area Ratio(A_2/A_1) on Centreline Velocity Profiles of Coaxial Jets at U_2/U_1=0.60 and Re=4X10^4

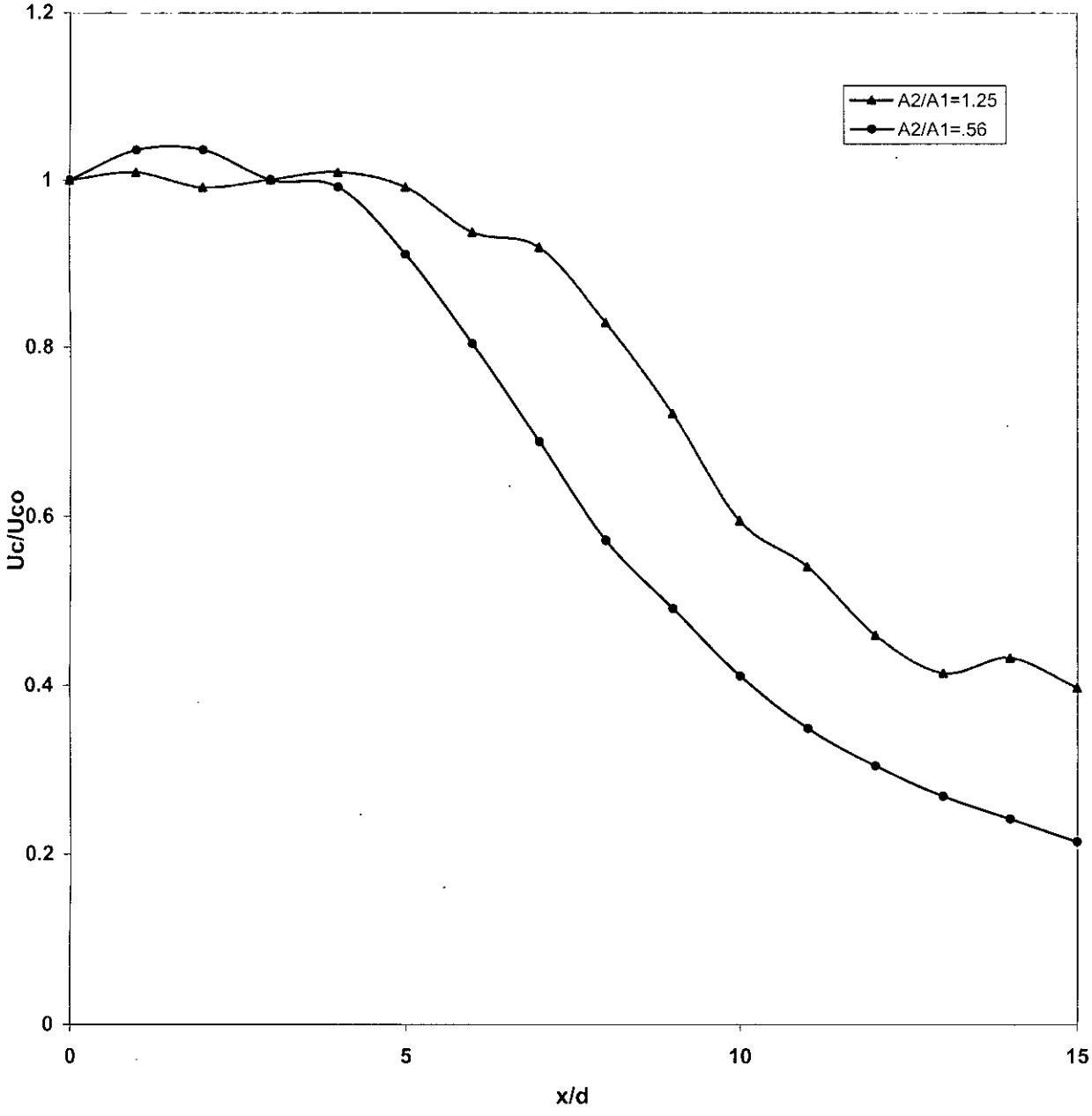

Fig 5.3.4: Effects of Area Ratio(A_2/A_1) on Centreline Velocity Profiles of Coaxial Jets at U_2/U_1=0.75 and Re=4X10^4

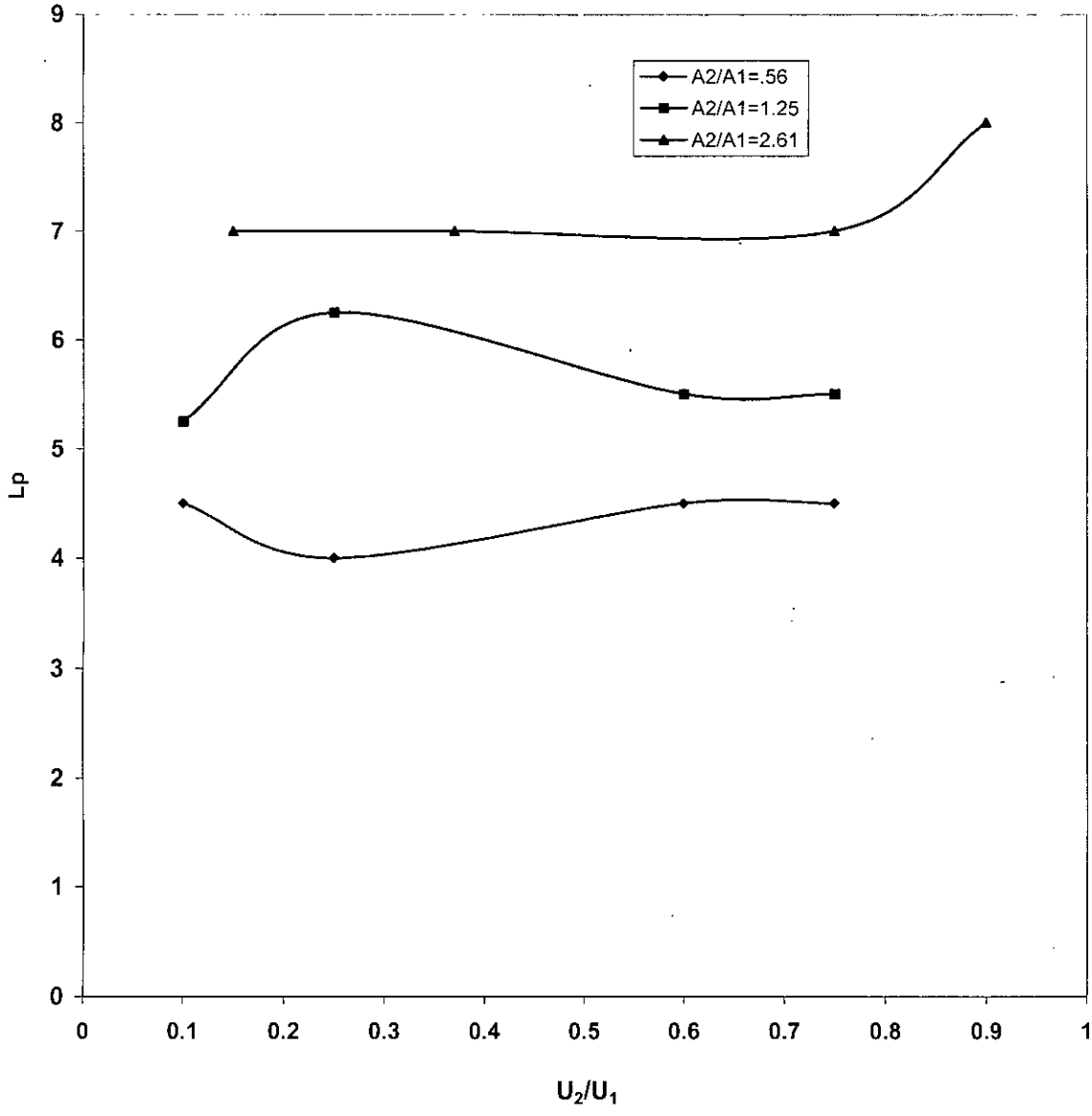

Fig 5.3.5 : Length of Potential Core as a Function of the Velocity Ratio for three area ratios

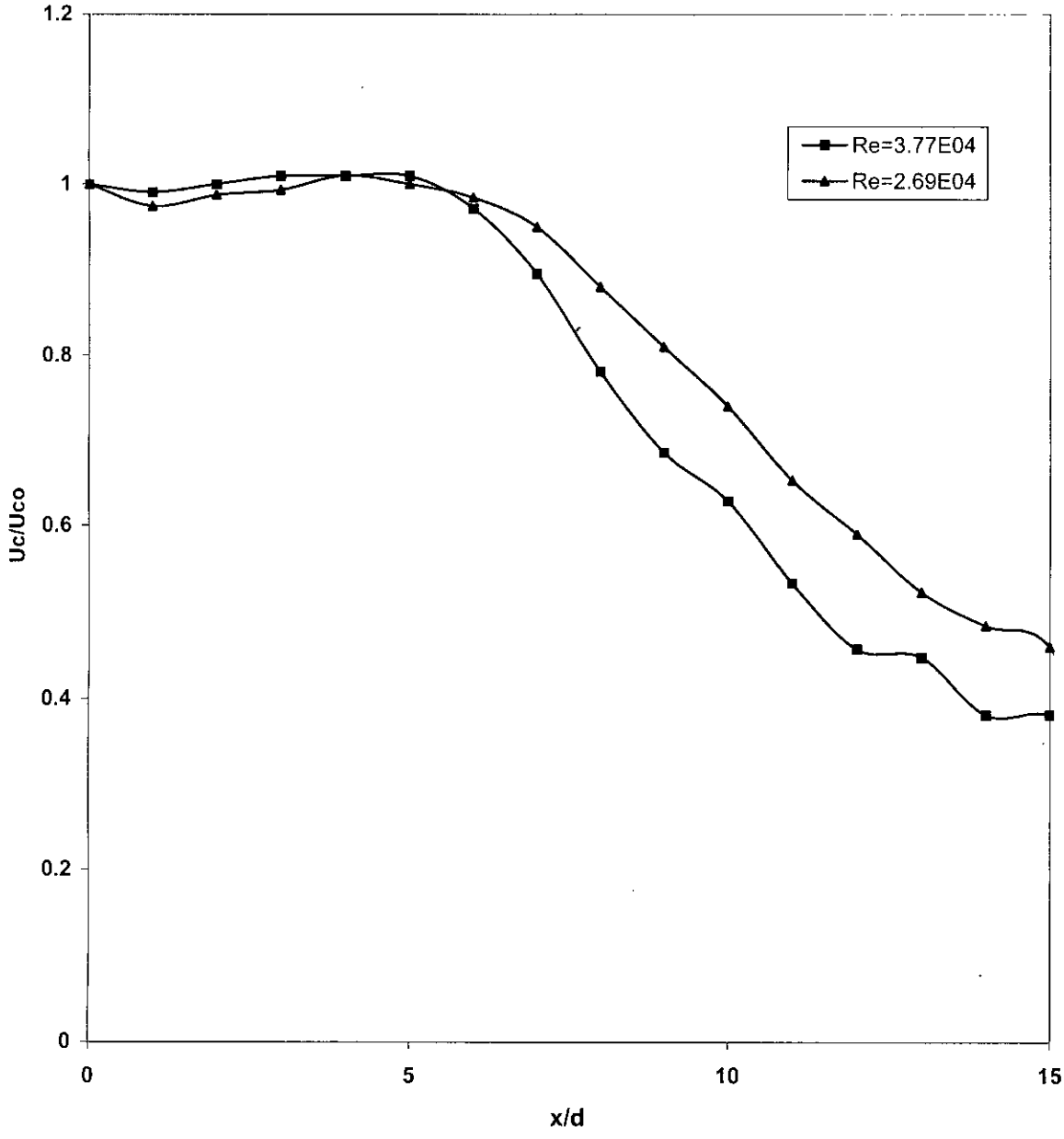

Fig: 5.3.6: Effect of Reynolds Number on Centerline Velocity Profile of Co-axial Jets at U_2/U_1=0.12

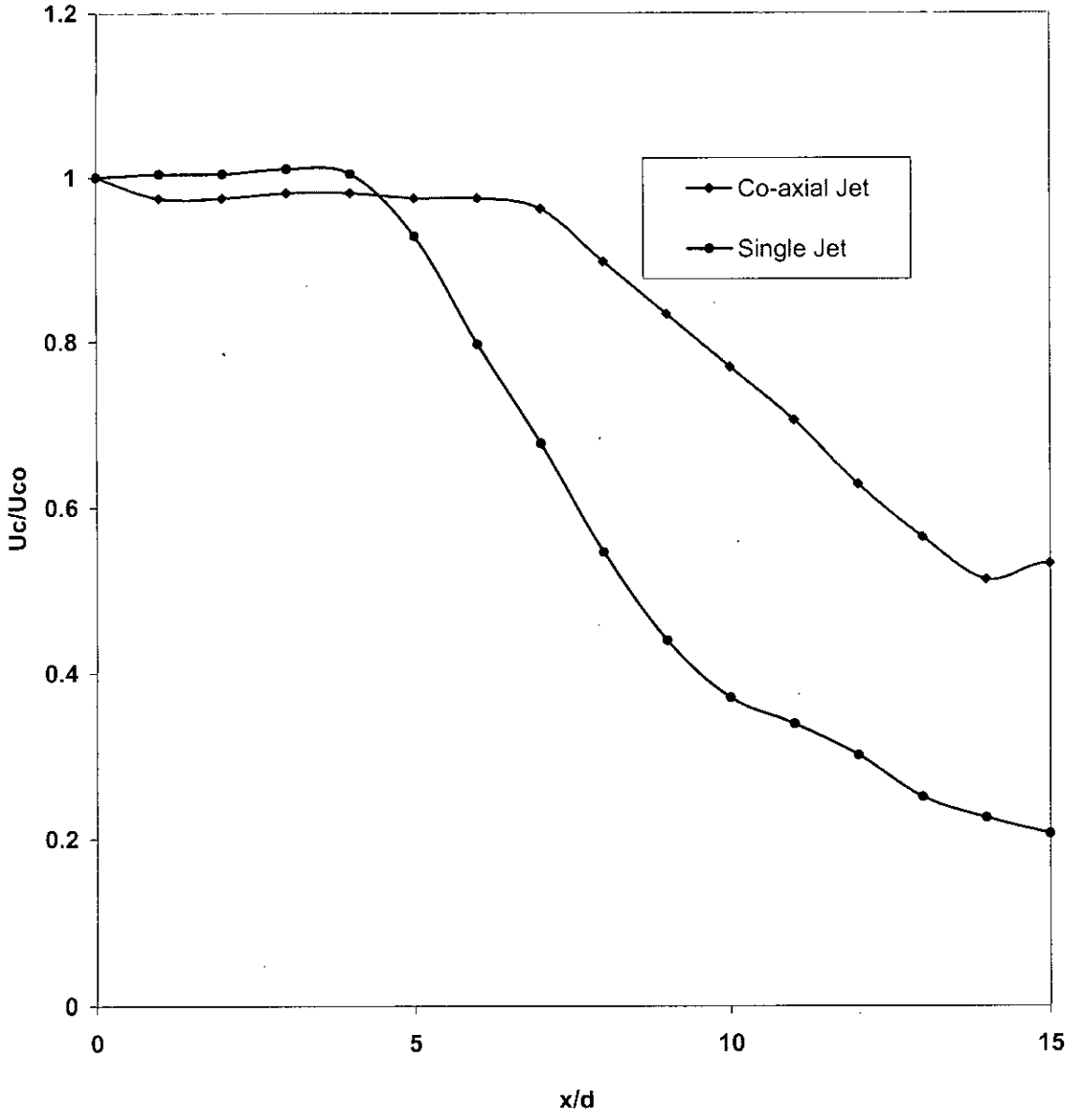

Fig. 5.3.7 : Centerline Velocity Profiles of Single Jet and Co-axial Jets(U_2/U_1=0.37)

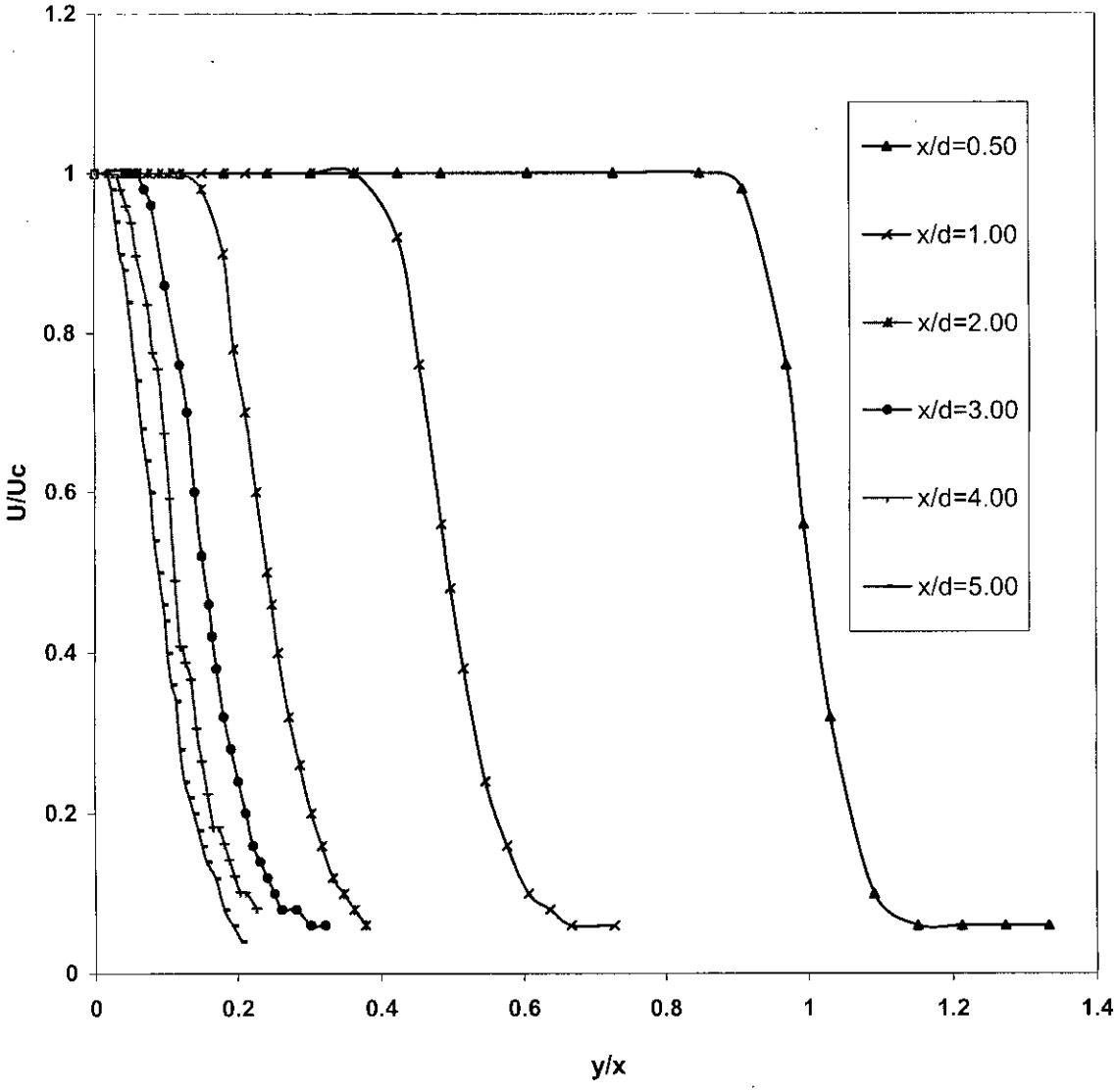

Fig 5.4.1: Sreamwise Evolution of Velocity Profiles of the 42 mmD Jet at Re=3.7x10^4

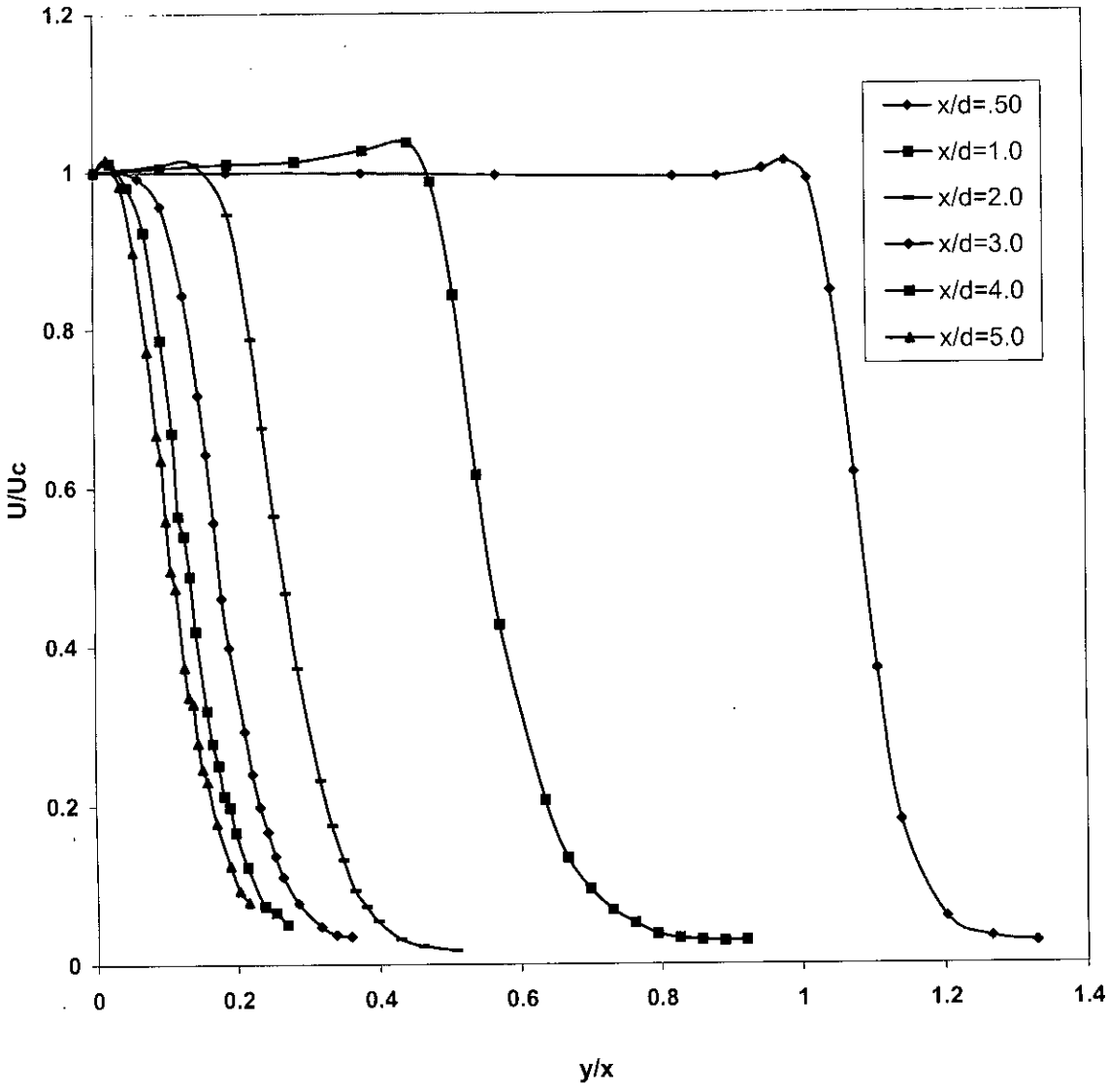

Fig. 5.4.2 Streamwise Evolution of Velocity Profiles of the 80 mmD Jet at Re = 5.3 x10^4

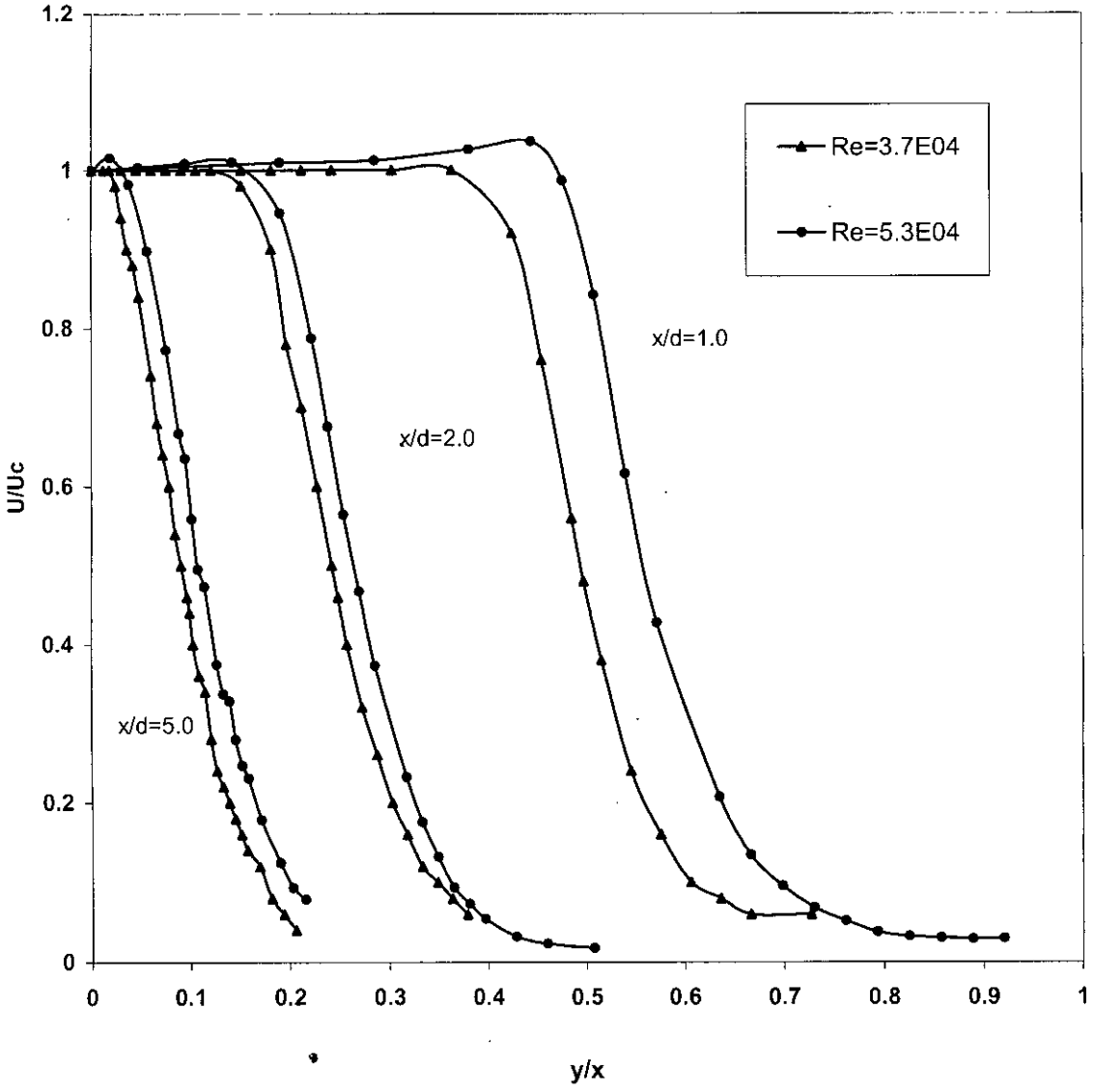

Fig:5.4.3 Effect of Reynolds Number on Streamwise Evolution of Velocity Profiles of Single Jets

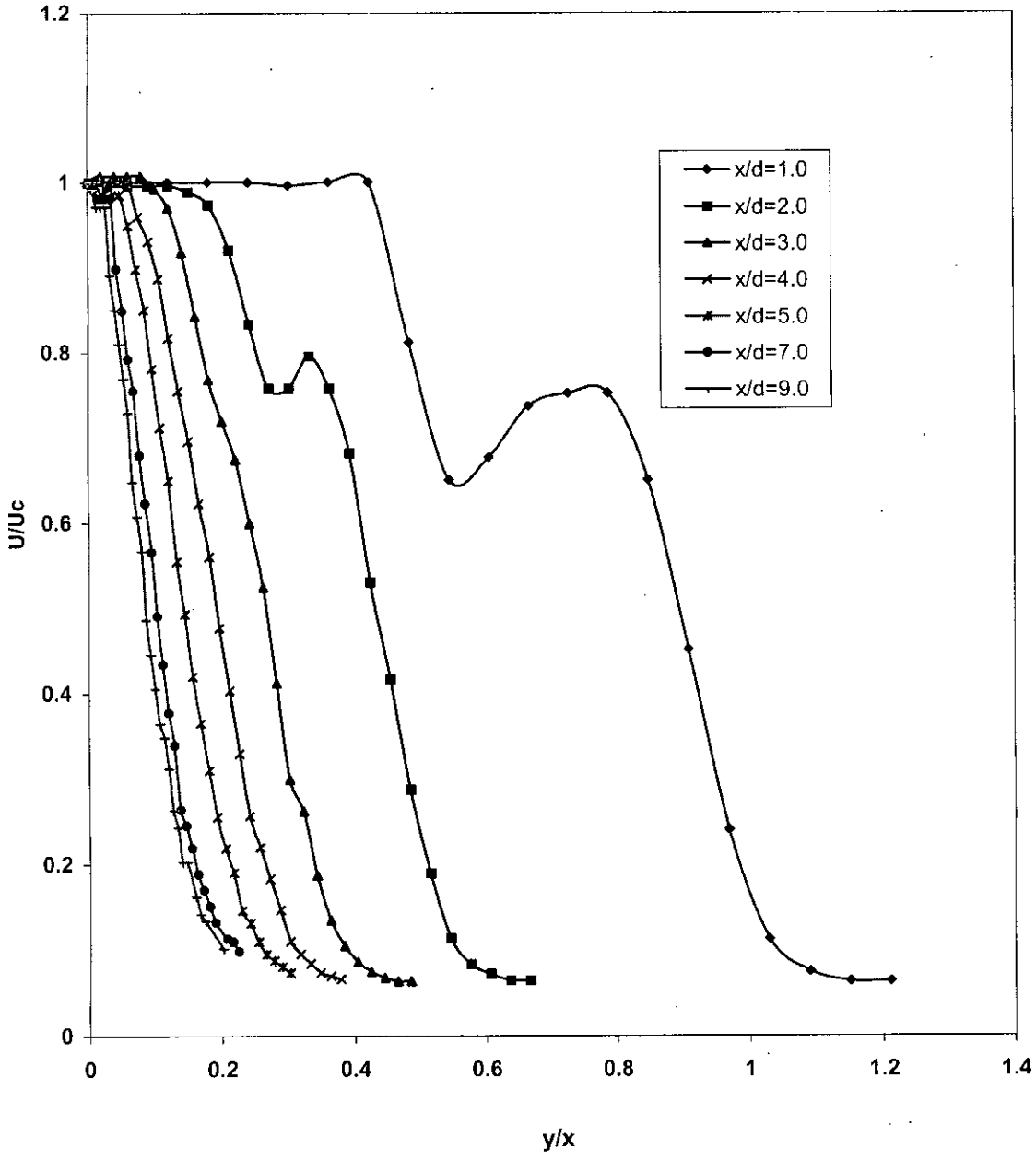

Fig 5.4.4 Evolution of Streamwise Velocity Profiles of Co-axial Jets of Area Ratio=2.61 and Velocity Ratio= 0.75 at Re=2.69x10^4

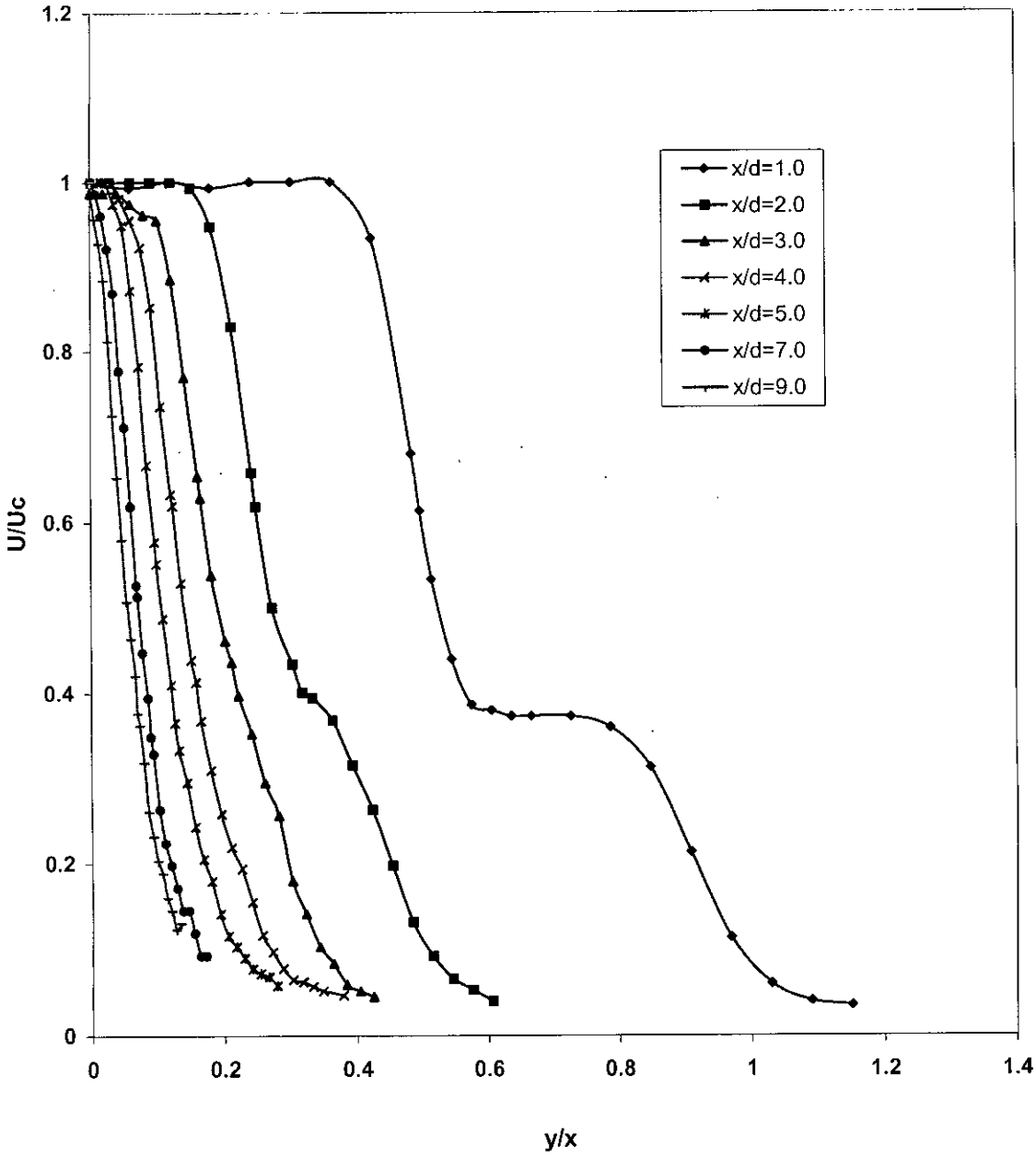

Fig 5.4.5 Evolution of Streamwise Velocity Profiles of Co-axial Jets of Area Ratio=2.61 and Velocity Ratio= 0.37at Re=2.69x10^4

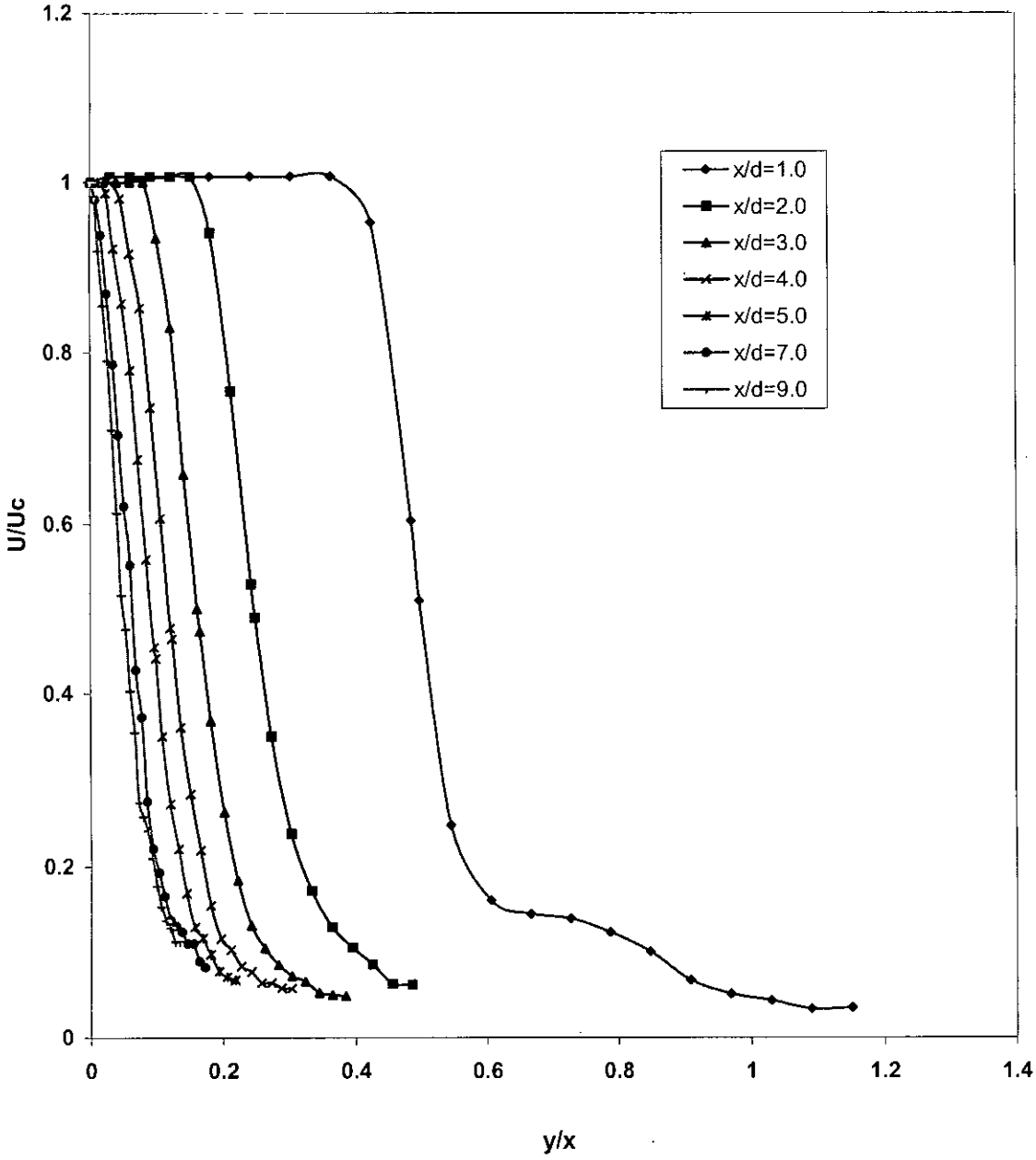

Fig 5.4.6 Evolution of Streamwise Velocity Profiles of Co-axial Jets of Area Ratio=2.61 and Velocity Ratio= 0.15at Re=2.69x10^4

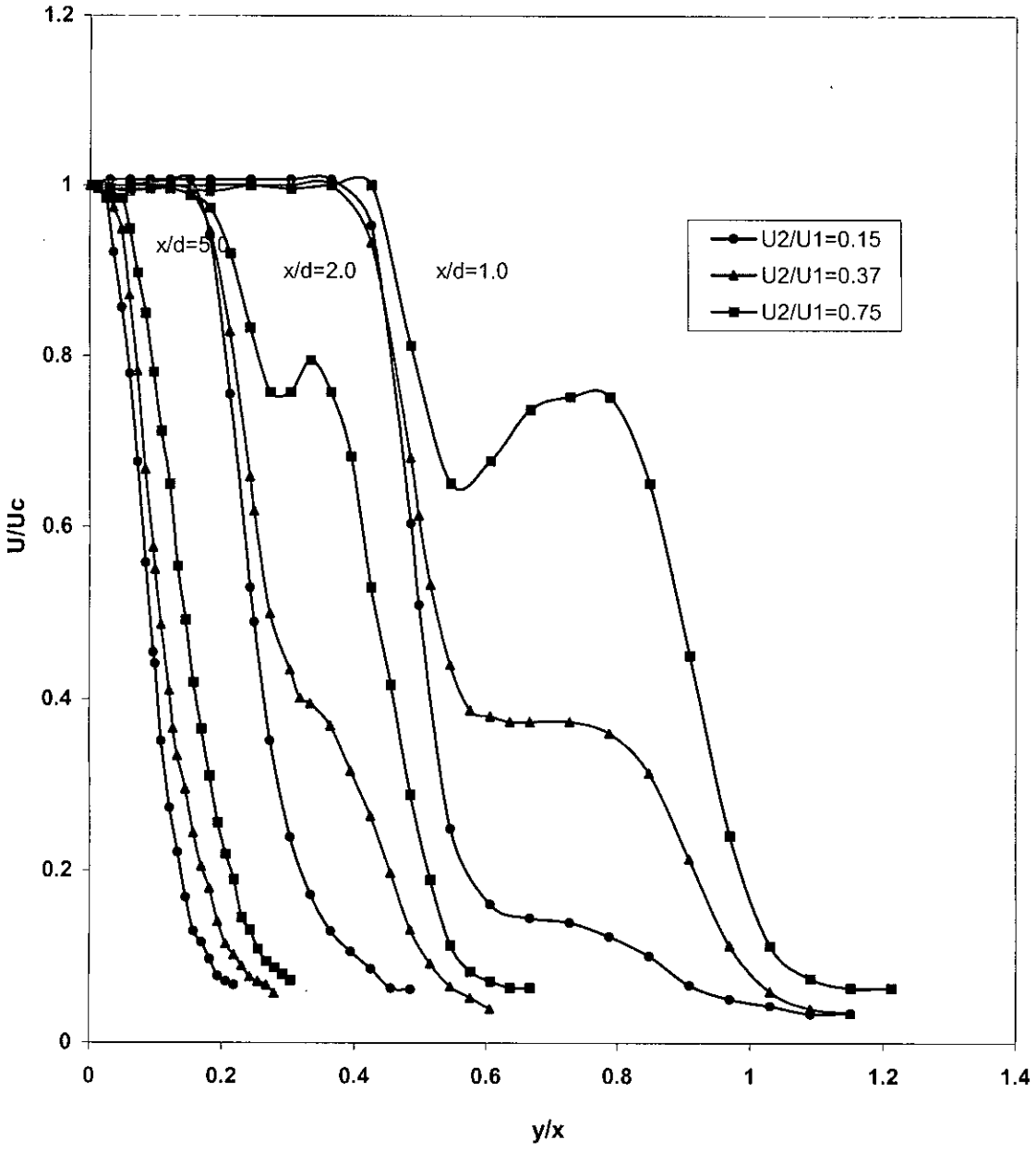

Fig 5.4.7 Effect of Velocity Ratio on Streamwise Velocity Profiles of Co-axial Jets of Area Ratio=2.61 at Re=2.69x10^4

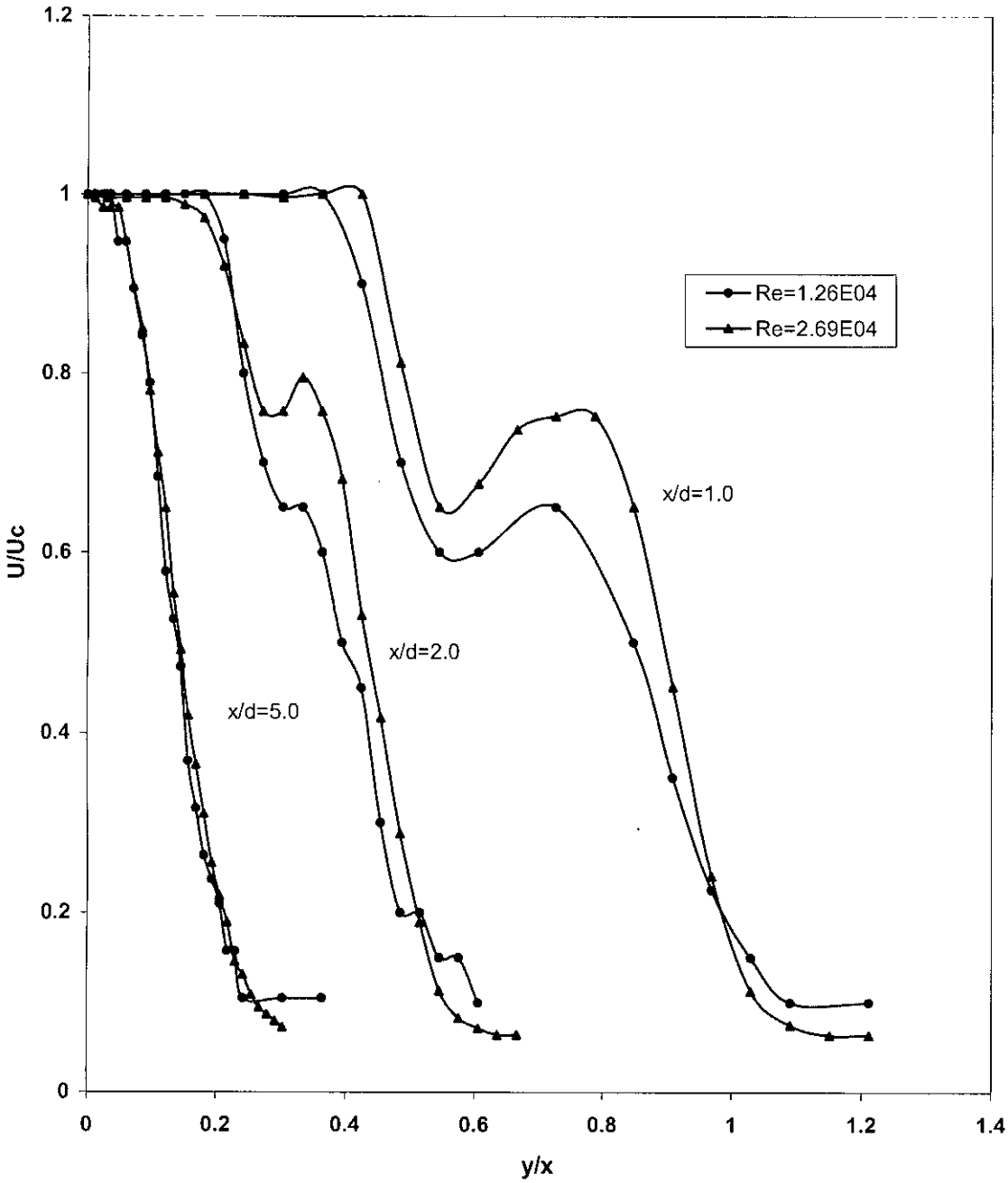

Fig 5.4.8 : Effects of Reynolds Number on Streamwise Evolution of Velocity Profiles for Area Ratio=2.61 at U_2/U_1=0.75

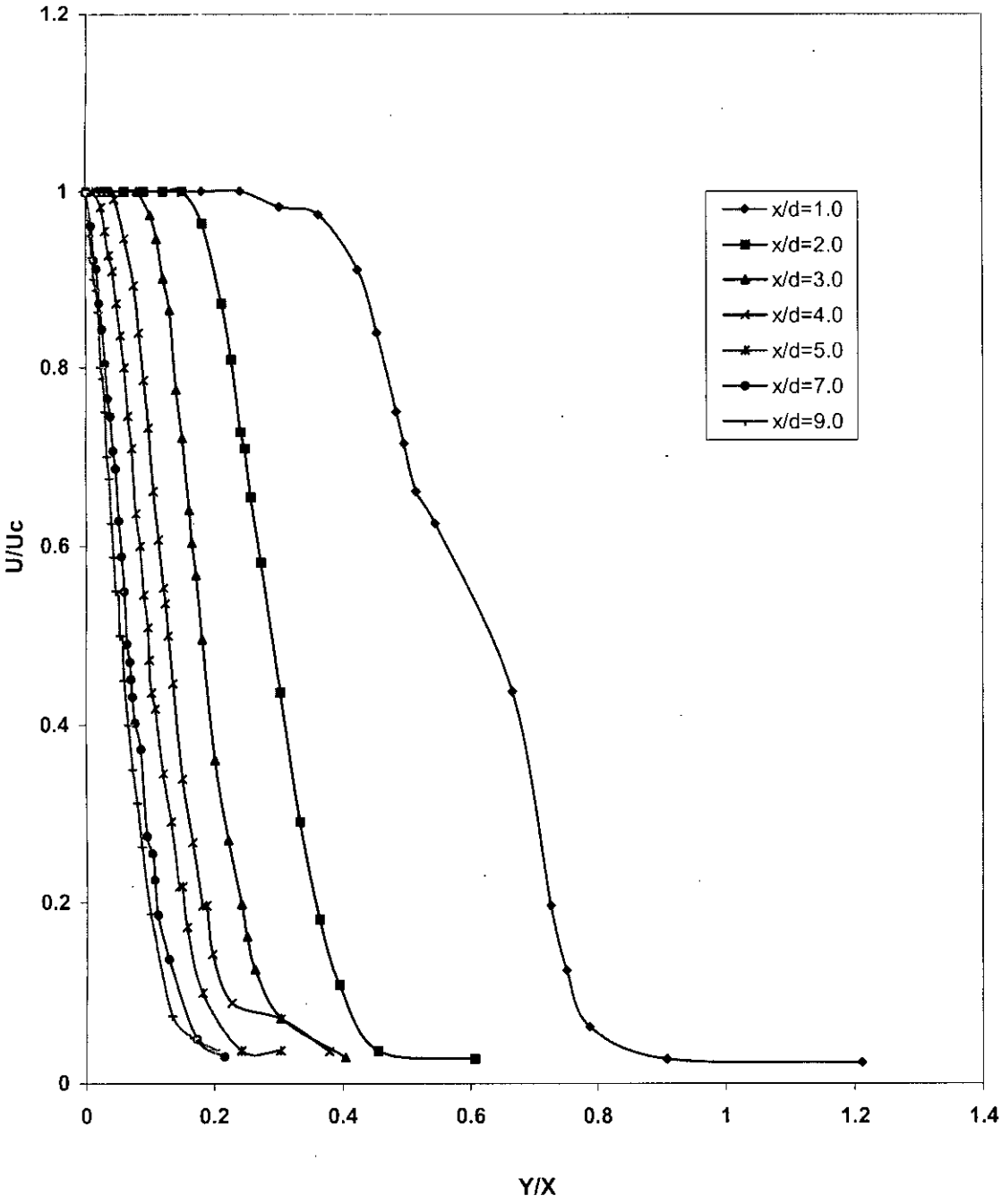

Fig 5.4.9: Streamwise Evolution of Velocity Profiles for Area Ratio=1.25 at U_2/U_1=0.75 and Re=4x10^4

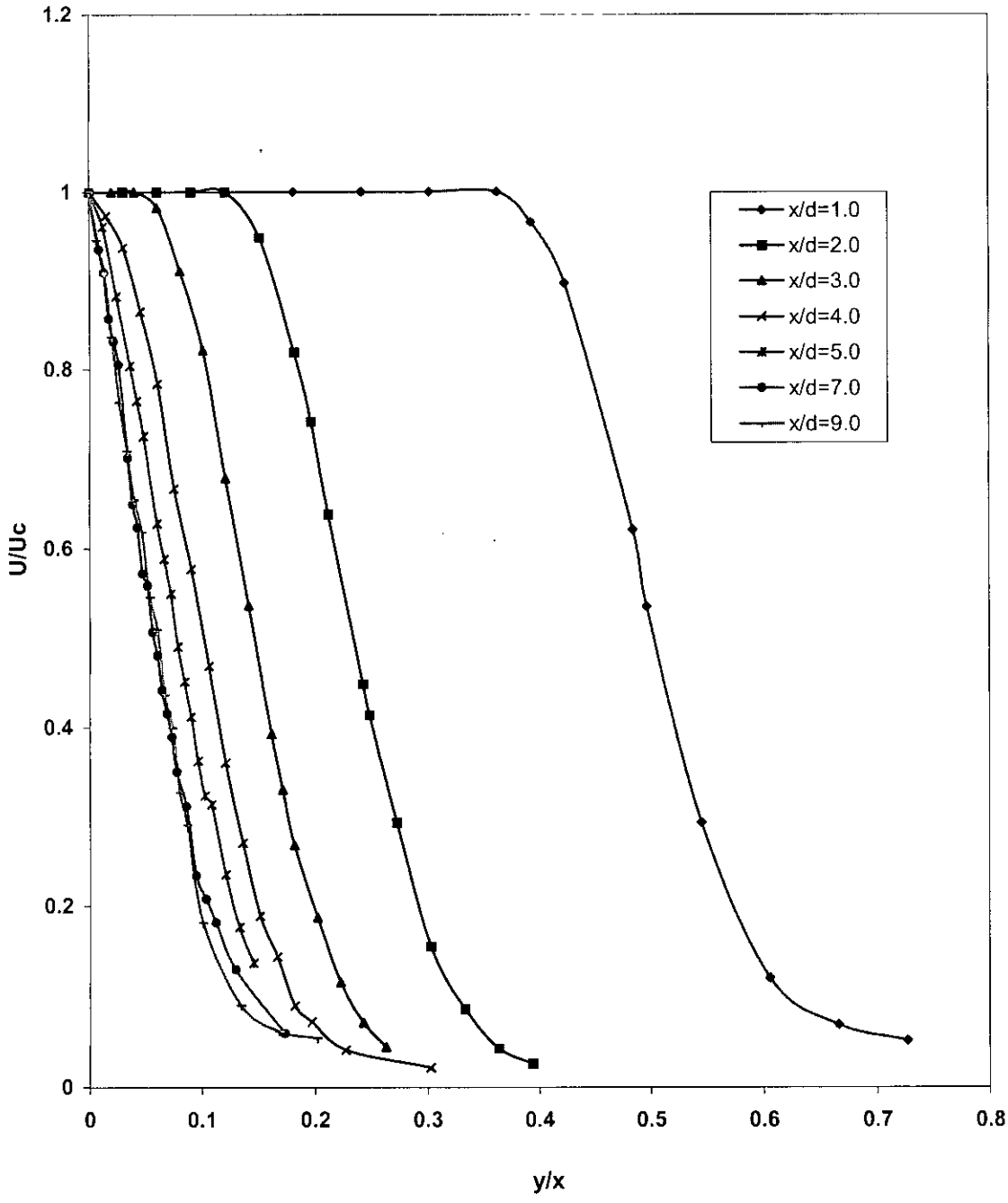

Fig 5.4.10: Streamwise Evolution of Velocity Profiles for Area Ratio=0.56 at U_2/U_1=0.75 and Re=4x10^4

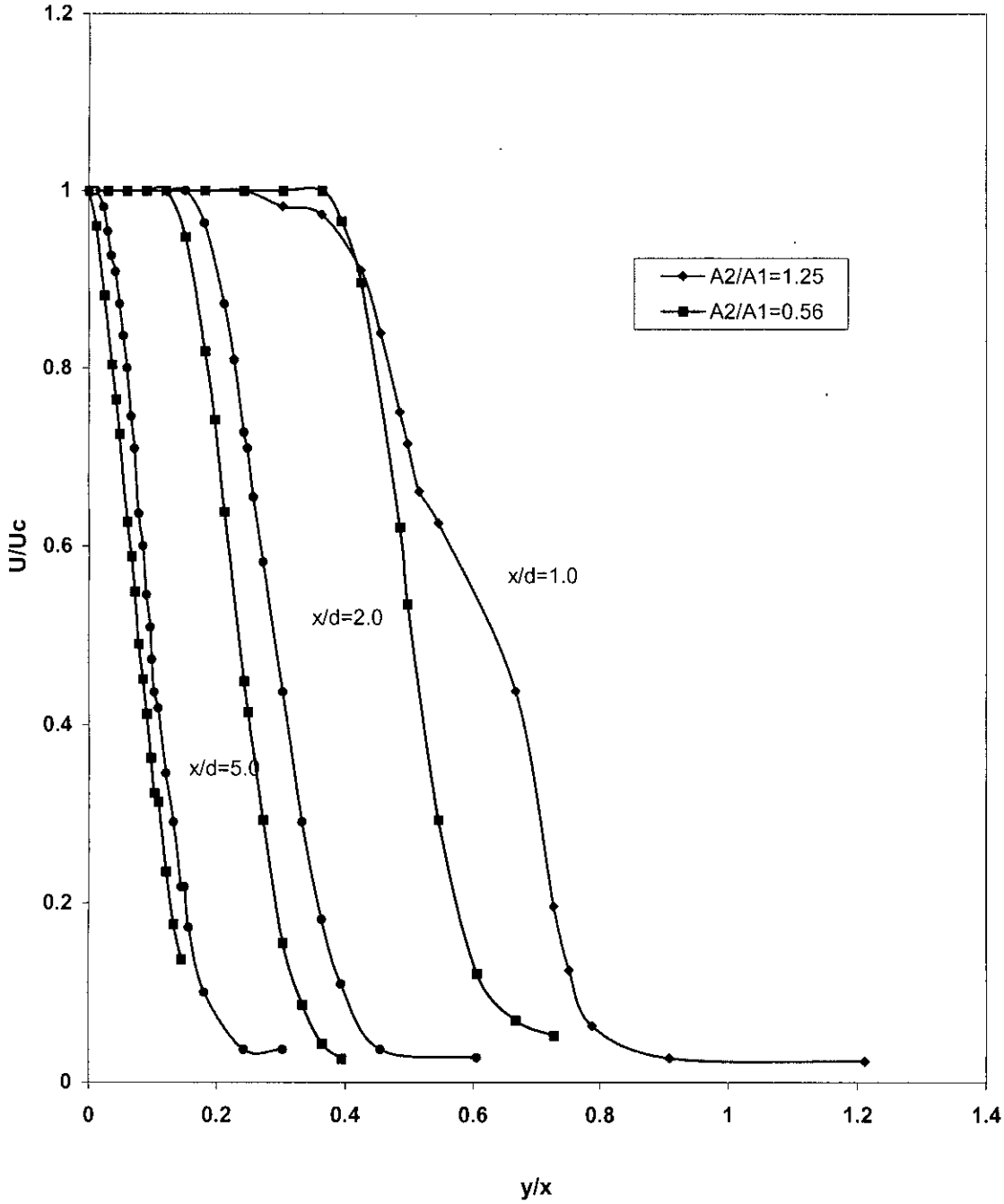

Fig 5.4.11: Effect of Area Ratio(A_2/A_1) on Streamwise Velocity Profiles at U_2/U_1=0.75 and Re=4x10^4

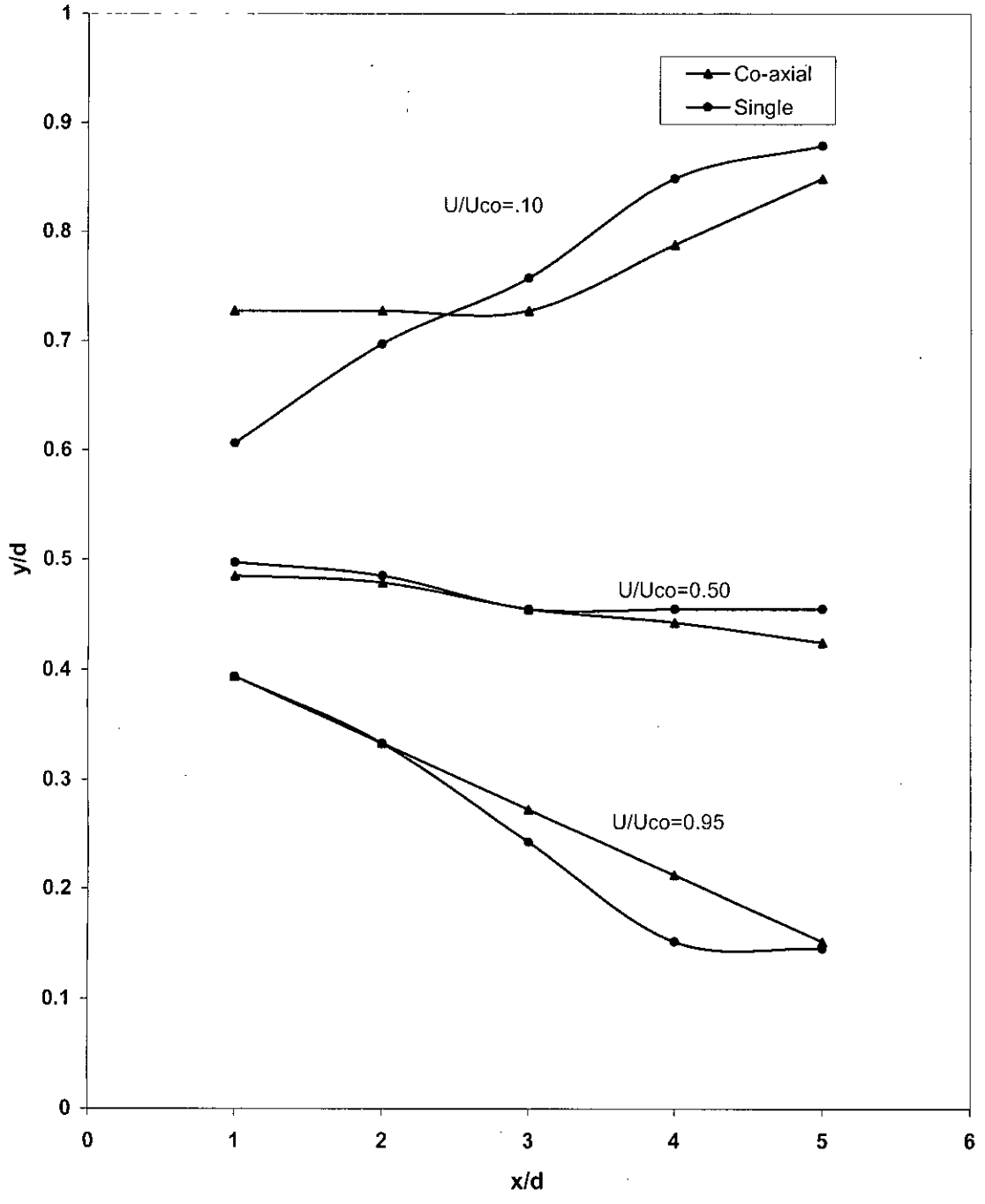

Fig 5.5.1 : **Comparison of Iso-Velocity Lines of Co-axial Jet and Single Jet**

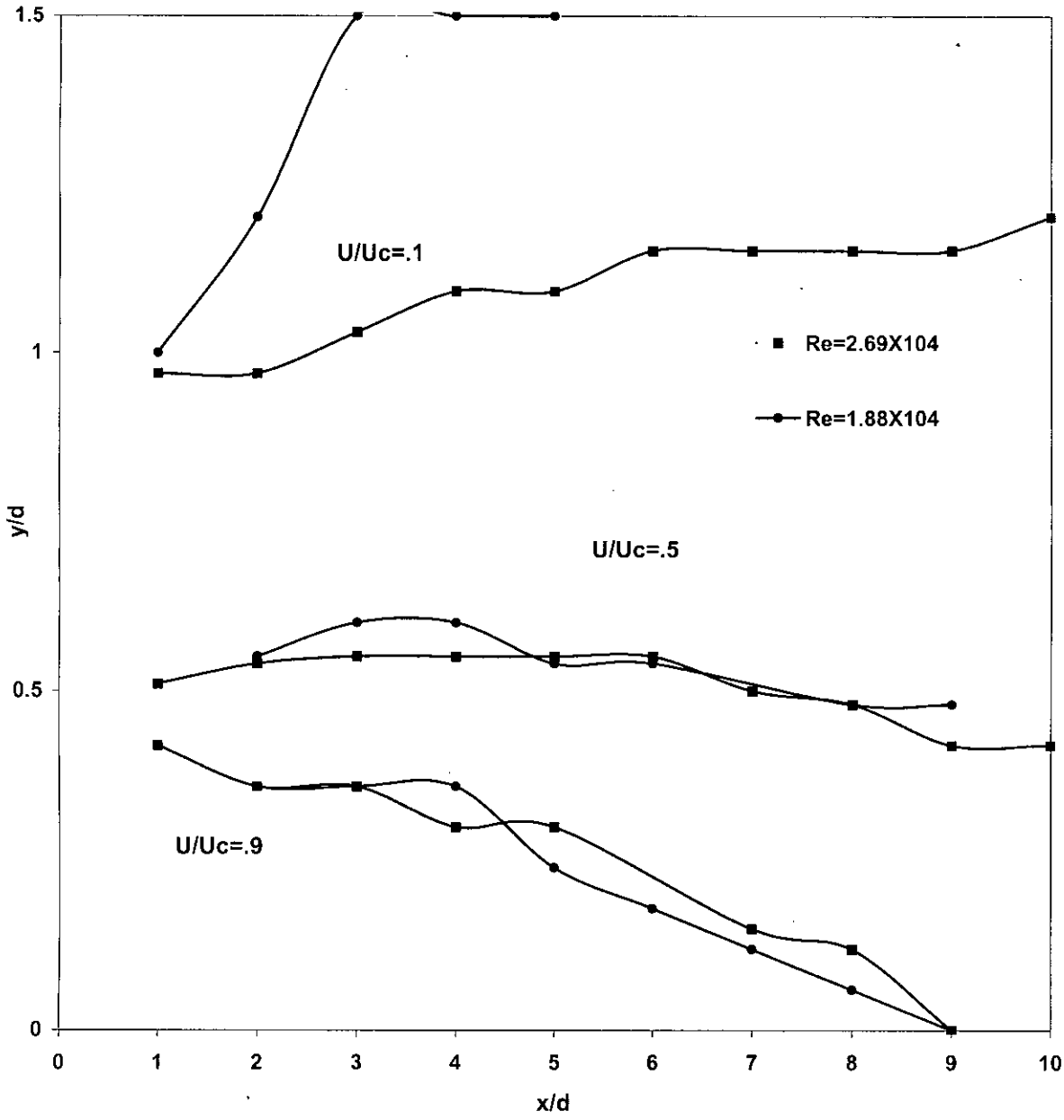

Fig5.5.2 Effect of Re on Iso-Velocity Lines at Area Ratio=2.61

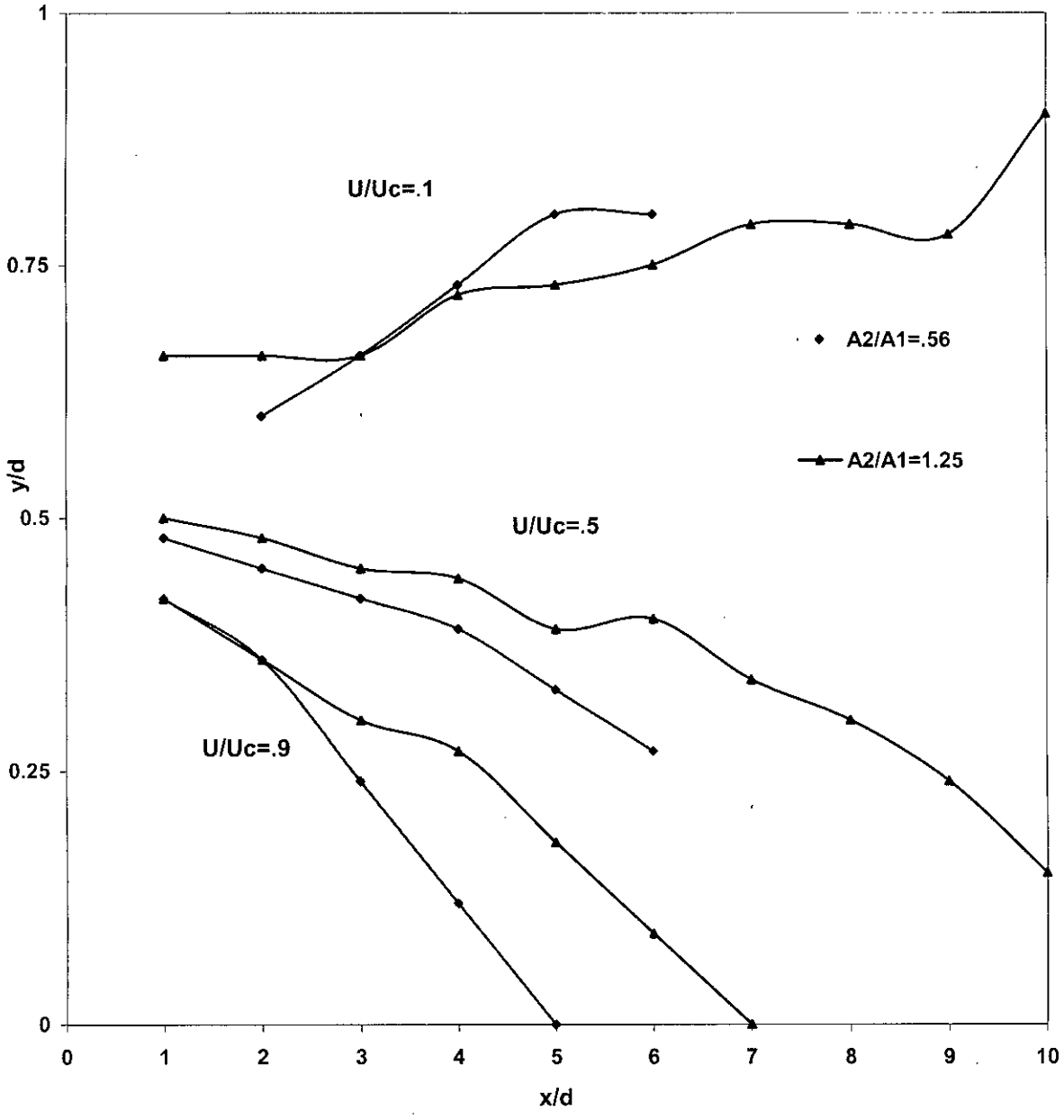

Fig 5.5.3: Effect of Area Ratio(A_2/A_1) on Iso-Velocity Lines at Re=$4X10^4$

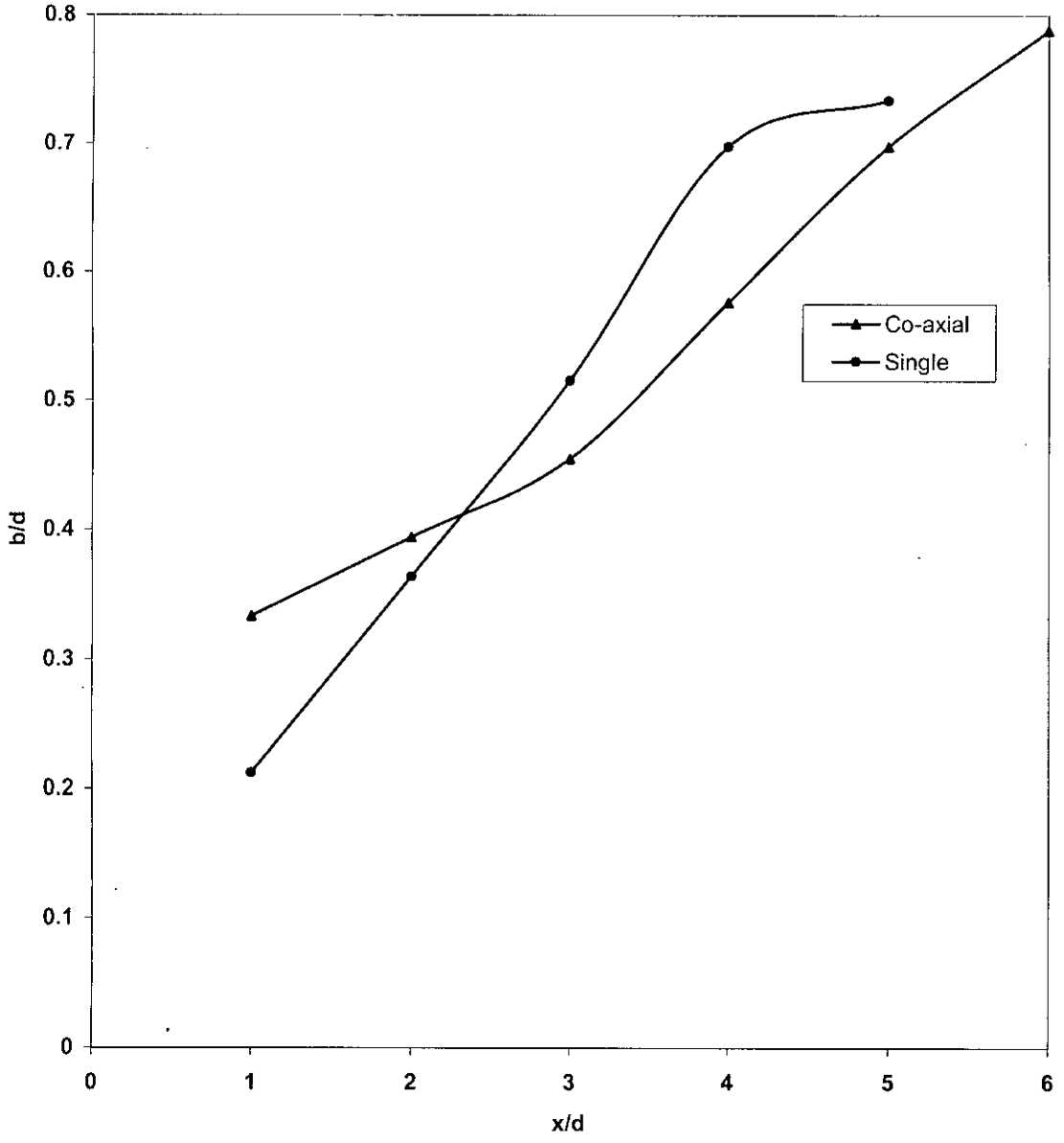

Fig 5.5.4 : **Comparison of Shear Layer Width of Co-axial Jet and Single Jet**

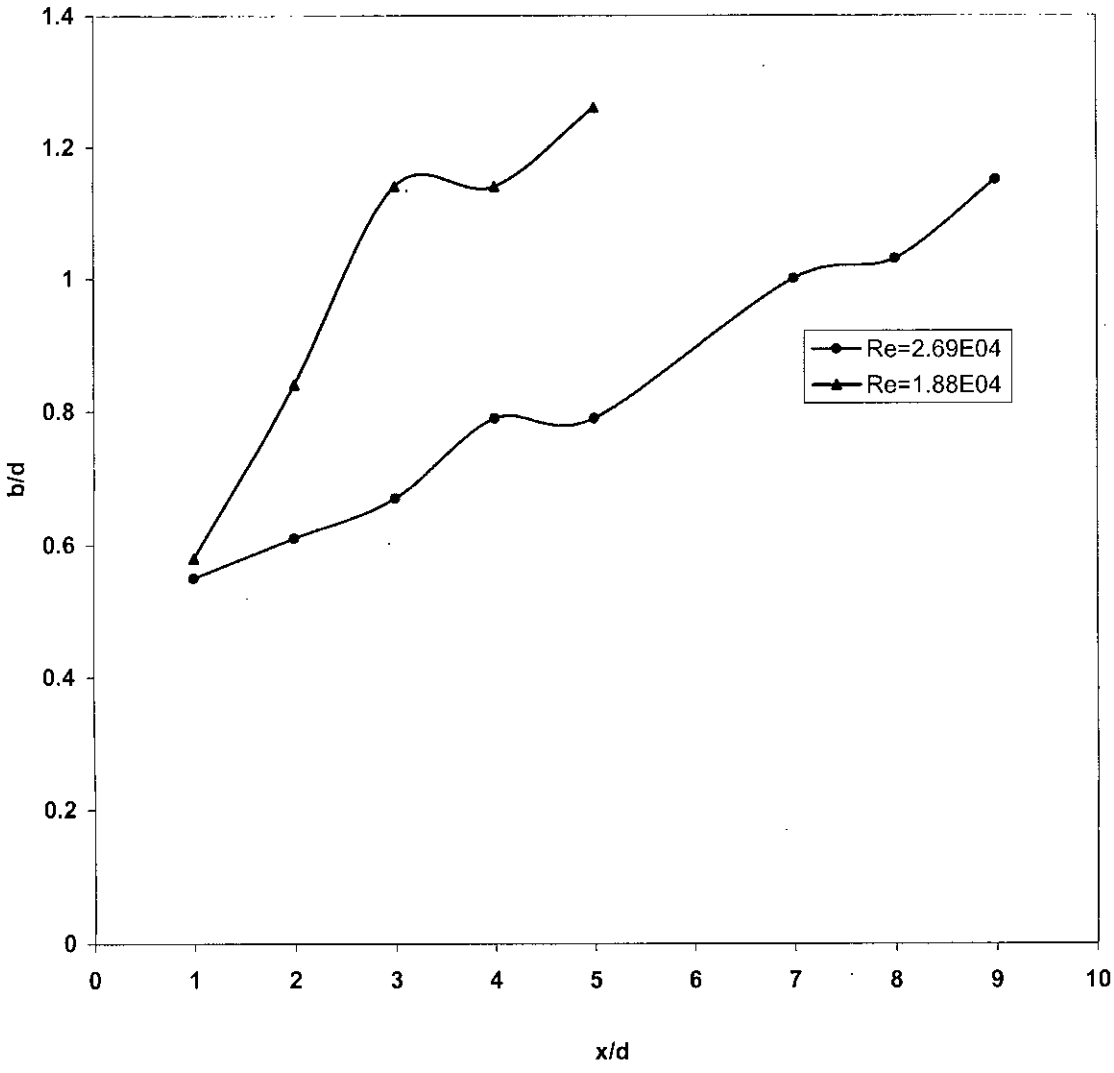

Fig 5.5.5 : Effect of Reynolds Number on the Shear Layer Width of Co-axial Jets at Area Ratio=2.61

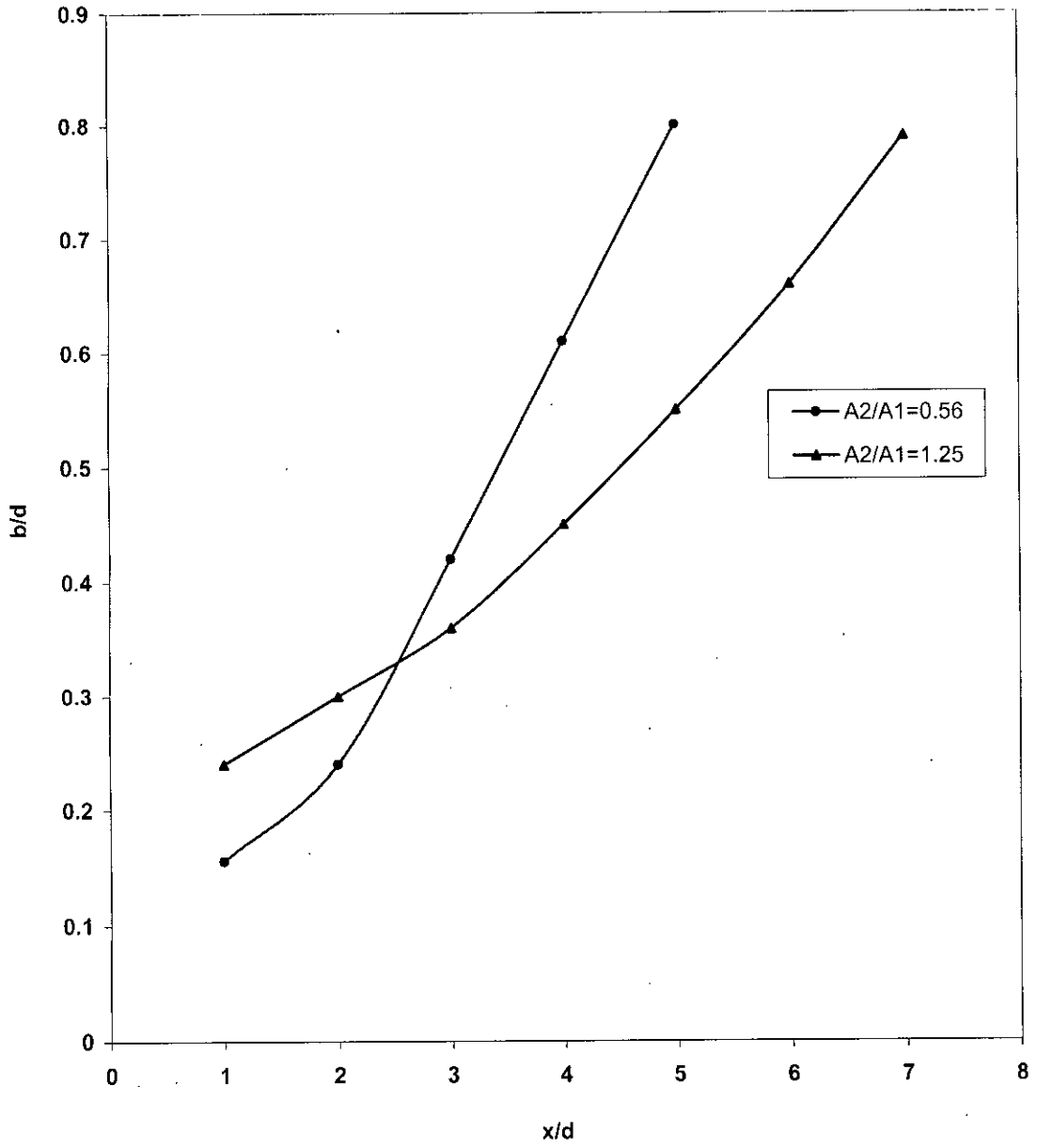

Fig5.5.6 : Effect of Area Ratio (A_2/A_1) on Shear Layer Width at Re=$4x10^4$

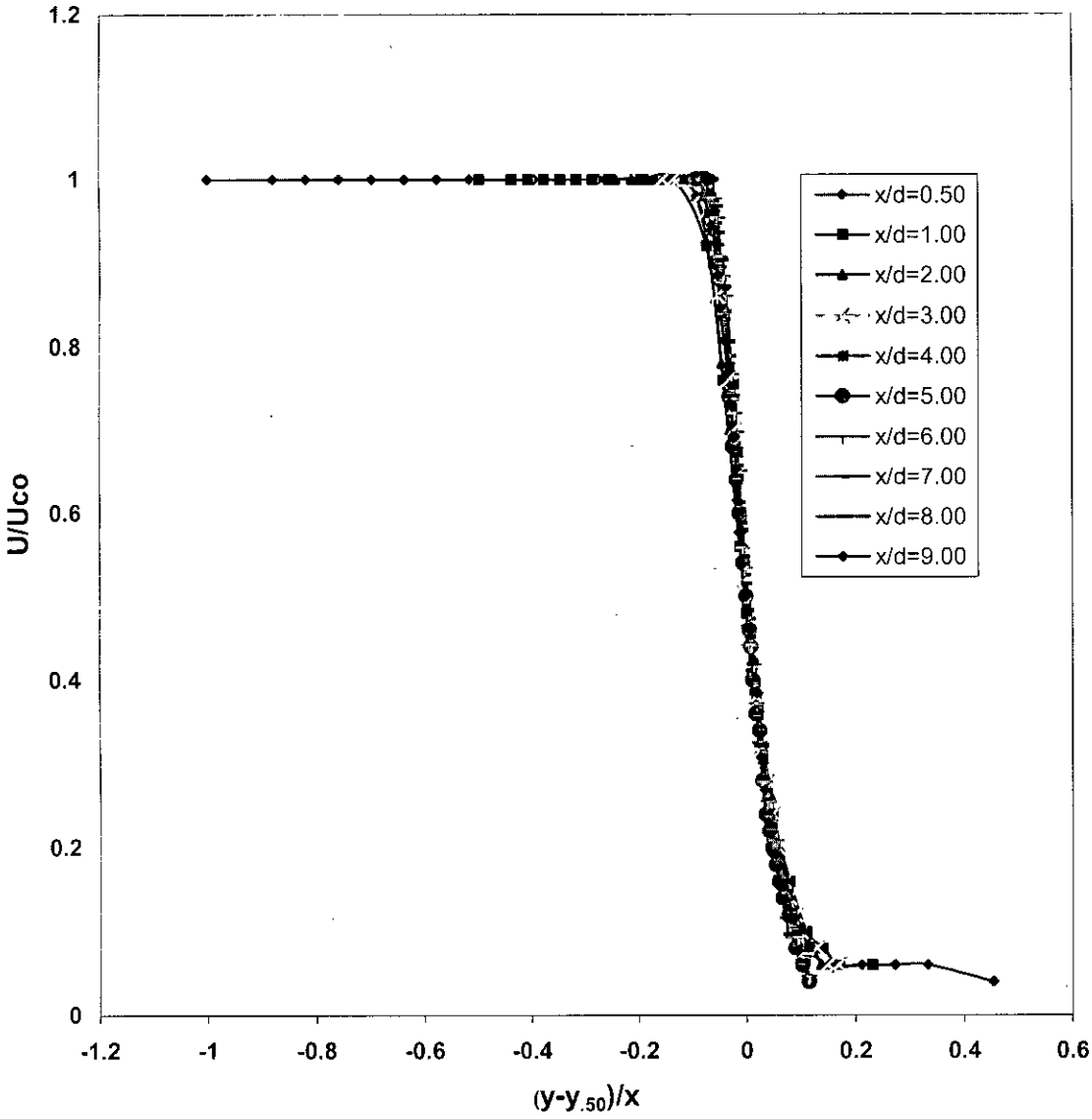

Fig 5.6.1 : Self-Preservation of Velocity Profiles for Single Jet at Re=3.7x10^4

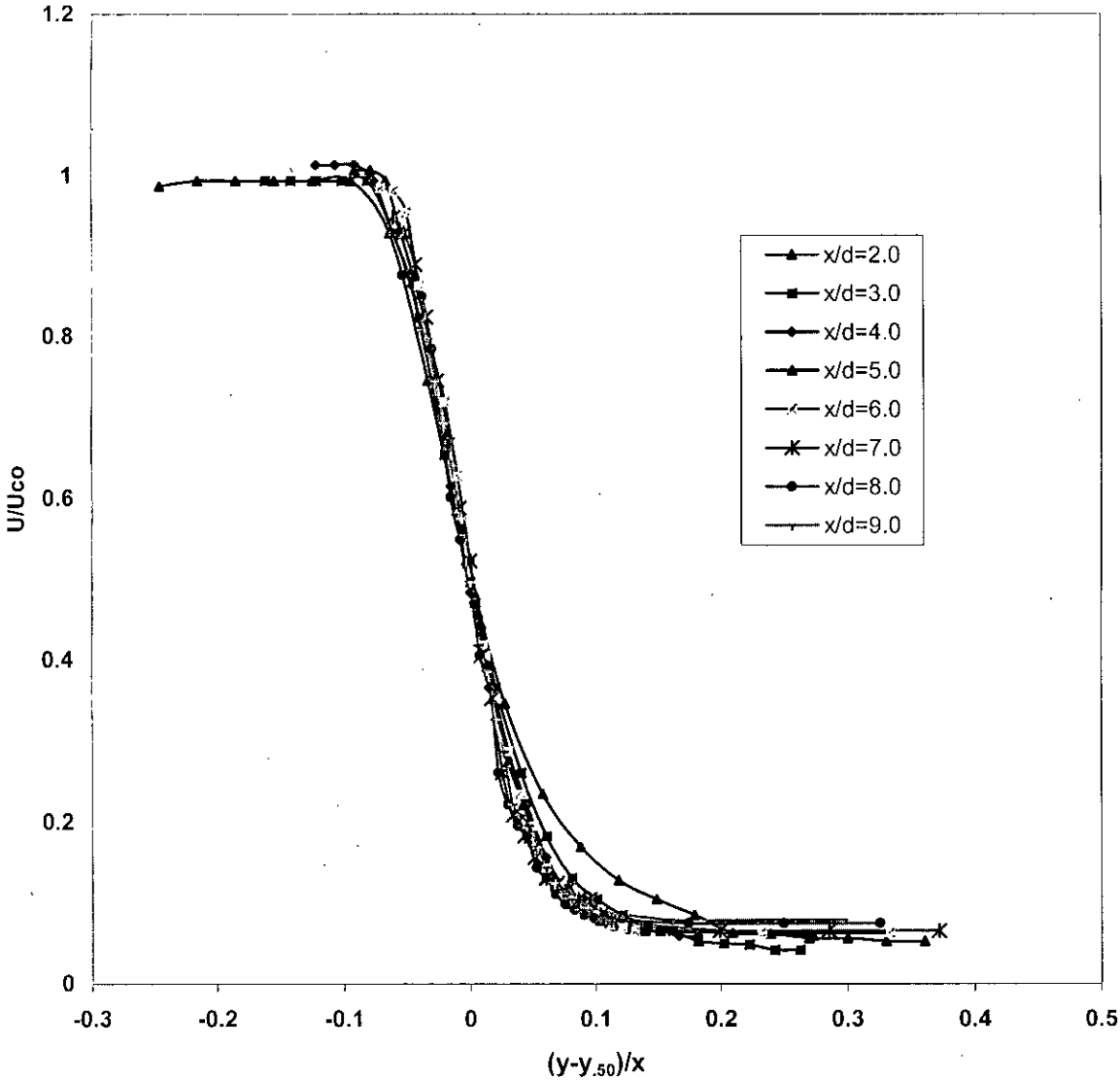

Fig 5.6.2 : Self-Preservation of Velocity Profiles of Co-axial Jets of A_2/A_1=2.61 at U_2/U_1=0.15 and Re=2.69x10^4

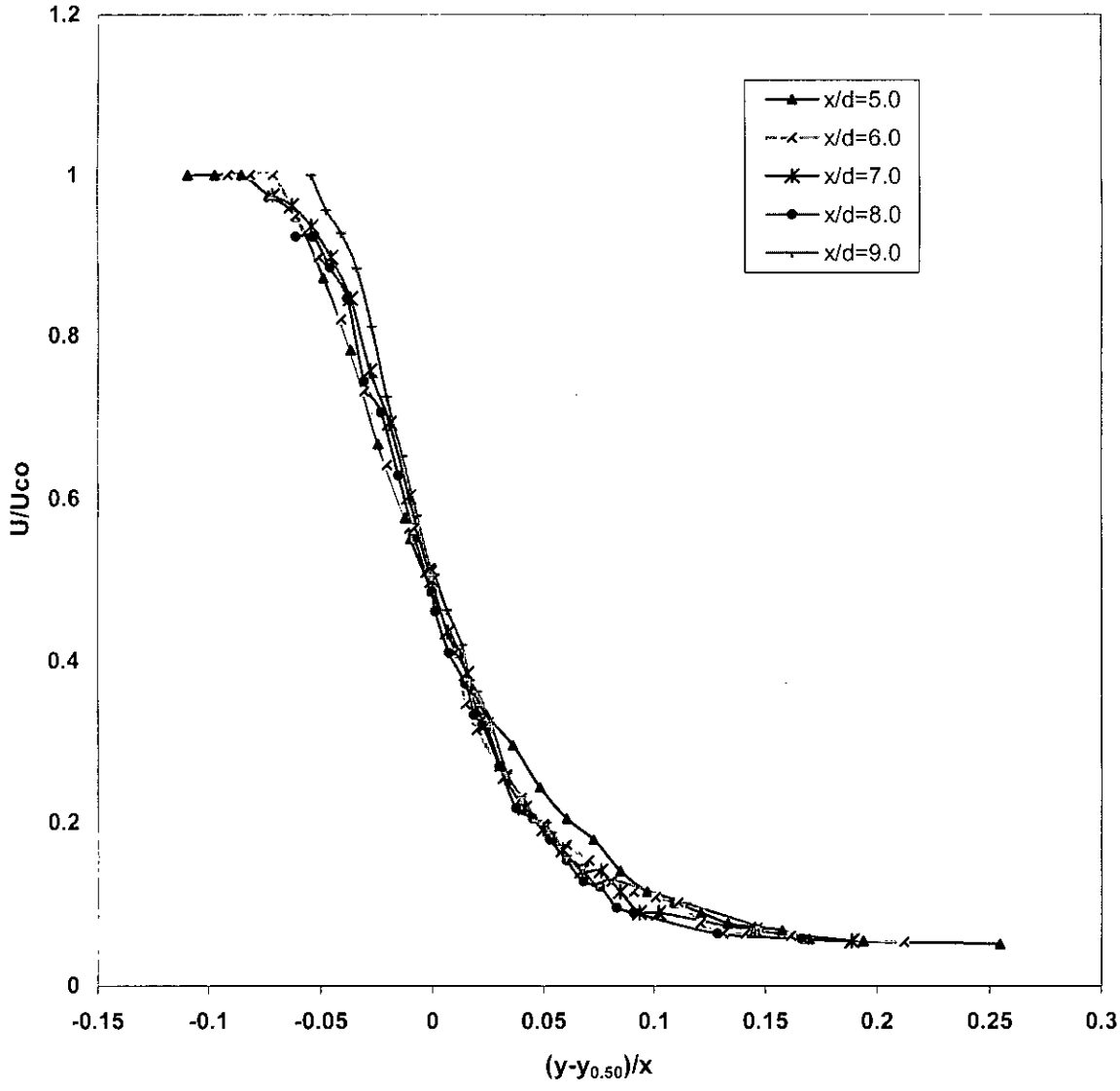

Fig 5.6.3 : Self-Preservation of Velocity Profiles of Co-axial Jets of A_2/A_1=2.61 at U_2/U_1=0.37 and Re=2.69x10^4

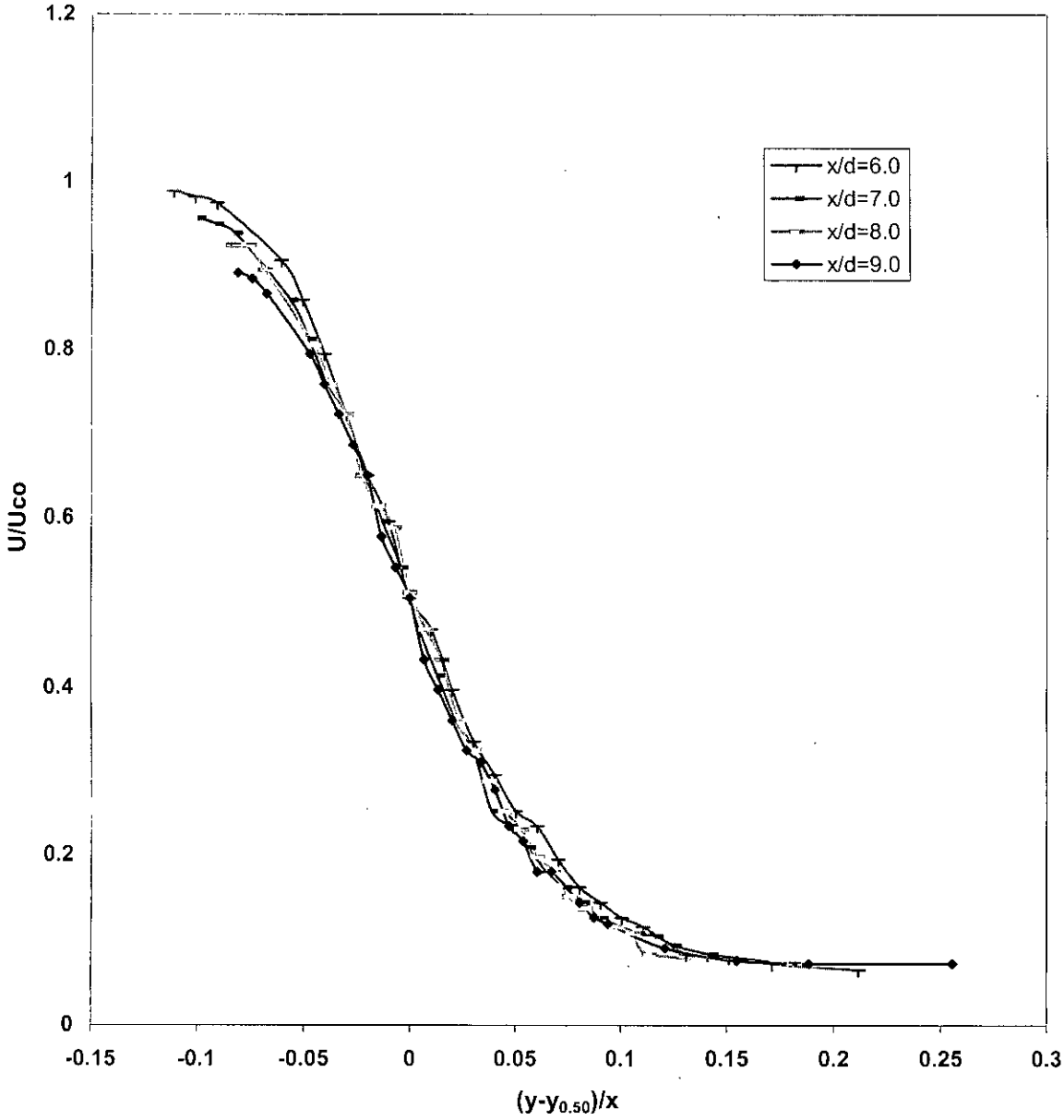

Fig 5.6.4 : Self-Preservation of Velocity Profiles of Co-axial Jets of A_2/A_1=2.61 at U_2/U_1=0.75 and Re=2.69x10^4

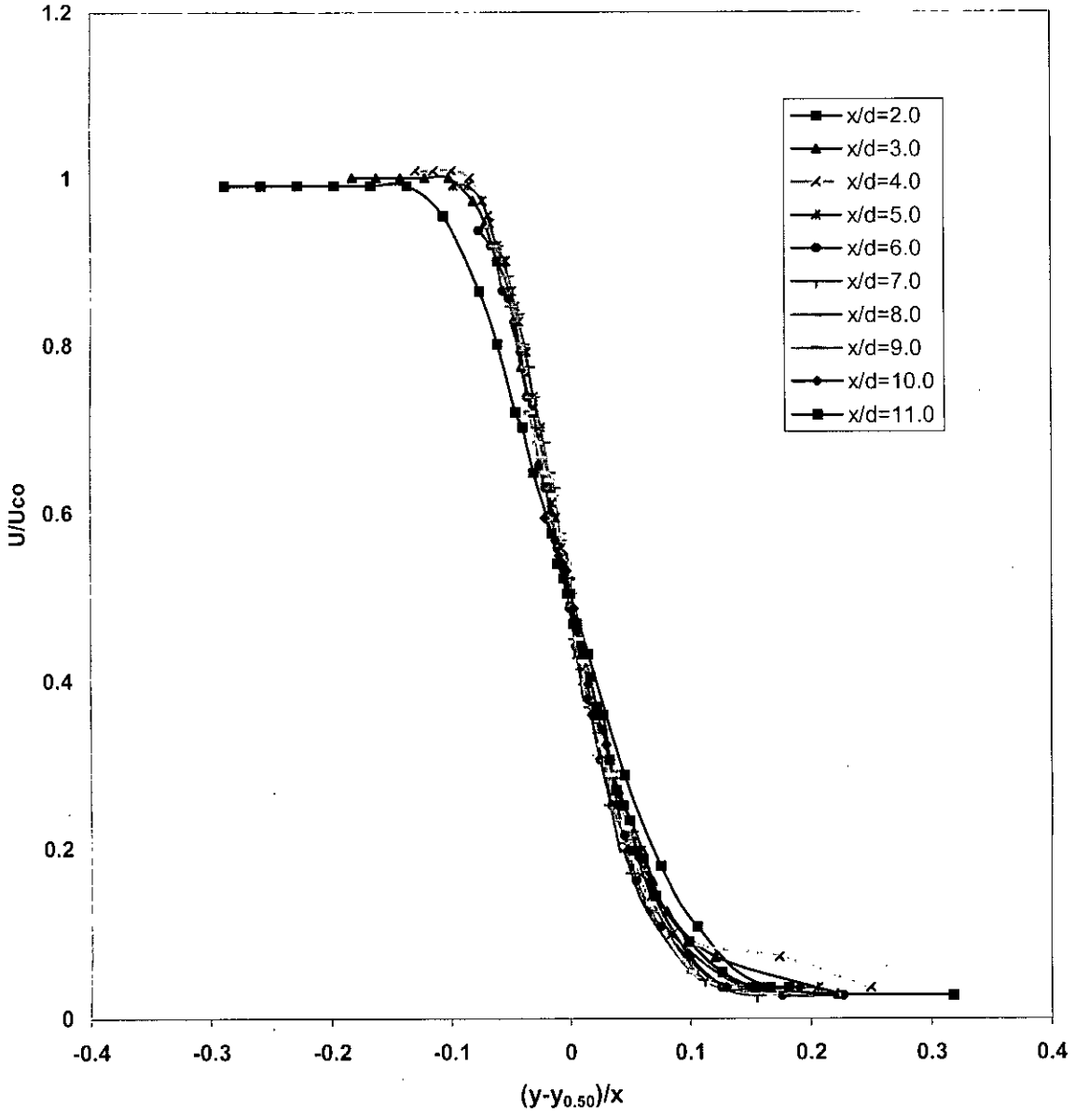

Fig 5.6.5: Self-Preservation of Velocity Profiles of Co-axial Jets of Area Ratio A_2/A_1=1.25 at U_2/U_1=0.75 and at Re=4x10^4

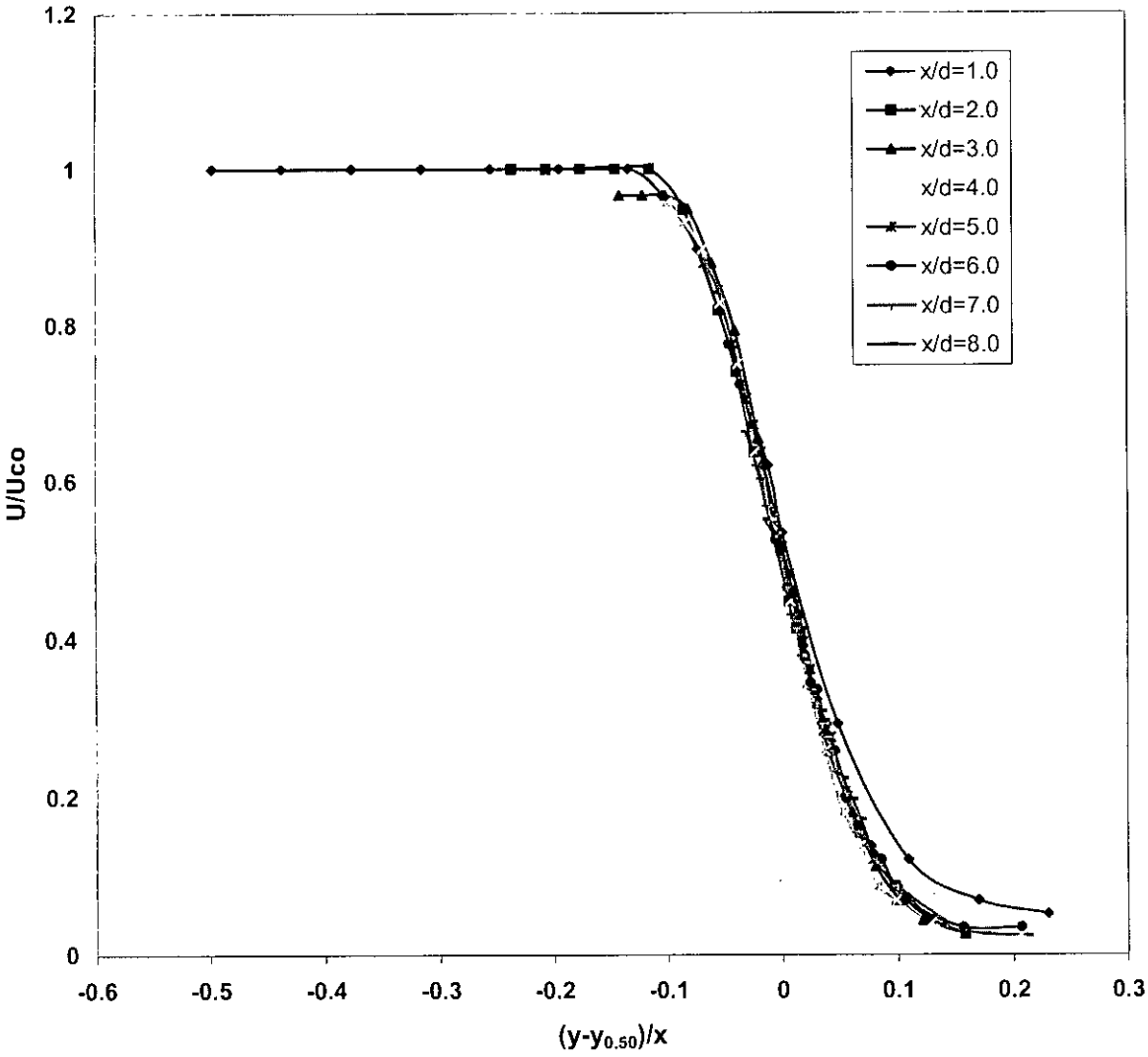

Fig. 5.6.6: Self-Preservation of Velocity Profiles of Co-axial Jets of Area Ratio(A_2/A_1) =0.56 at U_2/U_1=0.75 and Re=4x10^4

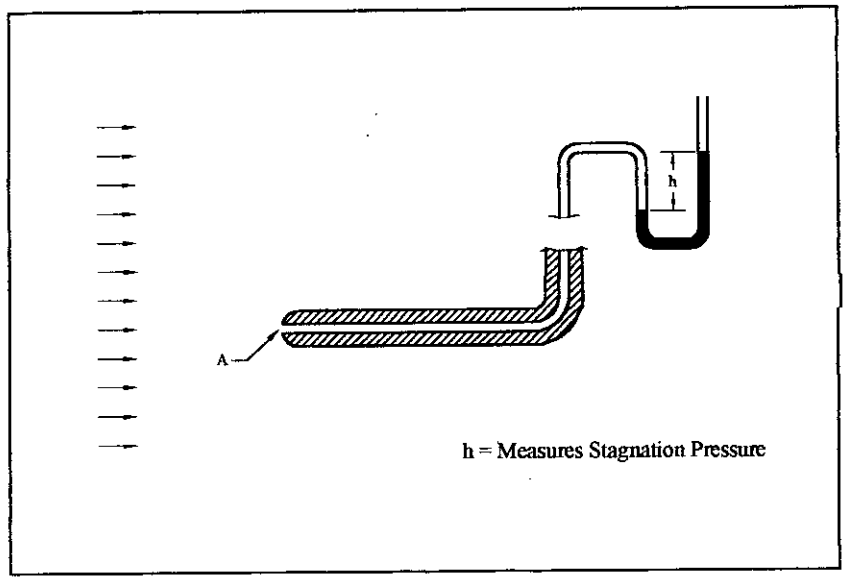

Fig. A.2.1 : Schematic Diagram of a Simple Pitot Tube.

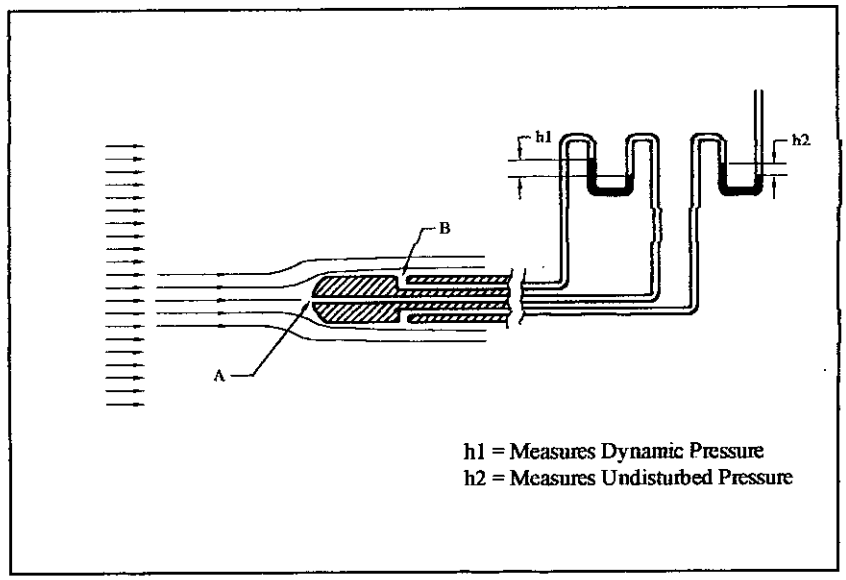

Fig. A.3.1. : Schematic Diagram of a Pitot-Satic Tube.

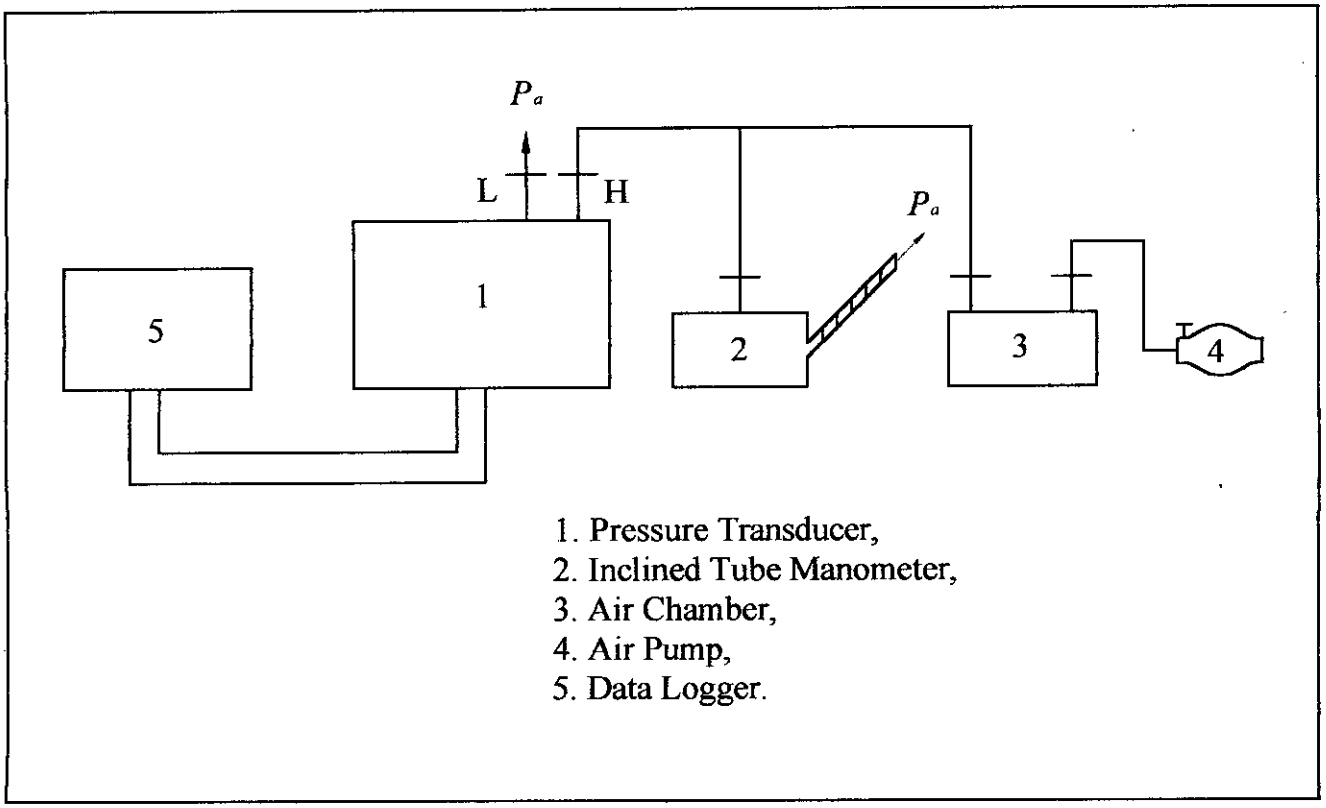

Fig. B.2.1. : Schematic Diagram of Pressure Tranducer Calibration.

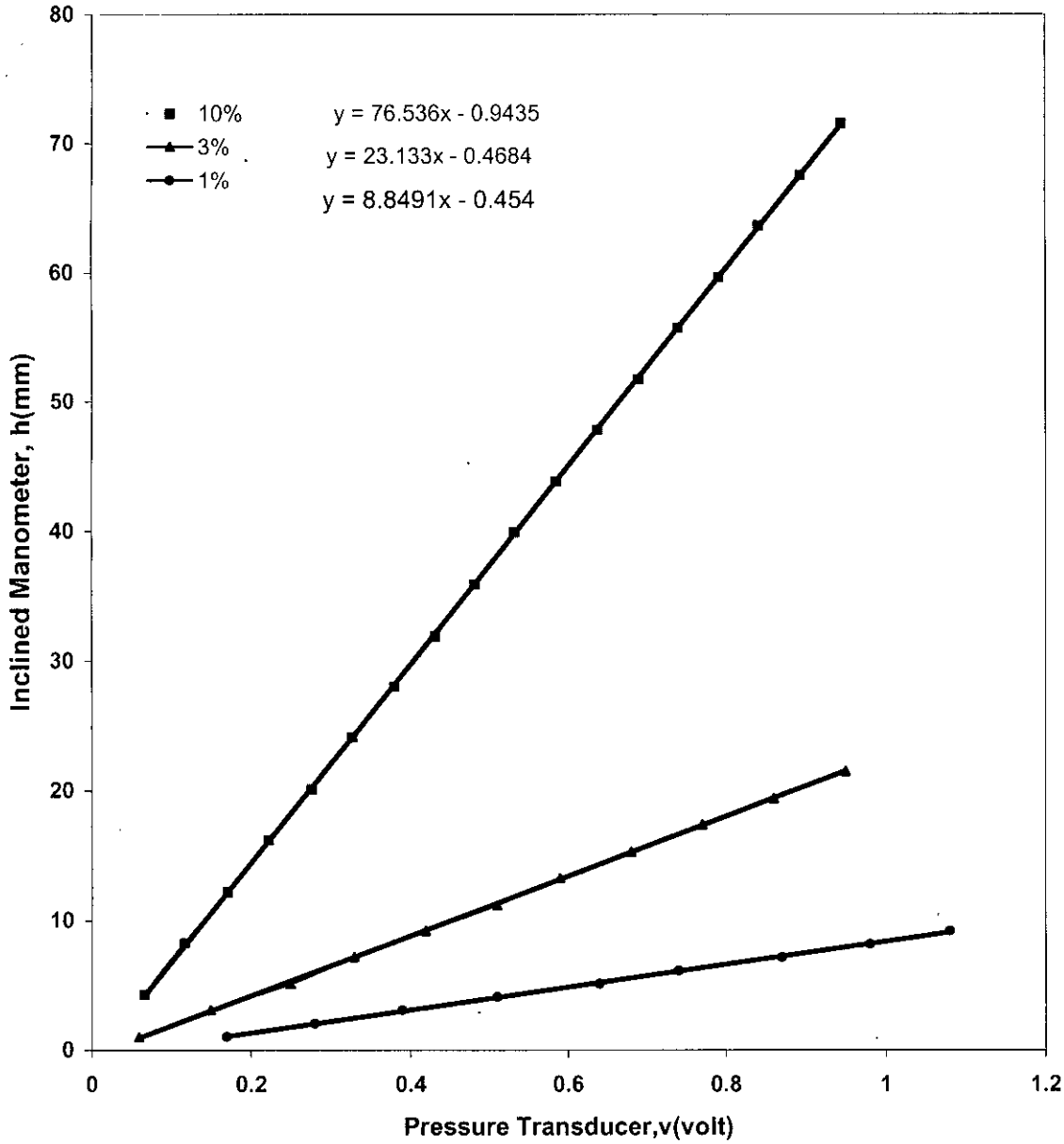

Fig B.2.2 : Calibration Curves of the Pressure Transducer

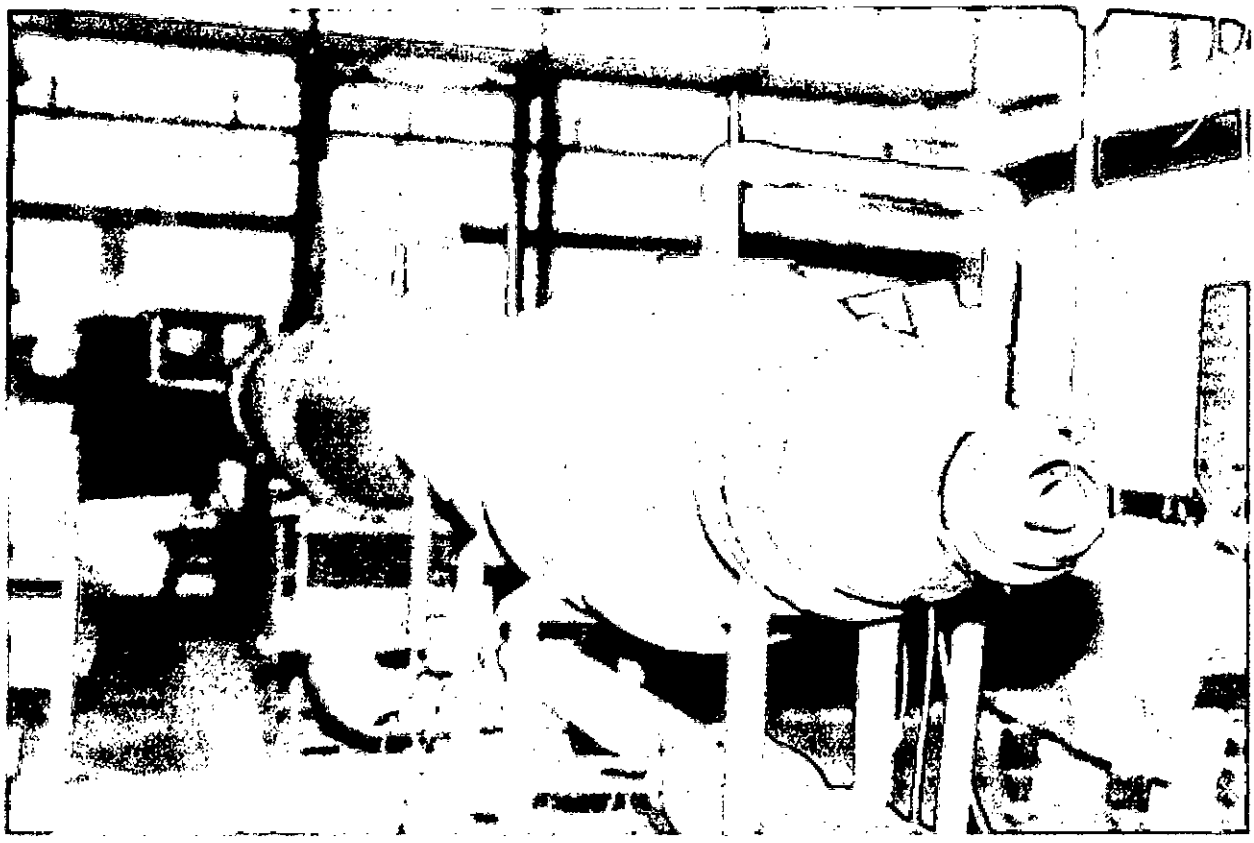

P.1 Co-axial Jet Flow System

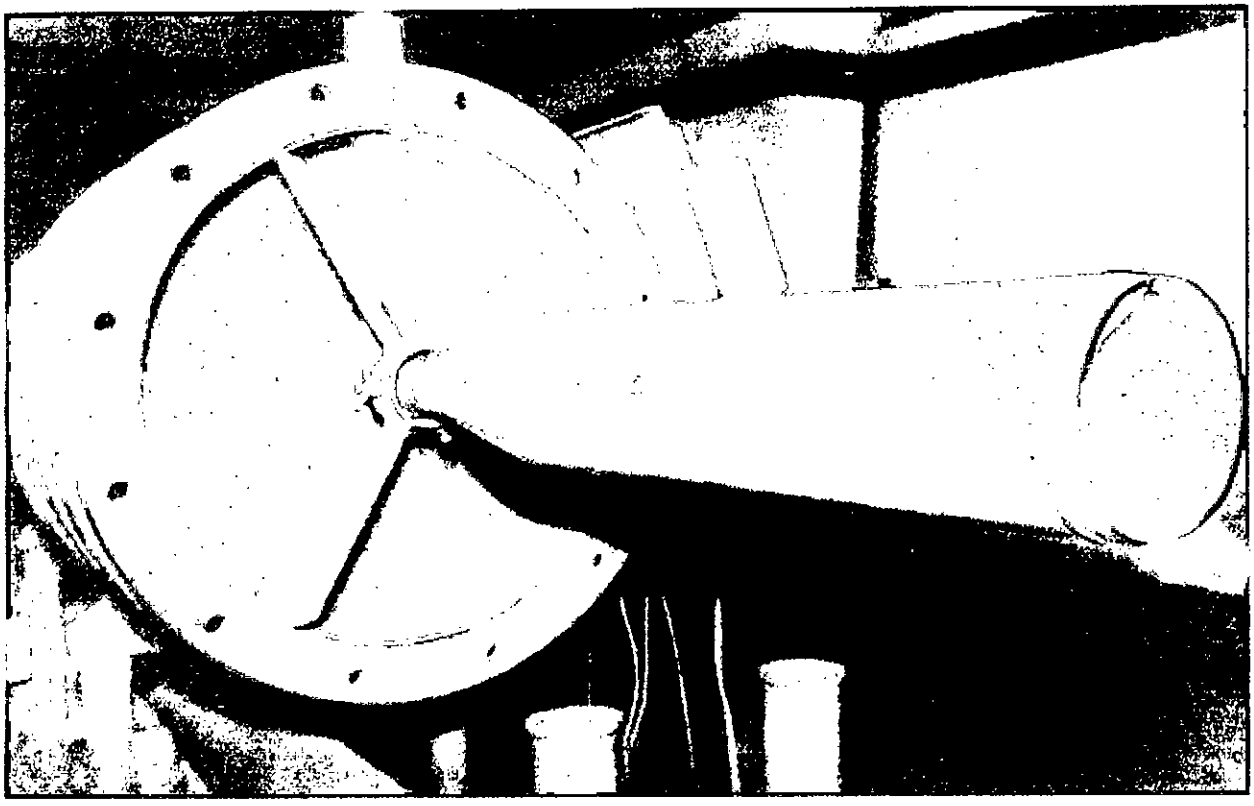

P.2a Centralizers at 475 mm Pipe Flange

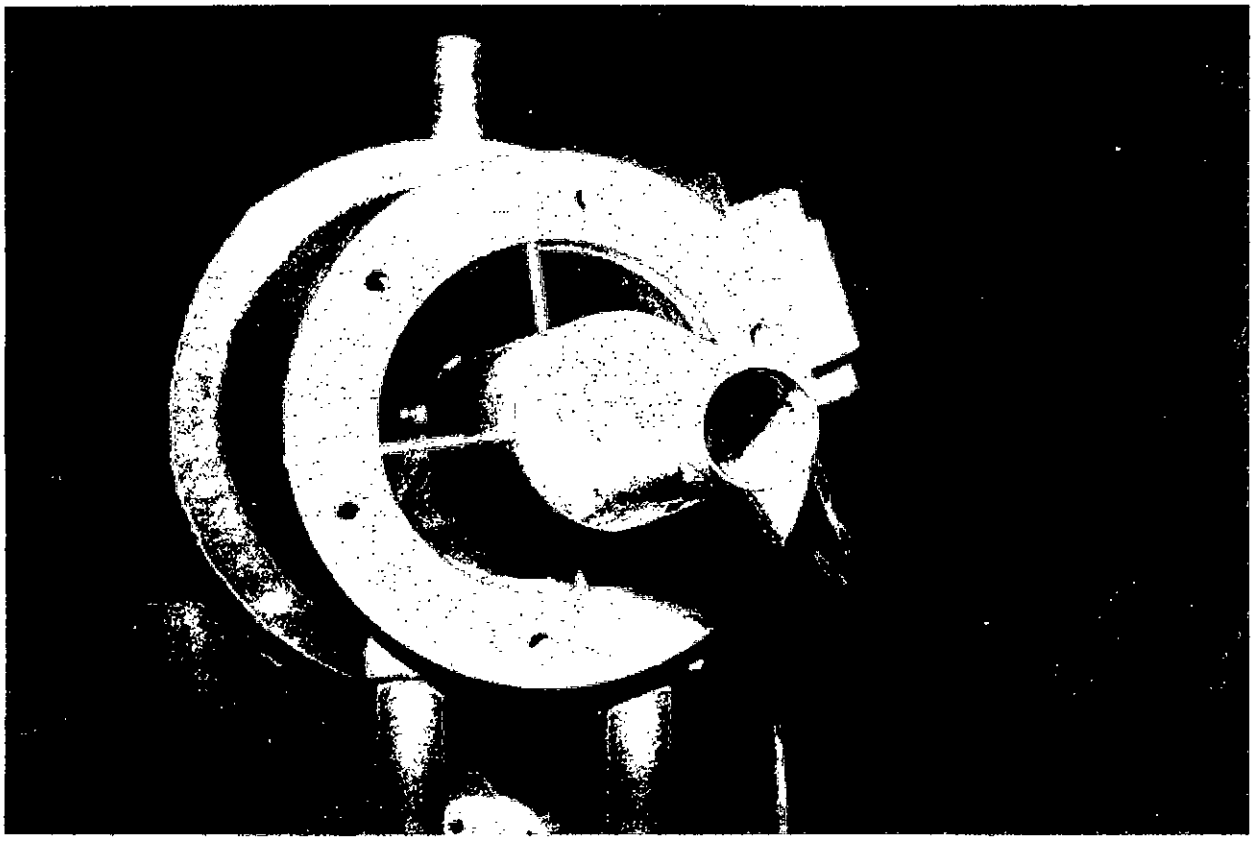

P.2b Centralizers at 250 mm Pipe Flange(Front view)

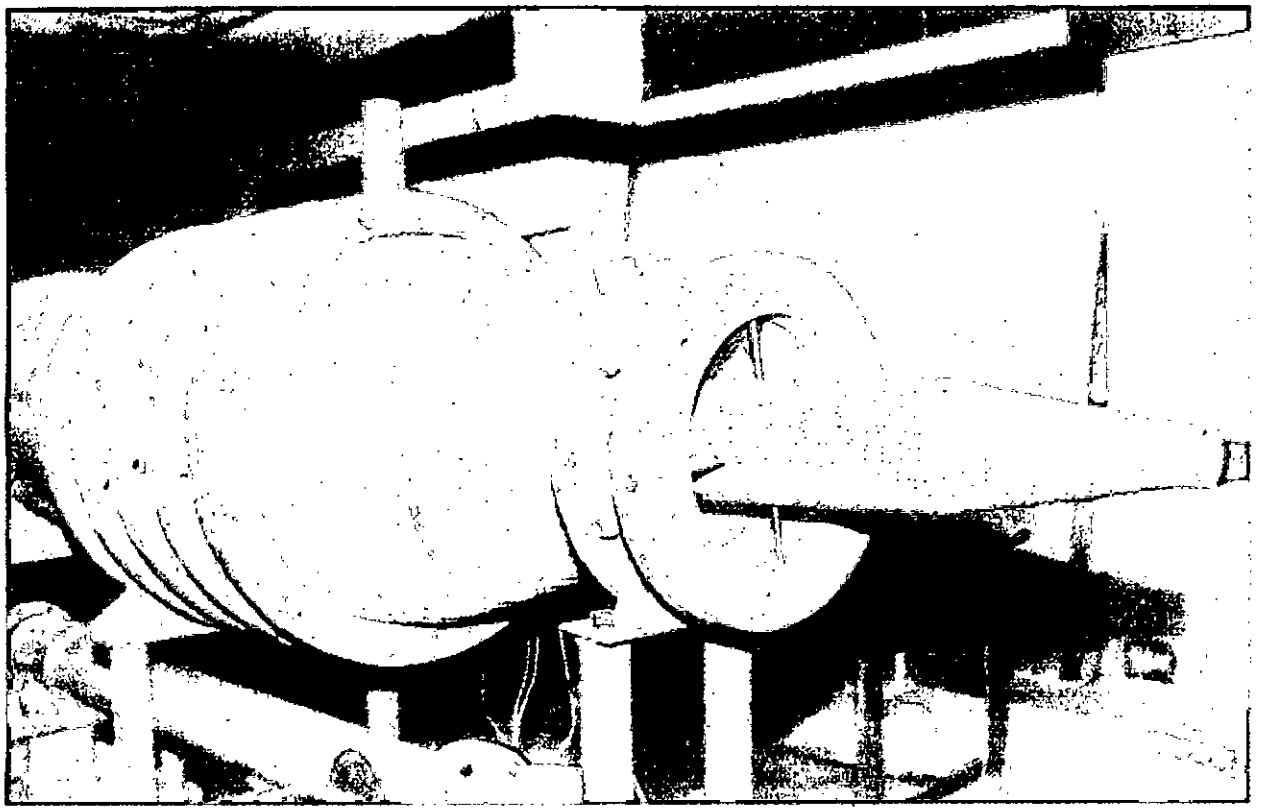

P.2c Centralizers at 250 mm Pipe Flange(Side View)

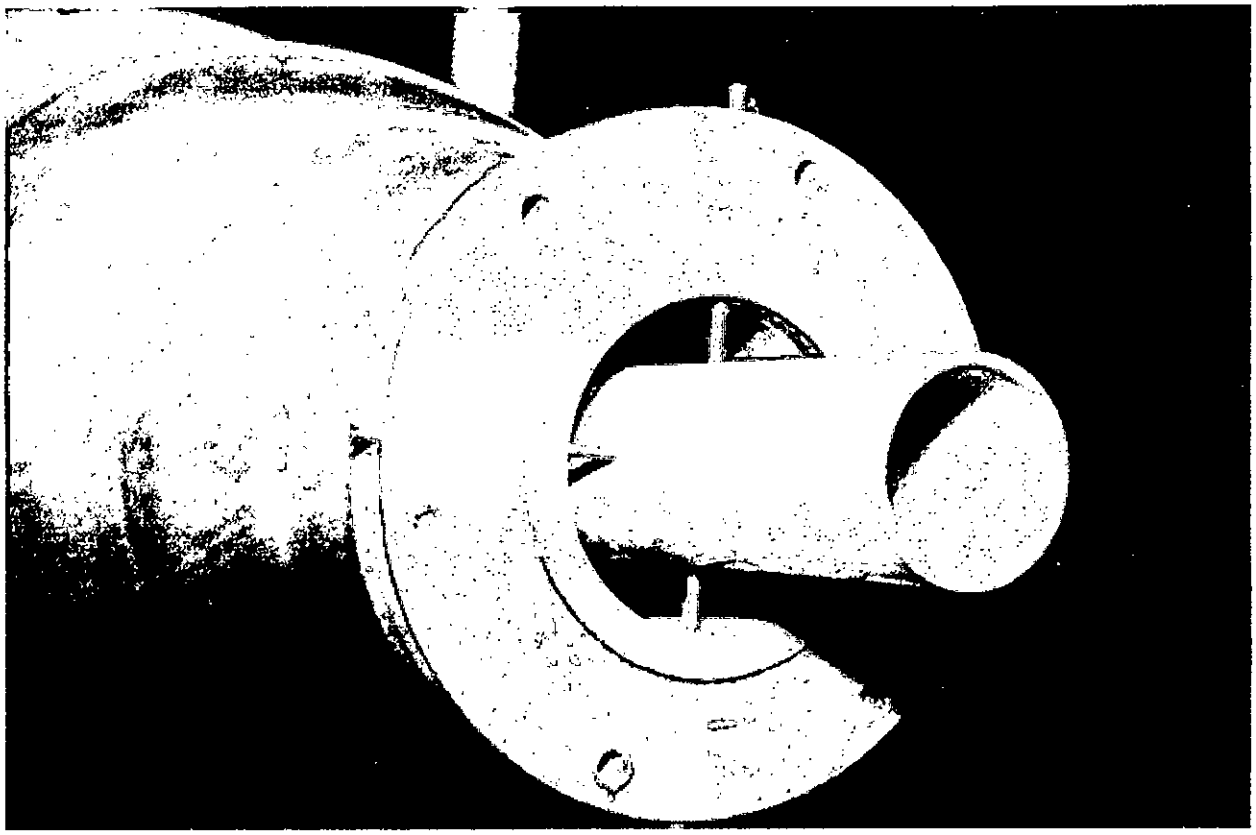

P.2d · Centralizers at 80 mm Discharge Flange

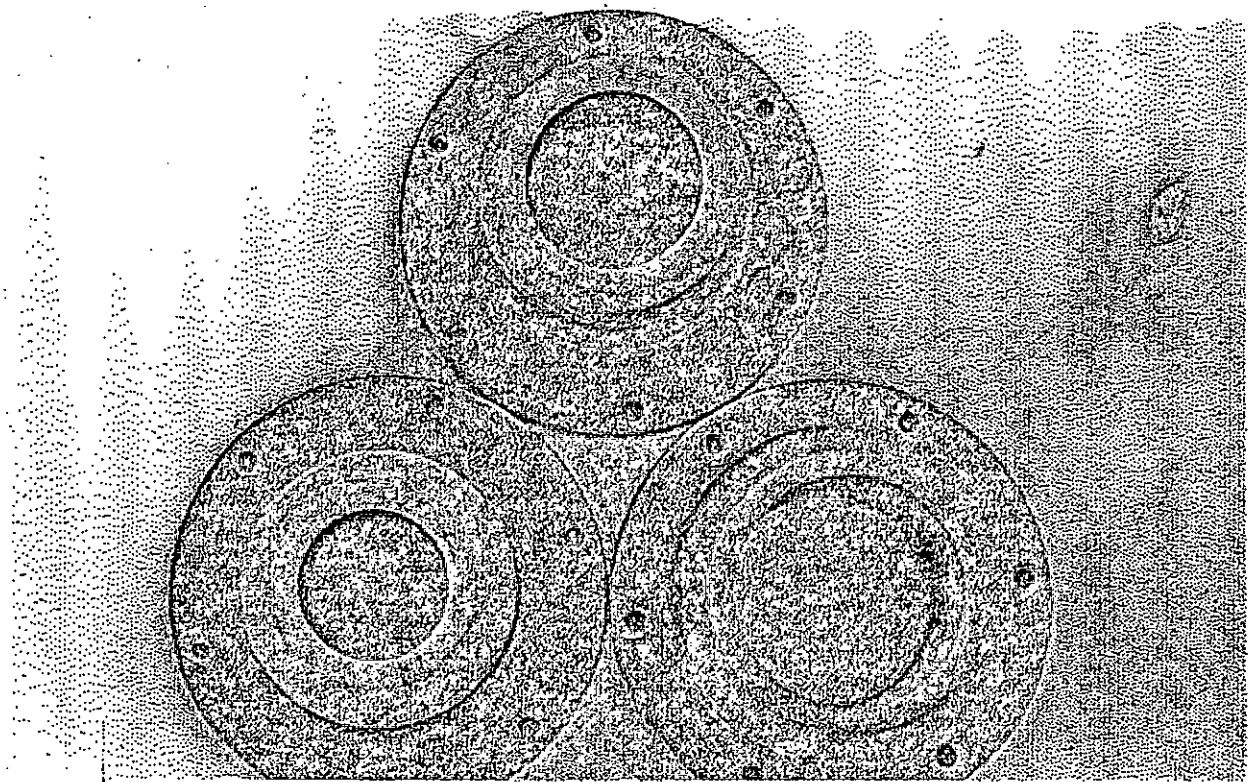

P.3 Annular Nozzles of Varying Diameter